Page VIII added 6-30-55

UNCLASSIFIED

CENTRAL RESEARCH LIBRARY
DOCUMENT COLLECTION

MARTIN MARIETTA ENERGY SYSTEMS LIBRARIES
3 4456 0349847 2

ORNL-1910
Special
Cy. 5

DISCRETE ELECTRON ENERGY LOSSES IN THIN METALLIC FOILS

A. W. Blackstock

CENTRAL RESEARCH LIBRARY
DOCUMENT COLLECTION

LIBRARY LOAN COPY

DO NOT TRANSFER TO ANOTHER PERSON

If you wish someone else to see this document, send in name with document and the library will arrange a loan.

OAK RIDGE NATIONAL LABORATORY
OPERATED BY
CARBIDE AND CARBON CHEMICALS COMPANY
A DIVISION OF UNION CARBIDE AND CARBON CORPORATION
UCC
POST OFFICE BOX P
OAK RIDGE, TENNESSEE

UNCLASSIFIED

UNCLASSIFIED

ORNL 1910

Copy No. 5

Contract No. W-7405-eng-26

HEALTH PHYSICS DIVISION

DISCRETE ELECTRON ENERGY LOSSES IN THIN METALLIC FOILS

A. W. Blackstock

DATE ISSUED

JUN 16 1958

OAK RIDGE NATIONAL LABORATORY
Operated by
CARBIDE AND CARBON CHEMICALS COMPANY
A Division of Union Carbide and Carbon Corporation
Post Office Box P
Oak Ridge, Tennessee

UNCLASSIFIED

MARTIN MARIETTA ENERGY SYSTEMS LIBRARIES

3 4456 0349847 2

ORNL 1910
Special

INTERNAL DISTRIBUTION

1. C. E. Center
2. Biology Library
3. Health Physics Library
4-5. Central Research Library
6. Reactor Experimental Engineering Library
7-31. Laboratory Records Department
32. Laboratory Records, ORNL R.C.
33. C. E. Larson
34. L. B. Emlet (K-25)
35. J. P. Murray (Y-12)
36. A. M. Weinberg
37. E. H. Taylor
38. E. D. Shipley
39. K. Z. Morgan
40. F. C. VonderLage
41. W. H. Jordan
42. C. P. Keim
43. J. H. Frye, Jr.
44. R. S. Livingston
45. J. A. Swartout
46. S. C. Lind
47. F. L. Culler
48. A. H. Snell
49. M. T. Kelley
50. P. M. Reyling
51. A. S. Householder
52. T. A. Lincoln
53. C. S. Harrill
54. C. E. Winters
55. D. W. Cardwell
56. J. A. Lane
57. E. E. Anderson
58. D. D. Cowen
59. R. A. Charpie
60. C. E. Clifford
61. M. J. Skinner
62. J. Neufeld
63. W. S. Snyder
64. H. H. Hubbell
65. G. S. Hurst
66. H. P. Yockey
67-81. A. W. Blackstock
82. R. H. Ritchie
83. M. Slater (Y-12)
84. J. S. Cheka
85. B. G. Saunders
86-115. R. D. Birkhoff
116. ORNL Document Reference Library, Y-12 Branch

EXTERNAL DISTRIBUTION

117. R. F. Bacher, California Institute of Technology
118. G. E. Thoma, USAF
119. U. Fano, National Bureau of Standards
120. L. Leder, National Bureau of Standards
121. L. Marton, National Bureau of Standards
122. H. Brooks, Harvard University
123. J. Bergstein, Los Alamos Scientific Laboratory
124. G. R. Harrison, Vanderbilt University
125. David Pines, Physics Dept., University of Illinois
126. Newton Underwood, Physics Dept., North Carolina State College
127. Division of Research and Medicine, AEC, ORO
128-133. Argonne National Laboratory
134-136. Atomic Energy Commission, Technical Library
137. Atomic Energy of Canada Limited
138-141. Brookhaven National Laboratory
142-143. Carnegie Institute of Technology

144-147. Chalk River Project, Canada
148. Columbia University (Failla)
149-150. Consolidated Vultee Aircraft Corporation
151-152. Iowa State College
153-154. Los Alamos Scientific Laboratory
155. Massachusetts Institute of Technology (Hardy)
156-157. National Bureau of Standards, Atomic Energy Project
158. National Bureau of Standards (Library)
159. National Research Corporation
160-162. National Research Council, Canada
163. Naval Medical Research Institute
164-166. Naval Research Laboratory
167. UCLA Medical Research Laboratory
168-169. University of California Radiation Laboratory, Berkeley
170-173. University of California Radiation Laboratory, Livermore
174-308. Technical Information Service, Oak Ridge
309-408. Oak Ridge Institute of Nuclear Studies

TABLE OF CONTENTS

		Page
I.	Statement of the Problem	1
II.	Review of Previous Related Studies	3
III.	Methods of Procedure and Sources of Data	18
	The Instrument	18
	Operation of the Instrument	21
	The Electrostatic Analyzer	23
	Auxiliary Equipment	27
	Foils	37
	Development of the Instrument	42
IV.	Text of Study	48
	Energy Distributions	48
	Discrete Energy Losses	54
	Comparison with Other Experiments	58
	Mean Free Path	62
	Stopping Power	81
	Cross Sections	87
	Theory	98
	Comparison of Experiment with Theory	106
	Other Considerations	114
	Calculations	124
V.	Summary of Findings and Conclusions	130
	Summary of Findings	130
	Conclusions	132
Bibliography		135

LIST OF TABLES

Table		Page
1.	Discrete Energy Losses	54
2.	Comparison of Discrete Energy Losses with Previous Measurements	59
3.	Mean Free Path in Aluminum as a Function of Incident Electron Energy	70
4.	Mean Free Path in Magnesium at Different Incident Electron Energies	74
5.	Mean Free Path in Copper at Different Primary Energies	79
6.	Stopping Power in Aluminum at Different Incident Electron Energies	82
7.	Stopping Power in Magnesium as a Function of Primary Electron Energy	84
8.	Stopping Power in Copper at Different Primary Electron Energies	88
9.	Cross Section per Free Electron in Aluminum as a Function of Incident Electron Energy	91
10.	Cross Section per Free Electron in Magnesium as a Function of Electron Primary Energy	93
11.	Cross Section per Free Electron in Copper at Various Electron Incident Energies	96
12.	Comparison of Observed Energy Losses with Calculated Values	107
13.	Comparison of Number of Free Electrons per Atom with Valence	108
14.	Comparison of Transitions between Atomic Energy Levels with the Observed Energy Losses	119
15.	Observed Discrete Energy Losses	130
16.	Extreme Values of Mean Free Path	131
17.	Extreme values of Stopping Power	131
18.	Extreme Values of Cross Section per Free Electron	132

LIST OF FIGURES

Figure		Page
1.	Schematic Diagram of Apparatus	19
2.	Photograph of Instrument	20
3.	Electron Energy Distribution with no Foil	22
4.	Cross Sectional Views of Electrostatic Analyzer and Faraday Cage Collector	26
5.	Electron Gun Power Supply	29
6.	Schematic Diagram of R.C.A. WV-84A Microammeter	33
7.	Circuit of the Model Q-826-B Electrometer	34
8.	Photograph of Apparatus	38
9.	Energy Distribution from 15 $\mu g/cm^2$ Aluminum Foil. Incident Electron Energy 45 kev	49
10.	Energy Distribution from 15 $\mu g/cm^2$ Aluminum Foil. Incident Electron Energy 100 kev	50
11.	Electron Energy Distribution from an Aluminum Foil. Incident Electron Energy 45 kev	51
12.	Energy Distribution from 72 $\mu g/cm^2$ Magnesium Foil. Incident Electron Energy 30 kev	52
13.	Energy Distribution from 72 $\mu g/cm^2$ Magnesium Foil. Incident Electron Energy 115 kev	53
14.	Energy Distribution from 66 $\mu g/cm^2$ Copper Foil. Incident Electron Energy 45 kev	55
15.	Energy Distribution from 66 $\mu g/cm^2$ Copper Foil. Incident Electron Energy 115 kev	56
16.	Electron Energy Distribution from a Silver Foil. Incident Electron Energy 45 kev	57
17.	Energy Distribution from 15 $\mu g/cm^2$ Aluminum Foil. Incident Electron Energy 75 kev	68

LIST OF FIGURES (continued)

Figure		Page
18.	Mean Free Path in Aluminum as a Function of Incident Electron Energy	72
19.	Mean Free Path in Magnesium as a Function of Incident Electron Energy	78
20.	Mean Free Path in Copper as a Function of Incident Electron Energy	80
21.	Stopping Power in Aluminum as a Function of Incident Electron Energy	83
22.	Stopping Power in Magnesium as a Function of Incident Electron Energy	86
23.	Stopping Power in Copper as a Function of Incident Electron Energy	89
24.	Cross Section per Free Electron in Aluminum as a Function of Incident Electron Energy	92
25.	Cross Section per free Electron in Magnesium as a Function of Incident Electron Energy	95
26.	Cross Section per Free Electron in Copper as a Function of Incident Electron Energy	97
27.	v^2/λ as a Function of ln v in Aluminum	113

ACKNOWLEDGMENTS

The author wishes to express his gratitude to Drs. R. D. Birkhoff, H. H. Hubbell, Jr. and Newton Underwood, under whose combined direction the investigation was performed. The problem was suggested by Dr. Birkhoff. The author also wishes to express his gratitude to the Oak Ridge Institute of Nuclear Studies for sponsoring the research through an Oak Ridge Graduate Fellowship and to Dr. K. Z. Morgan for making available the facilities of the Health Physics Division of the Oak Ridge National Laboratory. The writer is greatly indebted to Mr. R. H. Ritchie for many very helpful discussions of the theory involved and extends his thanks to Dr. M. Slater for his guidance during the early part of the work. The writer also wishes to thank Mr. G. R. Harrison, Mr. P. N. Hensley, Mr. R. H. Jones, Mr. H. W. Parker and other members of the Health Physics Shop for their help.

I. STATEMENT OF THE PROBLEM

The problem herein discussed is a study of discrete energy losses suffered by electrons with primary energies in the range 25 to 115 kev which are scattered through angles less than one degree in passing through thin foils of aluminum, magnesium, copper, and silver. The measurements were made with an electron accelerator and an energy analyzer of very high resolution resulting from the use of a stopping potential type energy analyzer together with a low-energy cylindrical electrostatic analyzer. The mean free paths, cross sections and stopping powers, as a function of incident electron energy, corresponding to these discrete losses have been calculated for aluminum, magnesium and copper. The results are compared with previous experimental measurements and with the "plasma oscillation" theory of Pines and Bohm (1952, 1953).

There have been previous applications of the stopping potential technique for measuring energies and previous measurements of discrete electron energy losses by other methods. The contribution of this investigation is the measurement of discrete electron energy losses by the stopping potential technique, the measurement of such losses over a considerably extended primary energy range and the evaluation of the corresponding mean free paths, cross sections and stopping powers as a function of primary energy.

Attempts have been made to attribute the discrete electron energy losses observed in metals to excitation of oscillations of the

electron plasma in the metals. Some of the previously observed losses agree with those predicted by the plasma oscillation theory; more of them do not. Pines (1953) obtained an expression for the mean free path for excitation of plasma oscillations. Prior to the present investigation, there were no experimental determinations of this mean free path. The measurement of the discrete energy losses over a much wider primary electron energy range and the evaluation of the corresponding mean free path should, in addition to providing a further test of the plasma oscillation theory, contribute to the understanding of the nature of these losses.

II. REVIEW OF PREVIOUS RELATED STUDIES

The stopping potential technique for measuring electron energy has been known for some time, having originated in the work of Franck and Hertz in 1914 on atomic excitation potentials. A recent application of this method has been made by Hamilton and Gross in 1950 in an electrostatic beta ray spectrograph utilizing a spherically symmetric retarding electric field and achieving an energy resolution of about 0.6 per cent for energies up to 30 kev. The spectrograph was used to study the low energy portion (0-30 kev) of the spectrum of sulfur 35. In another application Phillips in 1953 measured the energy loss in gases of protons with initial energies in the range 10 to 80 kev.

In 1930 Rudberg observed in the energy distribution of electrons scattered from incandescent solids a large, sharp peak corresponding to reflected electrons and several small maxima at slightly lower energies. These maxima were characteristic of the target material and their position with respect to the reflected peak remained constant for the range of bombarding voltages used, 90 to 540 volts. The measurements were confined to energy losses not exceeding 50 volts. These maxima were also independent of the scattering angle. The energy losses were measured by varying a magnetic field or by adding an accelerating potential equal to the energy loss. The results follow:

Energy Loss, ev				
Copper				
3.4 ± 0.11	6.9 ± 0.10	12.3 ± 0.15	25.5 ± 0.31	34.5 ± 0.31
Silver				
4.6 ± 0.06	7.4 ± 0.08	24.8 ± 0.26		
Gold				
7.3 ± 0.07	10.1 ± 0.29	25.9 ± 0.21	35.2 ± 0.19	
Platinum				
6.5 ± 0.09	9.4 ± 0.08	24.8 ± 0.16	33.7 ± 0.14	
Magnesium Oxide				
6.9 ± 0.10	11.7 ± 0.11	17.5 ± 0.11	22.7 ± 0.05	33.8 ± 0.13
Calcium Oxide				
9.4 ± 0.07	13.8 ± 0.07	20.0 ± 0.17	29.4 ± 0.10	36.7 ± 0.13
Strontium Oxide				
7.3 ± 0.13	9.6 ± 0.08	13.2 ± 0.11	24.9 ± 0.17	31.6 ± 0.12
Barium Oxide				
10.6 ± 0.14	16.8 ± 0.19	25.3 ± 0.20	32.7 ± 0.14	

In 1935 Haworth published results of studies on the energy distribution of secondary electrons from molybdenum under bombardment by electrons with primary energies up to 150 v. He observed, in addition to the usual sharp "elastically reflected" peak and the broad, low energy maximum, peaks at energies 10.6, 22 and 48 volts less than the primary energy which were due to critical energy losses among the

inelastically scattered electrons. The energies were measured with a 180° magnetic analyzer.

In 1936 Rudberg reported further results of measurements of the energy distribution of electrons scattered inelastically from solids for primary energies from 50 to 400 volts, using a method of magnetic deflection. For certain values of the energy loss suffered by scattered electrons the curves exhibited maxima, which were characteristic of the target material and independent of the primary voltage in the range studied. These maxima appeared to correspond roughly to the regions of high optical absorption for the same substance. His results follow:

Metal	Energy Loss, ev. (Approximate)		
Cu	4.2	7.2	
Ag	3.9	7.8	23
Au	3.0	6.0	24

Turnbull and Farnsworth reported in 1938 results of investigations on the energy distribution of slow electrons inelastically scattered from a (111) face of a silver single crystal using the magnetic deflection method. At 45° incidence, primary electrons were regularly reflected into the analyzer and diffraction beams observed at primary energies of 7.7, 23.2 and 83.2 ev. The energy distribution showed two discrete loss peaks at 3.9 and 7.3 ev, in general agreement

with those found by Rudberg (1936) for polycrystalline silver. The relative intensities of the two discrete loss peaks were found to depend on both the primary voltage and the target angle in the neighborhood of the diffraction beams, whereas Rudberg found that for polycrystalline targets the peaks were independent of these variables.

In 1941 Ruthemann reported discrete energy losses suffered by electrons of initial energy 3 to 8 kev in passing through foils a few hundred A thick of collodion, Al_2O_3, Be, Al, and Ag. These losses were independent of primary energy and foil thickness. The losses were most pronounced in Al and Be and five losses which were multiples of 15.1 ev were observed in Al. The measurements were taken with a semicircular magnetic spectrometer which had an energy resolution of about 0.05% at 5.3 kev. A photographic plate was used as a detector, the proper intensity distribution being determined from a photometer curve with the aid of a density curve. Using the same apparatus in 1942, Ruthemann observed energy losses of 22, 298, 400 and 546 ev suffered by electrons with 7.5 kev primary energy in passing through collodion films about 100 A thick. The last three losses correspond to the K excitation levels in C, N and O, respectively.

Hillier and Baker in 1944 used an instrument consisting of an electron gun, a two-stage, probe-forming lens system, a movable specimen stage, a projection lens, a 180° magnetic deflection type velocity analyzer and a photographic chamber to measure discrete electron energy losses. Their results are given in the following table.

Element	Z	ΔE (ev)	Level	E (kv)	ΔE (ev) (ICT)*
Be	4	129.3	K	46.5	----
C	6	286.2	K	26.0	284.2
N	7	404	K	26.0	397.6
O	8	525.8	K	26.0	526.2
Al	13	1605	K	46.0	1553.7
Si	14	2033	K	47.8	----
Fe	26	703.9	L	26.0	709.8 723.9
Fe	26	51.3	M	26.0	56.5
Zn	30	1160	L	46.0	1021.2 1044.4

* Values from International Critical Tables

The losses in C, N, and O were observed in collodion films. It was found that the values of the discrete energy losses corresponding to the K levels of carbon and oxygen increased with increasing accelerating potentials.

In 1948 Ruthemann published in a more detailed paper results on collodion, Al_2O_3, Be, Al and Ag in addition to those reported in 1941 on his preliminary investigations. Using the same semicircular magnetic analyzer with electrons of 2 to 8 kev primary energy, he found in Al five discrete energy losses of 14.72, 29.59, 44.34, 59.34 and 73.84 ev, respectively; in Be four of 18.97, 38.11, 57.31 and 75.98 ev; in Al_2O_3 two of 22.31 and 45.52 ev; in Ag two of 22.57 and 45.31 ev, and in

collodion one loss of 21.4 ev. In each case the higher losses were integral multiples of the lowest and the values were independent of the primary energy of the bombarding electrons. The mean values of the differences between successive losses were 22.3 ev in Al_2O_3, 19.0 ev in Be, 14.7 ev in Al, and 22.6 ev in Ag. The foils were 100 to 500 A thick.

Also in 1948 Lang reported additional measurements in Al and measurements in Cu and Ni taken with the same apparatus as that used by Ruthemann. Discrete energy losses were measured in Al foils of thicknesses 180A, 250A, and 350A using electrons with primary energies of 7.75, 7.75, and 7.54 kev. Two discrete energy losses were found in the 180A foil, three in the 250A foil, and six in the 350A foil with values of 14.5, 29.4, 44.2, 58.6, 75.2, and 90.4 ev, the higher losses being integral multiples of the smallest. The mean value of the difference between successive losses in Al was given as 14.8 ev. Single losses were found in both Cu and Ni with values of 19.1 and 24.2 ev, respectively. The uncertainty in the measurements was stated to be $\pm$ 3%. The energy resolution at 7.75 kev was about 0.06%.

Möllenstedt reported in 1949 measurements of discrete electron energy losses in thin foils made by means of a velocity analyzer composed of a 5 micron slit placed off the axis and in front of an electrostatic cylinder lens in an electrostatic electron microscope. Due to chromatic aberrations in the off-axis region, images of the slit due to electrons which had suffered discrete energy losses in passing through a foil were displaced on a photographic plate from

the image due to the unretarded electrons, the displacement being proportional to the energy loss. The foils were placed in the object position in the electron microscope. The electrons had initial energies in the range 25 to 40 kev. The resolution was 1 : 35,000. The intensity distribution was obtained from a photometer curve. The results are shown in the table below.

Substance	Energy Losses (ev)					
	Möllenstedt					Ruthemann - Lang Values 5 - 8 kev
Collodion	6	21				21.3
Aluminum	7	15	22			14.7
Aluminum, different exp.	9	18	36	54		
Aluminum Oxide, Al_2O_3	22.5					22.5
Nickel	22.6	65				24.2
Gold	15	30	45	60		
Tellurium	8	20				
Cadmium	9	21.5				
Antimony	15	20	31			
Platinum on Collodion	14	22.4	46	61.4		
Copper	20.4					19.1
Muscovite 400A	25					
Muscovite 700A	25	50				
Vacuum 10^{-3} mm Hg	3.5	7	12	66	130	

Reichertz and Farnsworth reported in 1949 measurements of the energy distribution of low speed electrons inelastically scattered from a (100) face of a copper single crystal by the electrostatic deflection method. A cylindrical electrostatic analyzer similar to that used in this research was used. With normal incidence of the primary electrons, observations were made in the neighborhood of two strong diffraction peaks, one at 59.5 ev primary energy and 60° scattering angle, the other at 114.5 ev and 40.5°. Discrete peaks were observed at 3.0, 6.0, 12.3, and 20.0 ev energy loss with intensities depending on both primary energy and scattering angle.

In 1952 and 1953 Pines and Bohm attempted to explain the discrete energy losses observed in metals as being due to excitation of plasma oscillations of the free electrons in the target materials. A more complete discussion of this theory will be given in the section on theory.

In 1952 Möllenstedt reported discrete electron energy losses measured in several gases, water and some organic compounds in the vapor state using the same equipment described earlier but modified to permit small amounts of the gases to be admitted through a needle valve just beneath the objective lens in the electron microscope. Also, the two projective lenses were removed. His results are shown in the following table. The primary energy of the electrons was 35 kev. These losses are due to excitation or ionization of the target atoms.

Substance	Energy Loss (ev)	
Nitrogen	13.1 ± 0.3	
Oxygen	8.0 ± 0.3	13.6 ± 0.5
Hydrogen	13.1 ± 0.3	
Helium	12.9 ± 0.3	19.8 to 20.9
Benzene, C_6H_6	6.9 ± 0.2	11.8 ± 0.3
Carbon Dioxide	11.9 ± 0.3	
Water	13.8 ± 1	
Xylene, $C_6H_4(CH_3)_2$	7.0 ± 0.5	14.0 ± 1
Ethyl ether $C_2H_5OC_2H_5$	11.5 to 13	

A paper by Cauchois in 1952 compares the discrete energy losses, V, observed by Ruthemann in 1941 in aluminum with the distances, Δ, between each dark band and the absorption discontinuity measured in the K absorption spectrum of metallic aluminum. The comparison follows:

V (ev)	15	32	47	63	82
Δ (ev)	9	29	47	63	85

The author states that if these coincidences are not fortuitous one can conclude that the spectrum of the transmitted electrons describes the density of excitation states for the conduction electrons in aluminum. The discrete energy losses observed by Ruthemann in aluminum correspond to the excitation of electrons

from the conduction band of the metal to the permissible unoccupied bands, which are of great density.

Lander reported in 1953 in a study of Auger peaks in the energy spectra of secondary electrons from various materials, in the region near the elastically scattered primary beam in aluminum and beryllium, peaks corresponding to those reported by Ruthemann in 1948. He found that slight oxidation changed drastically the character of this region of the curve. His equipment consisted essentially of an electron gun, an electrostatic electron velocity analyzer consisting of two electrodes which were sections of spheres, and a target at an angle of 45° with both the gun and the entrance to the analyzer. In this experiment, the phenomenon was observed in the spectrum of reflected electrons. He observed no peaks corresponding to the K excitation levels in carbon and oxygen as reported by Ruthemann in 1942.

Marton and Leder reported in 1954 discrete energy losses in the spectrum of 30 kev electrons passing through thin foils of a number of metals and insulators. The measurements were made with equipment very similar to that used by Möllenstedt. An electrostatic electron microscope was modified by replacing its two projection lenses with a slit and a "cylindrical" lens. The analysis of the scattered primary beam was accomplished by utilizing the off-axis chromatic aberration of the "cylindrical" lens. An energy resolution of 1 part in 35,000 was obtained. Thin films, which were between 50 and 100 A thick, were mounted in the normal

object position of the microscope. The spectra were detected on photographic plates. The authors state that where higher energy losses appear to be multiples of some lower one, this indicates the repeated occurrence of the same event. The results are shown in the following table:

Material	Energy Loss in ev					
Beryllium	6.5	18.9				
Na on quartz	5.4	10.7	13.3	17.5		
Na on collodion	5.1	10.8	17.5	18.6		
Magnesium	9.7	20.3				
Aluminum	6.2	13.9	19.2	27.8	35.0	
Silicon	5.2	16.9				
K on silicon	7.8	11.3	15.0	18.7	22.6	27.8
K on collodion	8.0	11.0	14.9	19.5	22.7	25.8
Titanium	11.4	21.4	42.9			
Chromium	9.7	21.8	45.0			
Manganese	9.9	22.1				
Iron	15.8	19.4	56.1			
Cobalt	5.7	18.3				
Nickel	5.8	9.4	13.2	17.6	23.4	
Copper	6.9	11.3	19.6			
Germanium	16.0	30.1				
Palladium	15.7	21.5				
Silver	16.0					
Cadmium	14.5					
Tin	4.5	12.4	18.0	23.9		
Antimony	14.2	24.3				
Gold	16.5	21.5				
Bismuth	13.0	25.2				
Collodion	4.5	19.3				
Quartz	5.5	19.4				
Air (nitrogen)	12.9					

Later in 1954 Leder and Marton reported characteristic energy losses of 30 kev electrons in passing through thin films of several metals and compounds of these metals. In each case the

peaks observed in the compounds were shifted to higher energies than those of the peaks in the metal. The results are shown in the following table:

Material	Energy Loss (ev)		
Si	4.8	16.9	
SiO_2	5.4	19.4	
Te	4.6	16.0	
TeO_2	9.5	17.5	
Pb	5.1	12.1	21.8
PbS	6.8	14.7	21.9
Sb	4.3	14.9	30.6
Sb_2S_3	6.3	18.0	35.4
Mg	9.7	20.3	
MgO*	11.4	25.0	

* H. Watanabe (private communication)

The authors state that these results suggest that some of the characteristic energy losses observed were not due to electron plasma interaction, since there would be no plasma in the compound, but were rather due to excitation of some outer orbit electrons.

Watanabe reported in 1954 discrete energy losses of 15-25 kev electrons in passing through a MgO foil. The electron velocity analyzer used in the measurements was of the same type as that of Möllenstedt (1949), described previously. Watanabe concluded that the positions of the peaks were independent of the accelerating voltage of the incident electrons. He considered the discrete energy losses to correspond to the transitions of the electrons in

MgO from the valence band to the empty bands above the valence band. His results are given in the following table:

Accelerator Voltage kv	First Peak Position ev	Second Peak Position ev	Second Peak Width ev	Third Peak Position ev
16	5.2	11.41	1.7	24.5
18	5.2	11.44	1.9	25.1
22	5.3	11.45	1.9	25.0
24.5	5.4	11.49	1.9	25.2

In another paper in 1954 Watanabe reported further discrete energy losses of 22 kev electrons in passing through thin foils of various materials. He used an electron microscope with an analyzing lens very similar to that of Möllenstedt (1949) and Marton and Leder (1954), which have already been described. He reported a resolving power of about 1/10,000 and a detectable energy loss of 2 ev for 22 kev electrons. The losses were detected photographically and the energy distributions obtained by means of a microphotometer. His results are given in the following table:

Substance	Foil Thickness (A)	Energy Losses (ev)				
Al	200	6.5	14.8	23	29.5	
Al_2O_3		22.5	46			
Ag		22				
Au		6.5	17.5	25	34	49
Be	300	19	38	56		
BeO		5.7	16.5	28	57	
$Ca(OH)_2$		7.5	12	15	22	37
Cr		26	54			
Cu		7	19.5			
Ge		17	34			
MgO	200	4.5	5.5	11.4	25	
NaCl		14.5	20	24	29	32
Ni		6.5	12	22.5	45	
Sb		6.5	18	24.5	46	
Sn		6.3	13	19.5		
SnO_2		5.5	12.5	19.5	35	63
Collodion		7	13	18	21.2	
Residual Gas in Vacuum		6	9	13.5		

He also compared the loss peaks in aluminum with the "valleys" near the K and L X-ray absorption edges. This comparison follows:

Valleys of K Absorption Edge (ev)	Valleys of L Absorption Edge (ev)	Loss Peaks (ev)
6.1	(3.8)	6.5
14.0	(10.0)	14.8
	23.0	23.0
		29.5
37.0	39.0	
55.0	54.0	

In still another short paper in 1954 Watanabe reported discrete energy losses of 25 kev electrons in passing through Mg foils, about 600A thick, using the same apparatus. His results are:

Energy Loss	(ev)	10.3	20.7	31.2	41.5
Half Width	(ev)	1.5	1.5	2	3

Prior to the work of Pines and Bohm (1952, 1953) there was no explanation of the observed discrete electron energy losses. Moreover, only some of the discrete losses observed in Be, Na, Mg, Al and K agree with the plasma oscillation theory; others observed in these metals and those observed in other metals do not. In addition, the measurements of discrete electron energy losses which have been described were made with initial electron energies up to only 40 kev. These facts indicate a need for further investigations of such discrete losses over an extended primary energy range.

III. METHODS OF PROCEDURE AND SOURCES OF DATA

The Instrument

A description of the instrument in its present form has been published by Blackstock, Birkhoff and Slater (1955). However, a more detailed description will be given here. Figures 1 and 2 are a schematic diagram and photograph of the apparatus, respectively. The instrument consists of an electron gun, an accelerating tube, a decelerating tube which derives its potential from the same source as the accelerating tube, a low energy cylindrical electrostatic analyzer, and a Faraday cage collector. The accelerating and decelerating tubes are typical of those used in Cockroft-Walton machines, each consisting of alternate ceramic insulators and accelerating electrodes sealed vacuum tight with vinyl cement. The potentials of the electrodes are established by six fifty megohm International Resistance Company voltage dividing resistors in series across the accelerator and six across the decelerator. The foil to be bombarded is located at the center of the machine, which is at ground potential. The same principal accelerating voltage is applied between the center and both ends of the system. In addition separate biasing voltages (δ and δ') of a few hundred volts are applied at each end of the system. δ' is a variable potential in the lead to the accelerator which provides additional acceleration to compensate for energy lost in the foil. δ is a fixed potential, usually set at approximately 100 volts, used in the lead to the decelerator to

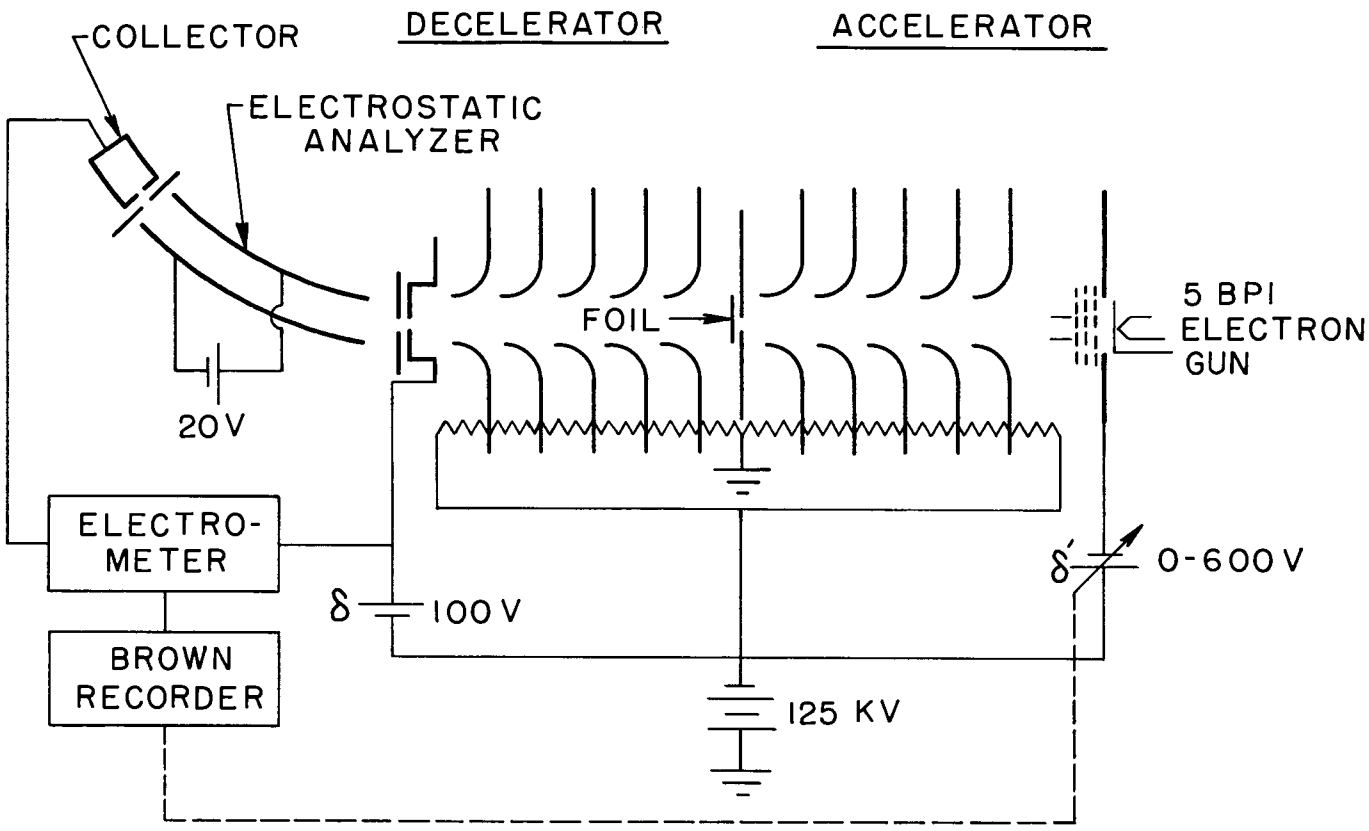

FIG. 1 - SCHEMATIC DIAGRAM OF APPARATUS

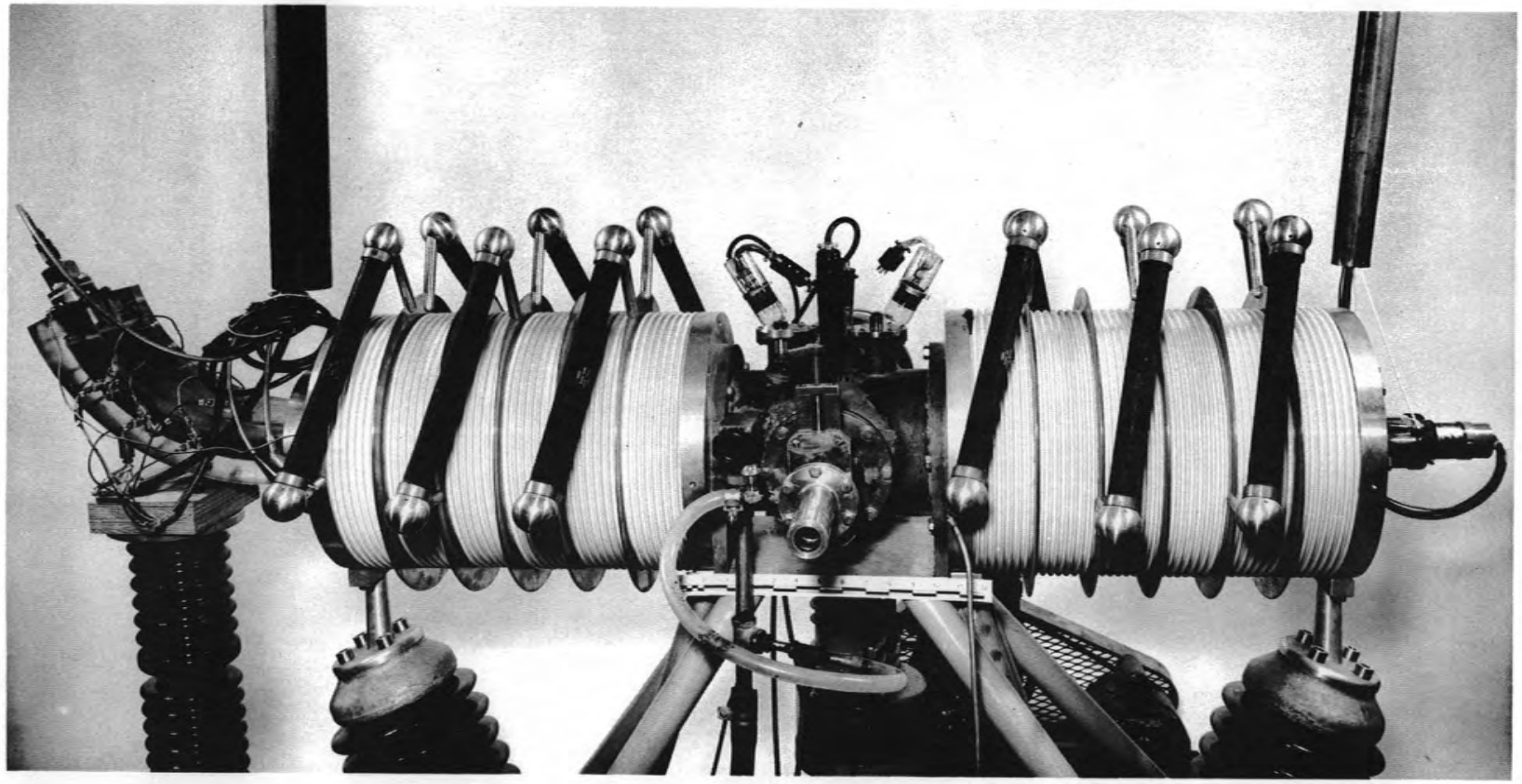

Fig. 2. Photograph of Instrument.

provide less deceleration than would result from the total high voltage.

Operation of the Instrument

The instrument permits the study of electron energy losses which do not depend critically on the primary energy of the electrons. Electrons from a cathode ray gun are accelerated in the accelerator, pass through the test foil, are slowed down in the decelerator, pass through the electrostatic analyzer and are collected in the Faraday cage. An aluminum baffle, with a 3/4 in. diameter hole in it, immediately in front of the foil insures that all electrons reaching the electrostatic analyzer and collector pass through the foil. Fluctuations in the high voltage affect both accelerator and decelerator similarly; thus, although the energy of the electrons incident on an absorber placed between the two tubes fluctuates, the energy of the electrons leaving the decelerator is unaffected, depending only on the processes occurring in the foil. The electrons enter the electrostatic analyzer with about 100 ev energy thus eliminating defocussing which occurs if collection is attempted at zero energy directly from the decelerator. The width of the energy distribution is essentially independent of the bombarding energy, a situation not generally found in accelerators in which the energy analyzer is a separate unit. The energy resolution of the instrument is 0.002% at 100 kev as given in Fig. 3 by the ratio of the width at half maximum to the accelerating voltage. The resolution is limited only by the spread in energy of the electrons from the cathode ray

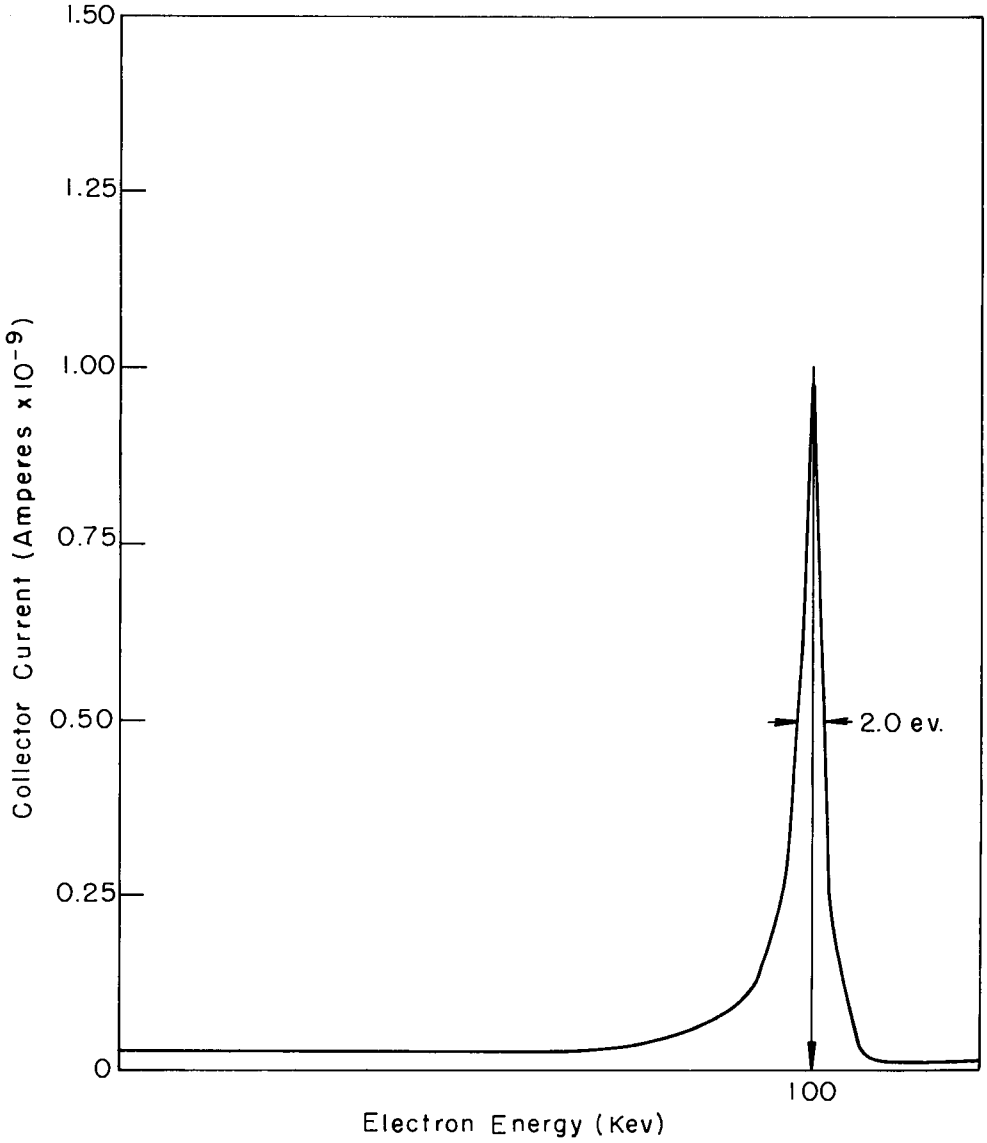

FIG. 3-ELECTRON ENERGY DISTRIBUTION WITH NO FOIL

gun, and the resolution of the electrostatic analyzer. The resolution for effects which depend critically on the bombarding energy is limited only by the stability of the high voltage supply and not by geometrical factors.

With δ' set at zero and no foil in the beam, electrons leave the decelerator with an energy of about 100 ev, pass through the electrostatic analyzer, which is set to select electrons of this energy, and then into the Faraday cage. When a foil is placed between the accelerator and decelerator, electrons which have lost energy in the foil may still be collected if the voltage δ' is increased to a value corresponding to the amount of energy lost. All electrons which are collected, regardless of the amount of energy lost, leave the foil with the same kinetic energy, are decelerated by the same amount, are deflected the same amount by any residual magnetic fields, and are deflected in the electrostatic analyzer by the same electric field. Such operation eliminates any ambiguities in energy which might arise in any of these steps if the energy of the electrons collected is scanned by varying the potential applied to the electrostatic analyzer, or by changing the δ voltage with δ' set at zero.

The Electrostatic Analyzer

The electrostatic analyzer used is similar to that described by Hughes and Rojansky (1929) and Hughes and McMillen (1929). Their analysis shows that in a radial inverse first power electrostatic

field good focussing of a beam diverging from a slit source and good resolution are obtained if the angle between the planes of the entrance and exit slits is 127° 17'. In an analyzer of this type the deflecting plates are sections of surfaces of two concentric cylinders. Herzog (1934) and Dempster (1937) give a more general treatment of the theory involved.

There have been several applications of electrostatic deflectors of this type prior to the present one. Mattauch and Herzog (1934) describe a mass spectrograph utilizing such an electrostatic deflector with an angle of 31° 50' in one case and an angle of 63° 39' in another. Bainbridge and Jordan (1936) describe a mass spectrograph in which an electrostatic deflector of this type with an angle of 127° 17' is employed. Such a deflector employing an angle of 90° was used by Allison, Skaggs and Smith (1938). In 1940 Rogers, McReynolds and Rogers used an analyzer of this type with an angle of 89° 51' and Hanson (1944) employed one with an angle of 15°. This type deflector with an angle of 127° was used by Backus (1945) as a beta-ray spectrometer. Warren, Powell and Herb (1947) used a 90° analyzer of this type and obtained an energy resolution of 5000 at 1 Mev, corresponding to an energy spread of 200 ev in the beam. A 90° electrostatic analyzer was described by Fowler, Lauritsen and Lauritsen (1947). After passage through the analyzer the beam had an energy spread of 300 ev at 1 Mev. In 1949 Reichertz and Farnsworth used a similar electrostatic analyzer which had a theoretical resolving power

$\Delta V/V = 0.0273$. Another 90° cylindrical electrostatic analyzer has been described by Allison, Frankel, Hall, Montague, Morrish, and Warshaw (1949). A cylindrical electrostatic analyzer using a deflecting angle of 63° 39' was used by Hunt (1952). The energy resolution was stated to be one part in a thousand at 340 kev, corresponding to an energy spread of 340 ev.

The electrostatic analyzer used in this research was designed by Dr. M. Slater. Cross sectional views of the analyzer and the Faraday cage collector are shown in Fig. 4. Because the radiation entering the analyzer was approximately parallel, the angle between the planes of the entrance and exit slits was made half the 127° given by the analysis of Hughes and Rojansky (1929), or 63.5°. However, to insure that a narrow, parallel beam enters the analyzer, the electrons are collimated by a double slit as shown in Fig. 1. A block of lucite was milled out to form the concentric cylindrical plates, which were made conducting by an aquadag coating. An O-ring between the lucite top and the body of the analyzer provides the vacuum seal. Brass screws, with O-rings under their heads, make electrical connections to the plates and to the guard electrodes, which serve to make the electric field between the plates more uniform. The radius of the inner plate is 9 inches and that of the outer plate 10 inches. The depth of the gap is 3 inches. With this geometry the ratio of the energy selected in ev to the potential difference between the plates in volts is 4.75. Thus a potential difference of 21 volts across the plates is

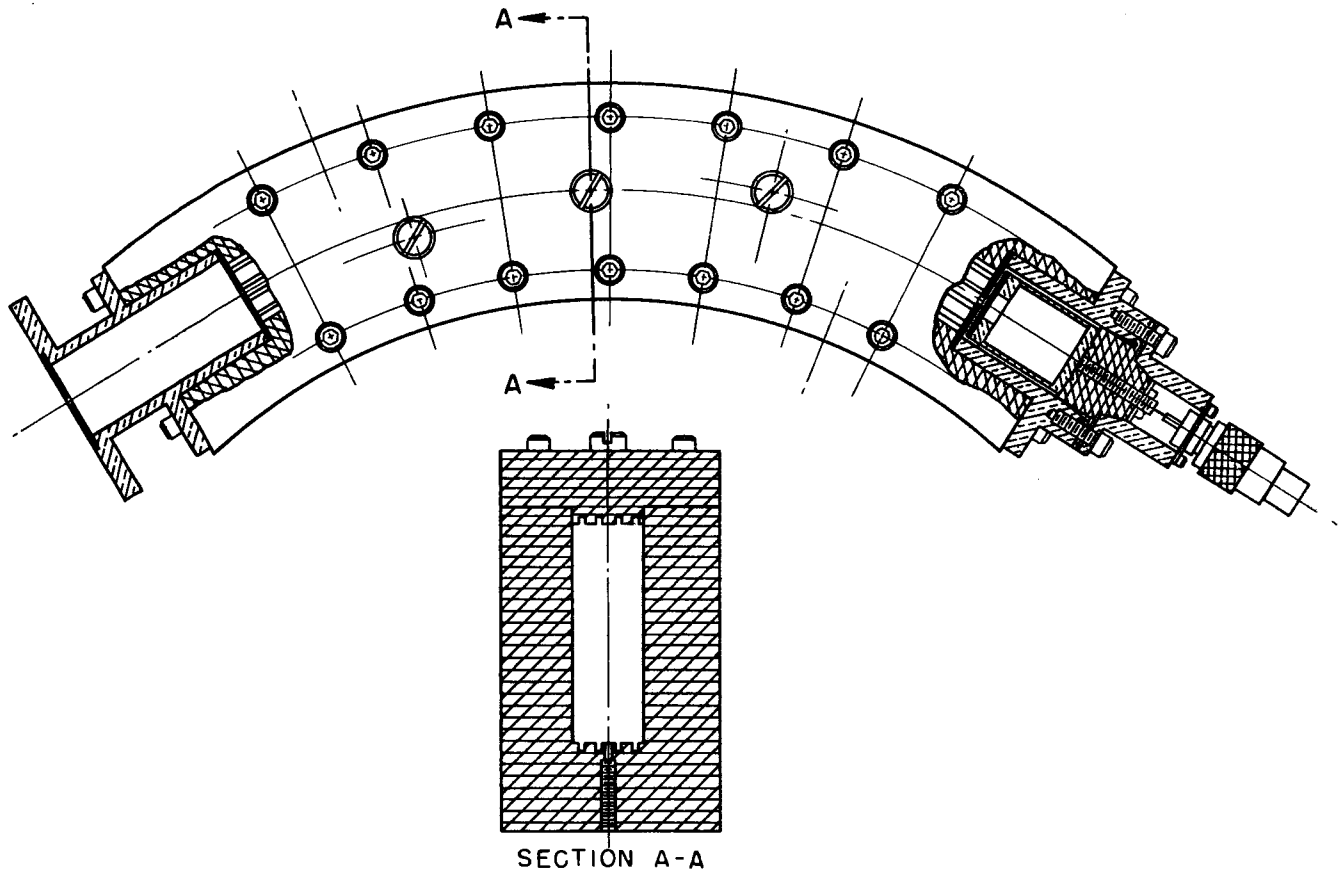

FIG. 4-CROSS SECTIONAL VIEWS OF ELECTROSTATIC ANALYZER AND FARADAY CAGE COLLECTOR

required to select electrons of 100 ev energy. The voltage across the plates is supplied by a battery, the upper and lower plates being at equal potentials above and below the potential of the entrance slits to the analyzer. The center guard electrodes are at the entrance slit potential and the other two pair are at potentials half way between this and that of the analyzer plates. The energy resolution of the electrostatic analyzer is about 1% at an energy of 100 ev, corresponding to an energy width of 1 ev at half maximum of the peak in the distribution curve.

The electrostatic analyzer gives the energy distribution directly, whereas in many of the experiments described in the literature the energy distribution was obtained by differentiating an integral distribution or by density and photometer measurements of a photographic plate, processes which are subject to considerable error.

Auxiliary Equipment

The source of electrons is an electron gun employing both electrostatic focussing and deflection from a 5BP1 cathode ray tube. To prevent deactivation of the cathode, the tube envelope is broken in an atmosphere of nitrogen, helium or argon in a dry box. The electron gun is transported in a plastic bag to the accelerator which has previously been flushed with one of the three gases mentioned.

The system is evacuated to a pressure between 5×10^{-6}

and 1 x 10^{-5} mm Hg using a Welch Duo-Seal forepump and a Distillation Products Industries VMF-260R oil diffusion pump. The pressure is measured with a Consolidated Vacuum Corporation VG-1A ionization gauge. A National Research Corporation Model 501 thermocouple gauge is used to indicate pressures above the range of the ionization gauge. A pressure interlock in the thermocouple gauge control circuit turns the diffusion pump off if the pressure gets too high. A valve between the diffusion pump and the rest of the system permits the system to be brought to atmospheric pressure without having to turn off the diffusion pump and allow it to cool.

As a power supply for the electron gun, at first an Atomic Instrument Company Model 316 power supply was used with the circuit given in the RCA Tube Handbook HB-3, Vol. 1-2, for a 5BP1-A cathode ray tube, a modification of the 5BP1. In this circuit the potentials of the gun elements were established by voltage dividing resistors. However, the current to the gun elements was a sufficiently large fraction of that in the voltage divider that when the voltage of one element, and hence the current to it, was altered, the potentials of the other elements were changed. This circuit was therefore replaced by the one shown in Fig. 5, in which the load is large enough, about 10 ma, so that changes in the potential of one gun element do not alter the potentials of the other elements. This circuit was designed and built by J. L. Blankenship. The voltage dividing resistors of the former circuit have been replaced by the voltage regulator tubes shown, which give

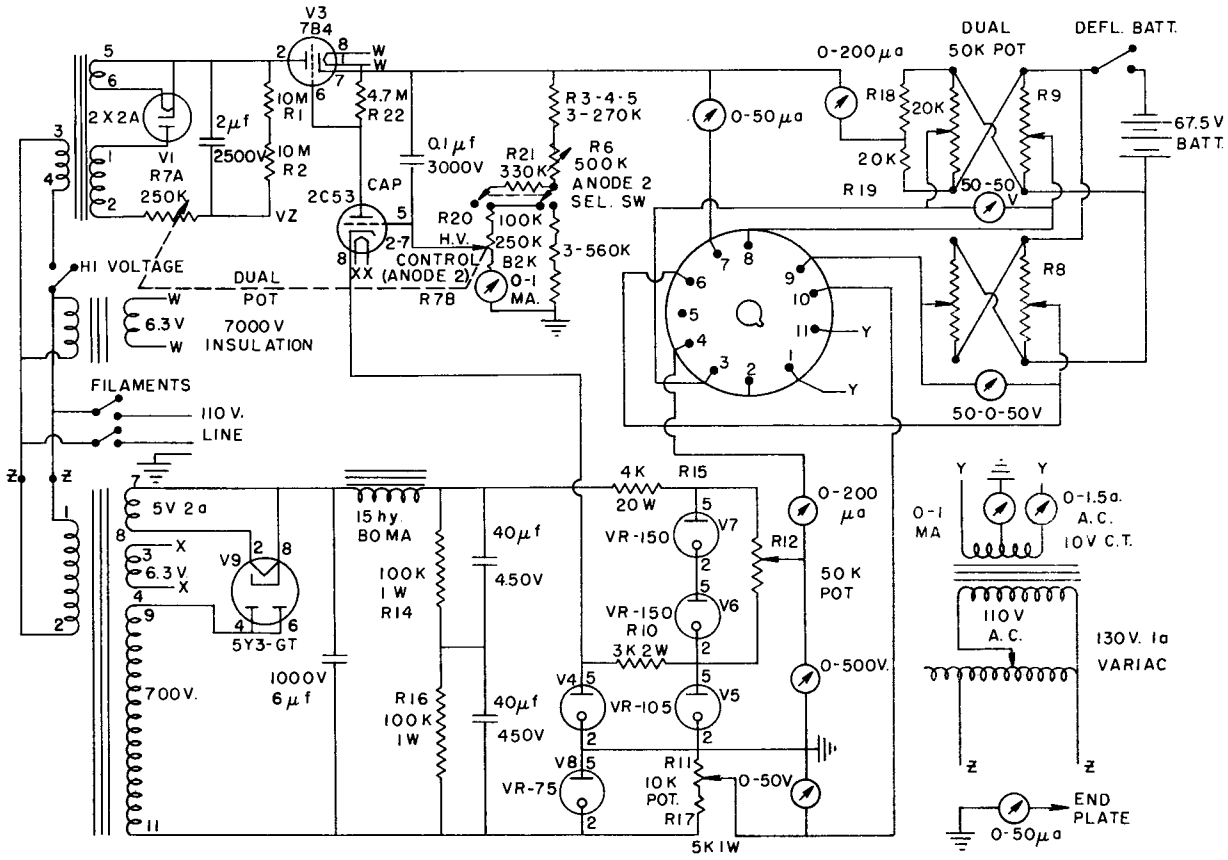

FIG. 5- ELECTRON GUN POWER SUPPLY

adequate regulation of the voltages supplied to the first anode, pin 4, and the control grid, pin 10. The grid voltage is variable from 0 to -50v and the first anode voltage from 150 to 450 volts. The series regulated high voltage supply provides a stabilized voltage, variable from 500 to 2500 volts, for the second anode, pin 7. The second anode potential is normally 1500 v. Dual potentiometers permit the potentials of each member of the two pairs of deflecting plates to be varied equally above and below the second anode potential. Pins 3 and 8 are connected to one pair of deflecting plates and pins 6 and 9 the other. Pins 1 and 11 are connected to the heater and pin 11 also to the cathode. Meters have been installed so that the voltages of and currents to all gun elements can be monitored. The electron beam is aimed by varying the potentials of the deflecting plates of the gun. It can also be aimed by tilting the gun by means of two horizontal and two vertical adjusting screws.

The high voltage is supplied by a Westinghouse 250 kv X-ray power supply. This supply is center grounded so that only the negative 125 kv can be used with the accelerator and decelerator, both ends of which are at high negative potential with the center grounded. An oil immersed switch designed by Dr. H. H. Hubbell, Mr. R. F. King, and Mr. R. W. Bennett permits either the accelerator or an X-ray tube to be operated from the same power supply. Separate controls, designed by Drs. Hubbell and M. Slater, permit the high voltage supply to be operated from the accelerator

control panel. The voltmeter which measures the high voltage is accurate to within 2%.

Horizontal and vertical coils, designed to neutralize the earth's magnetic field are used, in addition to the electron gun deflecting plates, to aim the electron beam.

The δ' voltage is supplied by batteries and is variable from 0 to 600 v. The voltage is measured with a voltmeter consisting of a Weston Model 861 D.C. microammeter with series resistors giving full scale ranges of 2, 6, 20, 60, 200, and 600 volts which are selected by a switch. The voltmeter was calibrated against Rubicon potentiometers Nos. 2730 and 2732. The δ' voltage can be accurately set on each range anywhere between 0 and the maximum value by means of a ten turn 100 K ohm Helipot potentiometer. This voltage is scanned by means of a continuous 50 K ohm model LS Helipot potentiometer driven by a one rpm type KYC-22 Bodine motor to cover the energy range to be investigated.

The δ voltage is supplied by a model A3A Oregon Electric Manufacturing Company regulated power supply, the output of which is variable from -300 to + 400 volts. This voltage is usually set at a value slightly less than 100 volts, which corresponds to the energy the electrostatic analyzer is set to select, so that the peak in collector current due to electrons which have lost no energy in passing through a foil will be separated slightly from the beginning of the scanning cycle.

The collector current is measured by an electrometer and is plotted directly as a function of the energy lost, measured by δ', by means of a Brown recorder, range 0 - 10 mv, driven by the electrometer. Two different electrometers were used. The first was an RCA WV-84A D.C. microammeter, a schematic diagram of which is shown in Fig. 6. The circuit is essentially a battery operated D.C. vacuum tube microammeter. Batteries E3 and E4 are arranged with tubes V1 and V2 to form a bridge circuit. The zero adjust control acts to balance the bridge, zero potential existing across the meter M1 when balance is obtained. The potential drop across the shunt, R1 to R6 selected by the range switch, is applied to the grid of V1 and changes the resistance of the tube in a direction which depends on the direction of the applied current. This change unbalances the bridge and causes a current through the meter. The current through the input terminals required to give full-scale deflection is dependent on the resistance of the shunt. The voltage drop for full scale deflection is 0.5 volt for all ranges. There are six ranges of 0.01, 0.1, 1, 10, 100 and 1000 microamperes full scale. However, in this application the shunt resistors for the 100 and 1000 scales were replaced by 500 and 5000 megohm resistors, giving ranges of 10^{-9} and 10^{-10} amperes full scale, respectively.

The RCA microammeter was replaced by a model Q-826-B ORNL Instrument Department electrometer, a circuit diagram of which is shown in Fig. 7. This instrument is described by Glass (1952).

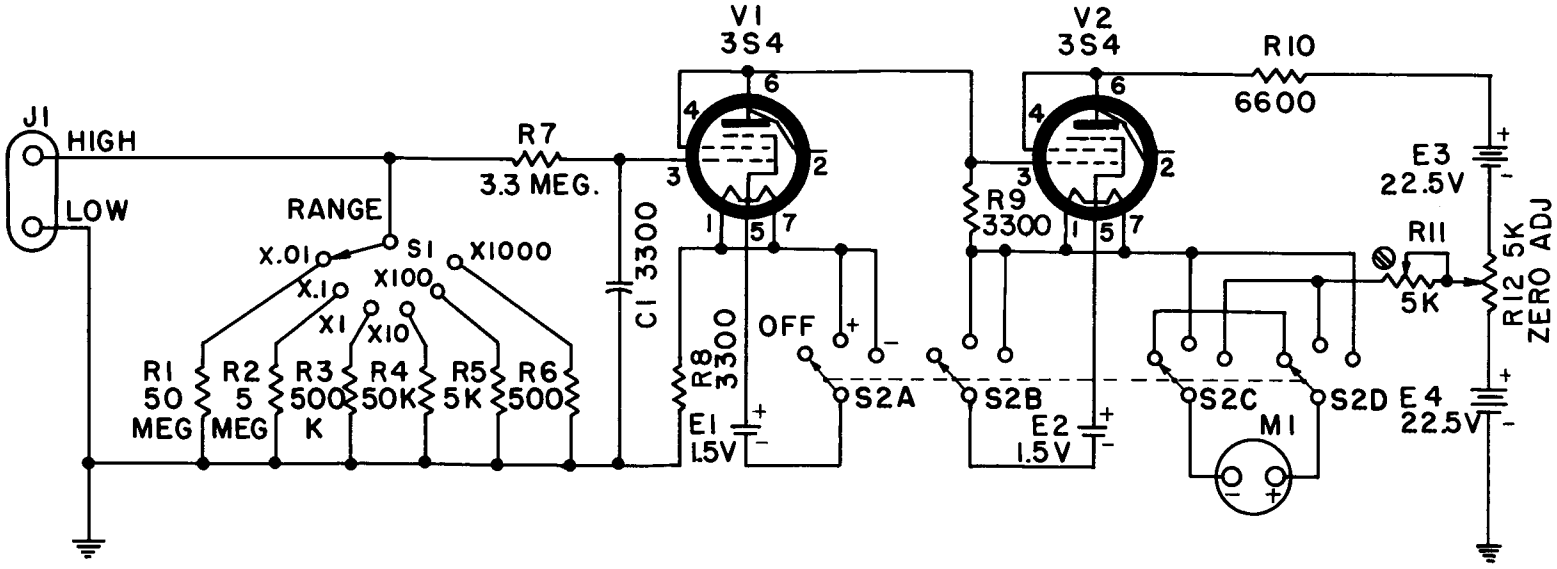

FIG. 6-SCHEMATIC DIAGRAM OF RCA WV-84A MICROAMMETER

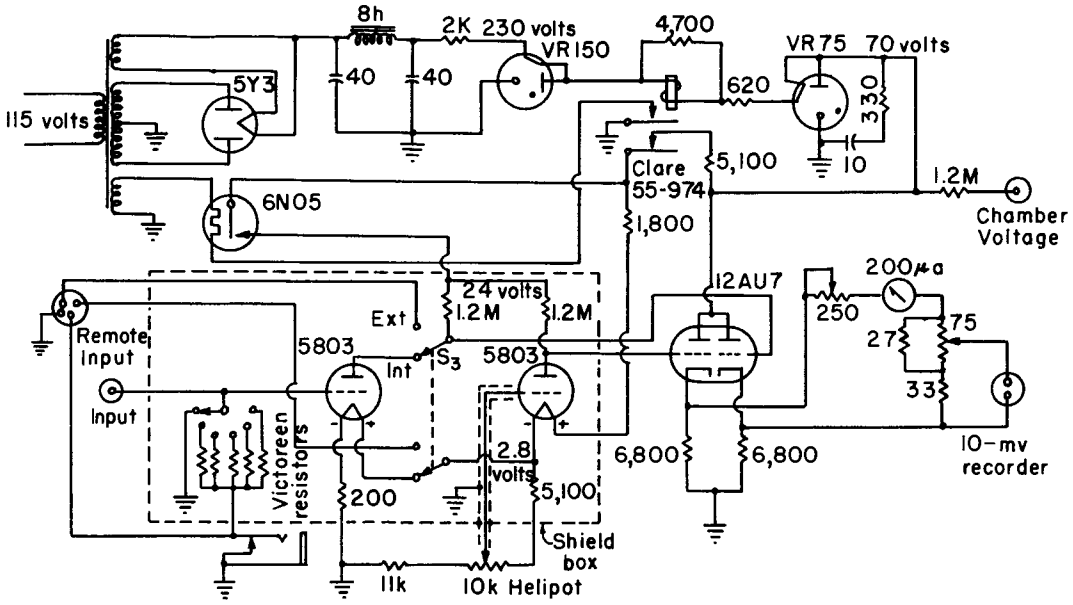

FIG. 7-CIRCUIT OF THE MODEL Q-826-B ELECTROMETER

Compensation for drift within the electrometer tube has been accomplished by the placement of a second electrometer tube in the opposite leg of the bridge. The 5803, a sub-miniature Victoreen tube, is used because of availability, high leakage resistance (10^{14} ohms), low microphonics and low grid current. Since the filament current is only 10 ma, the regulated plate supply is used for filament power. If the two tubes are aged for 72 hours and then carefully matched as to plate current for given grid and plate voltages, they will drift in the same direction at approximately the same rate, thus providing good drift compensation. Since less than 15 ma is required to supply both filaments and plates, sufficient regulation was obtained by cascading a VR-150 and a VR-75 tube. The degree of regulation required for the two circuits is less than that required for a single-tube circuit. However, additional compensation was added by making the bias voltage a function of both filament and plate voltages. As a result of these two features a 20% change in line voltage gives no change in the meter reading. The two relays shown prevent the plate voltage from being applied to the two electrometer tubes until after the cathode reaches operating temperature. The 5803 is used here as a voltage amplifier, directly coupled to a cathode follower. By dividing the current gain between the electrometer tube and the cathode follower, optimum operating conditions for low grid current, good linearity and long tube life can be realized. For good stability, the 12AU7 must be aged

and the two halves matched. In the instrument used a high impedance range switch using fluorothene as an insulator was installed. Resistances of 10^7, 10^8, 10^9, 10^{10}, and 10^{11} ohms were used. Since the full scale voltage is 0.25 volts, these give ranges of 2.5×10^{-8}, 2.5×10^{-9}, 2.5×10^{-10}, 2.5×10^{-11} and 2.5×10^{-12} amperes full scale. Grid resistors larger than 10^{12} ohms should not be used since the grid current is then not small compared with the full scale current. With the 10^{11} ohm resistor, the RC time constant of the input circuit is about 1 second.

In operation the electron gun, the initial end of the accelerator, the final end of the decelerator, the electrostatic analyzer and the collector are all at high negative potential. Hence all equipment connected to these, which includes the electron gun power supply, the δ' supply, the scanning circuit, the δ supply, the analyzer voltage supply, the electrometer and the Brown recorder, must be at high voltage also. Therefore all this equipment is mounted on two insulated tables. One hundred ten volts A.C. is supplied to the equipment which requires it through oil immersed insulating transformers. Two such transformers are cascaded at each table. The primary and case of the first transformer is at ground potential, its secondary and the primary and case of the second is at half the high voltage, and the secondary of the second transformer, which is connected to the table, is at the full high voltage. The potentials are established by voltage dividing resistors. The accelerator and

the two tables with the auxiliary equipment at high voltage are all enclosed by a screen wire cage. Insulating rods attached to the equipment at high voltage permit this equipment to be operated from outside the cage. The thermocouple and ionization gauge controls, the power supply for the neutralizing coils and the accelerator high voltage controls, which are all at ground potential, are mounted in a relay rack which is located at a gap in the cage. The cage has a door and a grounding hook. When the high voltage is off, the grounding hook is hung from a copper tube housing the leads to the initial end of the accelerator. When the high voltage is on, this copper tube is at high voltage. Interlocks require that the grounding hook be suspended from another hook just inside the cage door, that the door be closed, and that the powerstat controlling the high voltage be turned all the way down before the high voltage can be turned on. When the door is opened, the high voltage is turned off, if this has not been done previously. An overload relay causes the high voltage to be turned off when excess current is drawn due to an arc or some other cause. Figure 8 is a photograph showing the cage, the accelerator and the backs of the control panel and auxiliary equipment on the two tables.

Foils

The metal foils were evaporated onto Zapon or Formvar backings. A Zapon backing was prepared by dropping one drop of

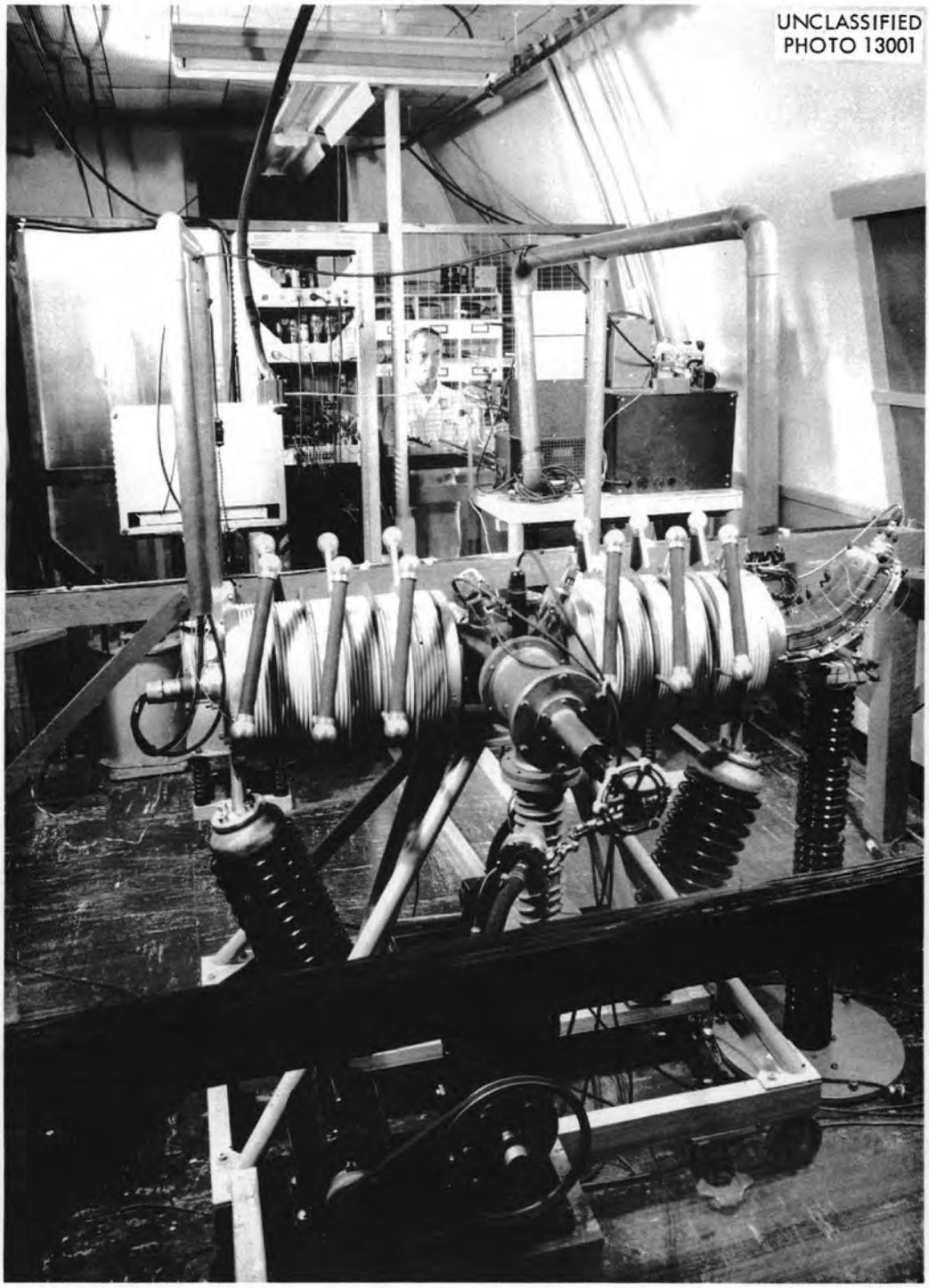

Fig. 8. Photograph of Apparatus.

a solution of Zapon Aquanite "A" in Zaponite Thinner No. 5 on water and picking up the resulting film by raising in a vertical position a thin rectangular piece of aluminum with a 1-5/8 in. circular hole in it. The film was then transferred to a rectangular piece, about 1-3/8 in. by 7/8 in., of 0.010 in. stainless steel or 0.016 in. aluminum sheet with a 5/8 in. circular hole in it. Solutions of one part Zapon in five parts thinner were usually used. The Formvar films were prepared in the same manner using a solution of one gram of Formvar 15/95E in 100 cc, or equivalent proportions, of ethylene chloride or 1,4 dioxane or p-dioxane. Zapon films could be made thinner and more uniform than Formvar films. However, Formvar films were stronger than Zapon films of the same thickness. According to Chen (1950) Formvar films are about seven times as strong as Zapon films. Magnesium foils on Zapon backings ruptured very easily, whereas they were much sturdier on Formvar backings. However, aluminum and silver foils on Zapon backings were quite durable. Copper foils on Formvar backings were stronger than those on Zapon backings. Zapon films as thin as $8\mu g/cm^2$ and Formvar films as thin as $12\mu g/cm^2$ were used as backings.

Prior to July, 1954, the foils were evaporated by the ORNL Instrument Division. Since that time the evaporation has been done in an evaporator set up by G. R. Harrison in the Health Physics Division. This evaporator consists of a bell jar resting on a brass plate, a rubber gasket coated with vacuum grease making a vacuum seal between the two. Teflon washers provide insulation

and a vacuum seal between the brass plate and the two filament electrodes passing through the plate. The bell jar is evacuated to a pressure of 1×10^{-4} mm Hg or less by two Distillation Products Industries MC 500 oil diffusion pumps in parallel feeding into a Kinney forepump. The filament is then heated until the metal evaporates. Tungsten wire is used as a filament for aluminum, gold and magnesium and a tantalum "boat" for copper, silver, tin and indium. Fifteen foils are usually evaporated at once. The amount of metal evaporated is determined by weighing the filament before and after the evaporation.

As soon as the metal foils are removed from the evaporator they are placed in a desiccator, which is immediately evacuated. The foils are kept in a vacuum until they are introduced into the accelerator. The foil is then mounted on the end of an aluminum rod 18 in. long and 0.95 in. in diameter. A vacuum lock permits the foils to be introduced into the accelerator without opening the system to the air.

After measurements on a foil have been completed, it is removed from the accelerator through the vacuum lock and placed again in the desiccator which is evacuated. The foils are kept in the evacuated desiccator until ready for weighing. The metal and backing within the 5/8 in. circle is cut away from the foil holder and weighed on a quartz fiber Precision Torque Balance manufactured by Vereenigde Draadfabrieken, Nijmegen, Holland. Although the smallest scale division on the balance is 10 μg, the weights of the foils can be estimated to the nearest μg using a telescope

focussed on the scale. Each foil is weighed at least three times and the average of the values taken. There was no consistent increase in the successive weights, indicating moisture was not adsorbed during the weighing. Several blank Zapon or Formvar films which were prepared at the same time as those on which the metal was evaporated are also weighed. The weight of the backing is subtracted from the weight of the metal plus the backing to give the weight of the metal. The thickness of the metal foils in $\mu g/cm^2$ is obtained by dividing the weight by the known area.

Attempts were made to remove Zapon backings from aluminum foils by dissolving the Zapon in Zaponite thinner, but the metal foils always ruptured. However, since no energy losses were observed in Zapon or Formvar films in the energy range in which the discrete losses were observed in the metals, it was not considered necessary to remove the backings.

The thickness in $\mu g/cm^2$ of the metal foil was also calculated using the inverse square law, assuming isotropic evaporation, from the relation $t = \frac{mh}{4\pi r^3}$ where m is the mass of the metal evaporated, h is the perpendicular distance between the source of evaporation and the plane of the foil, and r is the distance from the source to the foil. When a "boat" is used as a filament 2π instead of 4π geometry is assumed. Agreement between the thickness values determined by the two methods will be discussed later.

Development of the Instrument

An account of the development of the instrument, including improvements made since the writer began working with it and some difficulties encountered, is appropriate here. The design, construction and assembly of the accelerating and decelerating tubes, insulators and supporting frame were carried out by Dr. H. E. Banta, Mr. R. W. Bennett and Mr. R. F. King of the High Voltage Group at ORNL. The instrument was leak tested and made vacuum tight by Dr. R. D. Birkhoff and Mr. A. W. Smith of the Health Physics Division; Mr. J. Bergstein made preliminary measurements on the performance of the instrument. Brief descriptions of the instrument were given by Bergstein and Birkhoff (1953) and Blackstock, Birkhoff and Slater (1954).

The cage had just been built around the instrument when the writer began work on it. The first task was to rewire the auxiliary equipment in a permanent manner.

At this time a tungsten filament electron gun served as the source of electrons. The filament was bent in the shape of a V, the point of which was ground flat. The filament fitted into a small hole in the center of a disk so that the flat part was flush with the surface of the disk. The accelerating anode was another disk, with a 3/32 in. hole in the center, separated from the first disk by a distance variable between 0.040 and 0.300 inches. The potential of the accelerating anode could be varied from 0 to 600 v.

At that time the current collector consisted of a large steel cylinder with a steel plate on the end. It was necessary to make the collector 20 volts or more positive with respect to the end of the decelerator to suppress secondary electrons produced in the collector. The current had been measured by a galvanometer, but this was replaced by the RCA microammeter, which has greater sensitivity.

The plate on the end of the current collector could be replaced by a fluorescent screen consisting of a lucite plate on which zinc sulphide had been deposited. A fluorescent screen which could be rotated in and out of the beam could also be placed at the center of the instrument in the foil position and viewed through a lucite plate on the side of the instrument. The effects on the spots produced by the electron beam at these two positions caused by varying separately several parameters were observed. These parameters were the current in the coil designed to neutralize the vertical component of the earth's magnetic field, the gun filament current, the focussing anode voltage, the secondary electron suppressor voltage, the high voltage and the δ voltage. The spot at the collector became badly defocussed at δ voltages less than 50 volts. A coil forming a thin magnetic lens was designed to improve the focussing at low δ voltages, but did not improve it significantly. A coil to neutralize the horizontal component of the earth's magnetic field was added and proved useful in aiming the beam.

A considerable number of measurements of the operating

characteristics with no foil in the instrument were taken. At that time the δ voltage was varied manually in small steps and the collector current recorded at each step. A graph of the data yielded an integral distribution of the collector current as a function of δ voltage. With no foil, the collector current should rise sharply to a maximum in the vicinity of $\delta = 0$ and remain at this value as δ increases. The differential distribution, obtained by differentiating the integral curve, should exhibit a sharp peak at $\delta = 0$. Instead a δ of 40 volts or more was required to obtain maximum current, resulting in a relatively broad peak in the differential curve. The parameters mentioned in the previous paragraph were varied to see if the resolution could be improved. In addition, various geometries of apertures and grids of different mesh sizes were tried at the entrance to the collector to attempt to better define an equipotential plane at the barrier or δ potential. However, none of these methods improved the resolution.

An attempt was made to use a time varying δ produced by an oscillator to sweep the δ and observe the collector current signal on an oscilloscope. This proved unsuccessful due to stray pickup which could not be eliminated and was replaced by the method previously described of sweeping the δ and recording the current with a Brown recorder.

The defocussing of the electron beam was eliminated by adding the electrostatic analyzer and not allowing the electrons to

have energies below 100 ev. In addition the electrostatic analyzer yields the differentiated collector current distribution directly, from which the resolution can be obtained immediately. No secondary electron suppressor voltage was necessary with the Faraday cage current collector used with the electrostatic analyzer. This collector replaced the large steel collector. But still the resolution was improved little. By means of a fluorescent screen the beam after passing through the analyzer was observed.

With an oscilloscope a test was made for a phase shift in the voltage between the initial end of the accelerator and the final end of the decelerator, but none was found. With an oscilloscope a test was made for any high frequency oscillations in the energy of the electrons which might cause an energy spread in the beam or a phase difference in the potentials of the initial end of the accelerator and the final end of the decelerator. None were found. Additional filtering was added in the two neutralizing coil supplies, the focussing anode supply and the high voltage supply, but the resolution was not improved.

An electrometer more sensitive than the RCA microammeter was installed but did not operate satisfactorily probably because of too low leakage resistances and too high stray capacitances. However, the ORNL Instrument Department Q-826-B electrometer was installed later and works quite well on all ranges except the most sensitive, 2.5×10^{-12} amperes full scale.

The poor resolution might have been due, in part at least,

to an energy spread in the electrons leaving the gun. The replacement of the tungsten filament gun with an electrostatic electron gun from a cathode ray tube was decided upon as a means of trying to reduce the energy spread in the beam. The cathodes of these guns, however, are deactivated when exposed to air. Attempts were made to replace the cathode in one of these guns with a tungsten filament, which proved to be a very tedious task. Although several filaments were installed, it was impossible to measure any current at the collector from any of them, probably because the filaments were not properly aligned with the axis of the gun or not properly spaced from the grid.

The envelopes of cathode ray tubes were broken in an atmosphere of an inert gas as has been described. This method proved successful and was adopted. War surplus 5BP1 electron guns are used since they are available at no cost. Many of the guns have sufficient emission for only a week, but several have lasted much longer.

Although the resolution was improved by the use of the cathode-ray tube guns, not until the double slit was inserted at the entrance to the electrostatic analyzer was the present resolution attained.

Insulating coatings have been found deposited on the central baffle, the analyzer entrance slits, the collector entrance slit and the accelerating electrodes. These coatings probably result from diffusion pump oil vapor since there is no trap between the diffusion pump and the remainder of the system. The coatings

evidently become charged and deflect the beam so that it does not reach the collector. This seems to be true for the accelerating electrode coatings even though the inside diameter of the electrodes is 5 in., much larger than the beam diameter. These coatings must be removed at intervals with emery cloth.

Difficulties were also encountered in weighing the foils. These were overcome by using a vacuum desiccator to keep moisture from collecting on the foils.

As these improvements were made, the data also improved. Several thousand graphs of collector current versus energy loss were taken in order to obtain enough good data.

IV. TEXT OF STUDY

Energy Distributions

The energy distribution of electrons with an incident energy of 45 kev after passing through a 15 $\mu g/cm^2$ aluminum foil is shown in Fig. 9. The peak to the right represents electrons which have lost no more than one ev of energy and will be referred to as the "no loss peak." The next peak corresponds to a group of electrons which have lost 14.2 ev of energy. The higher losses are very nearly integral multiples of the smallest one.

The energy distribution of electrons with 100 kev incident energy after passing through the same foil is shown in Fig. 10. Figure 11 shows the energy spectrum resulting when 45 kev electrons pass through a thinner aluminum foil. The thickness of this foil is not known very accurately, since at the time the data were taken no balance of sufficient sensitivity to weigh the foil accurately was available. However, from an estimate of the thickness made on the basis of the inverse square law assuming isotropic distribution in evaporation of the foil, it is definitely thought to be thinner than the first foil, perhaps about 5 $\mu g/cm^2$.

Figure 12 shows the energy spectrum resulting when 30 kev electrons pass through a 72 $\mu g/cm^2$ magnesium foil. The energy distribution resulting when 115 kev electrons pass through the same foil is shown in Fig. 13. In both figures the larger losses are seen to be very nearly integral multiples of the first.

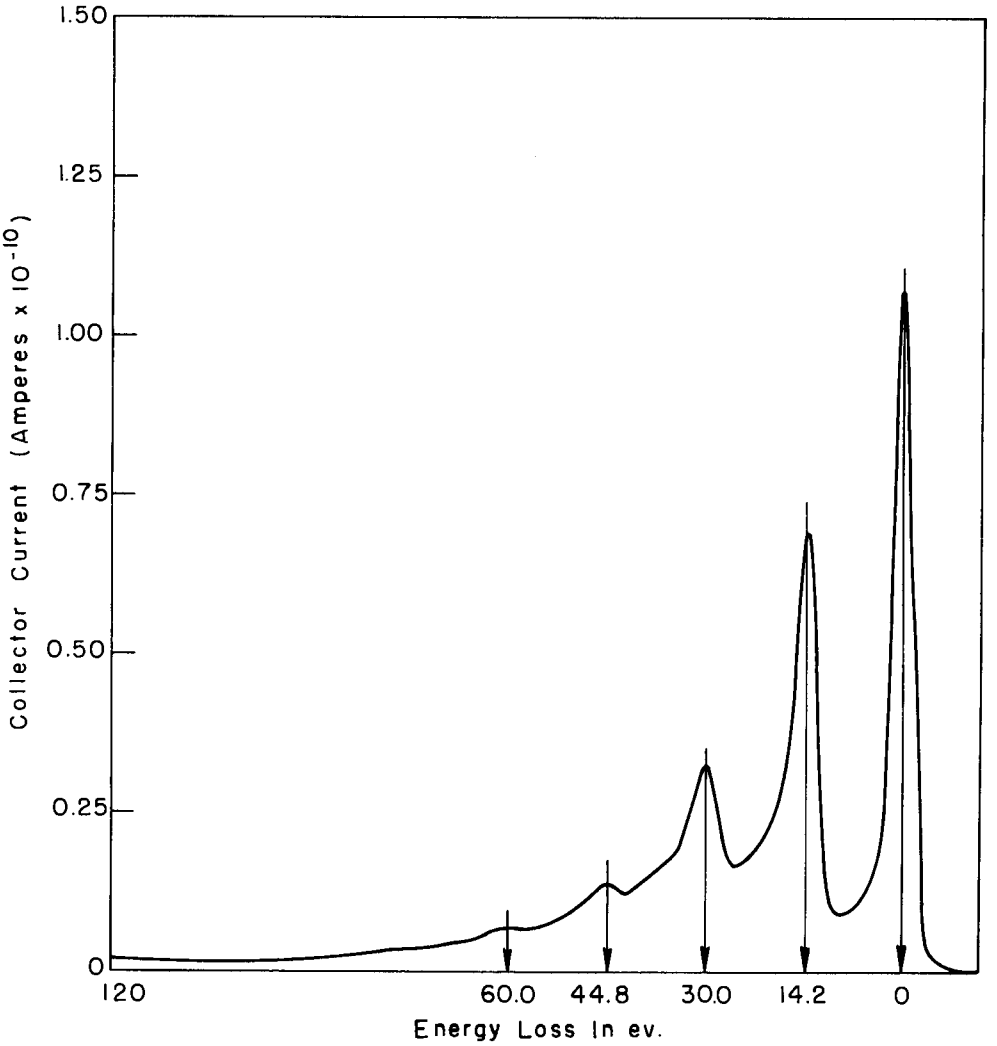

FIG. 9 - ENERGY DISTRIBUTION FROM
15 $\mu g/cm^2$ ALUMINUM FOIL
INCIDENT ELECTRON ENERGY 45 Kev.

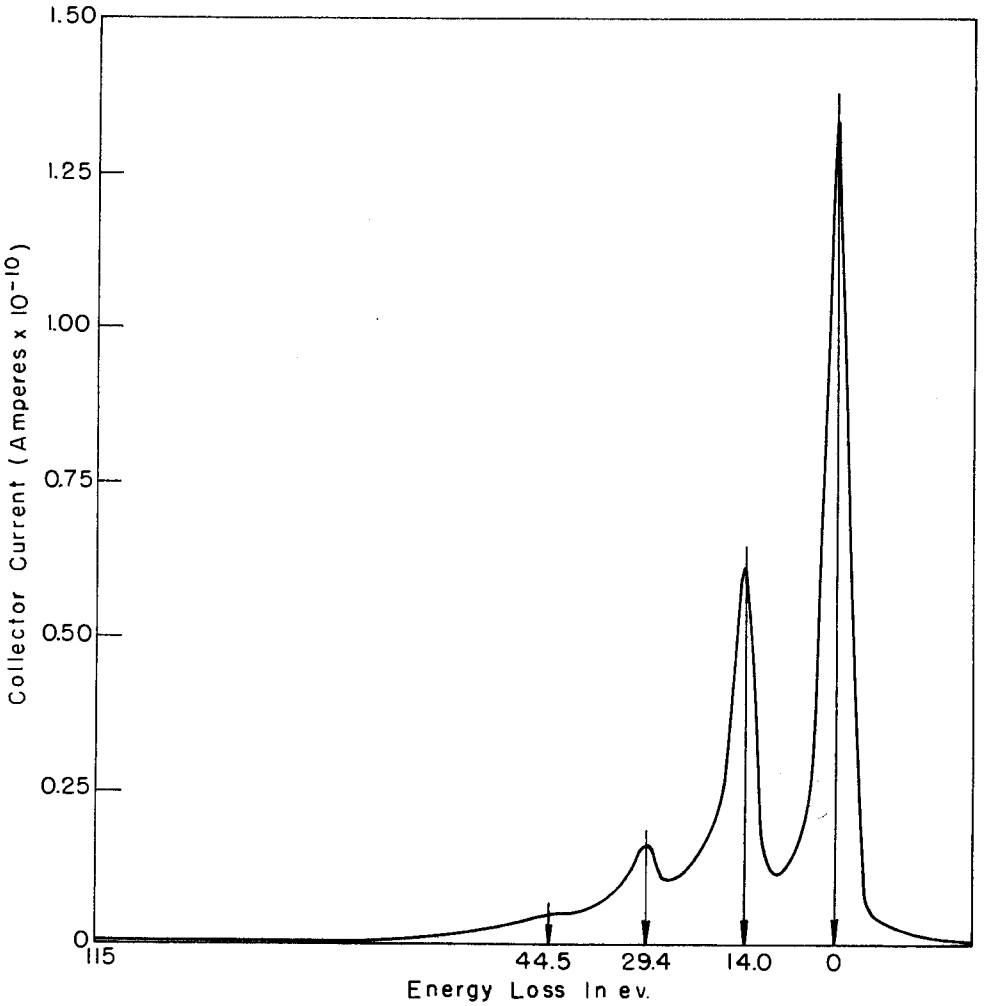

FIG. 10 - ENERGY DISTRIBUTION FROM
15 $\mu g/cm^2$ ALUMINUM FOIL
INCIDENT ELECTRON ENERGY 100 Kev.

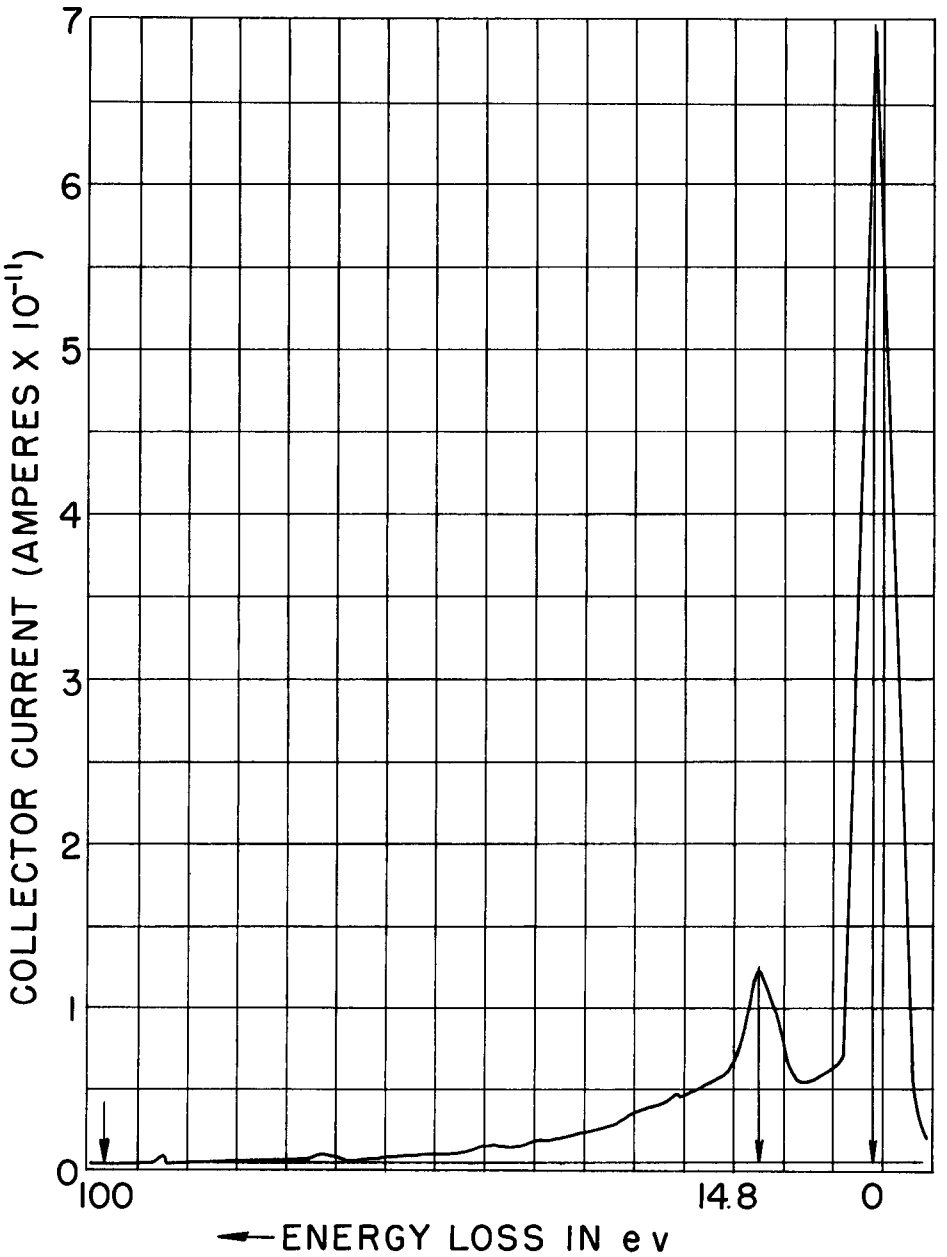

Fig. 11 - Electron Energy Distribution from an Aluminum Foil. Incident Electron Energy 45 Kev.

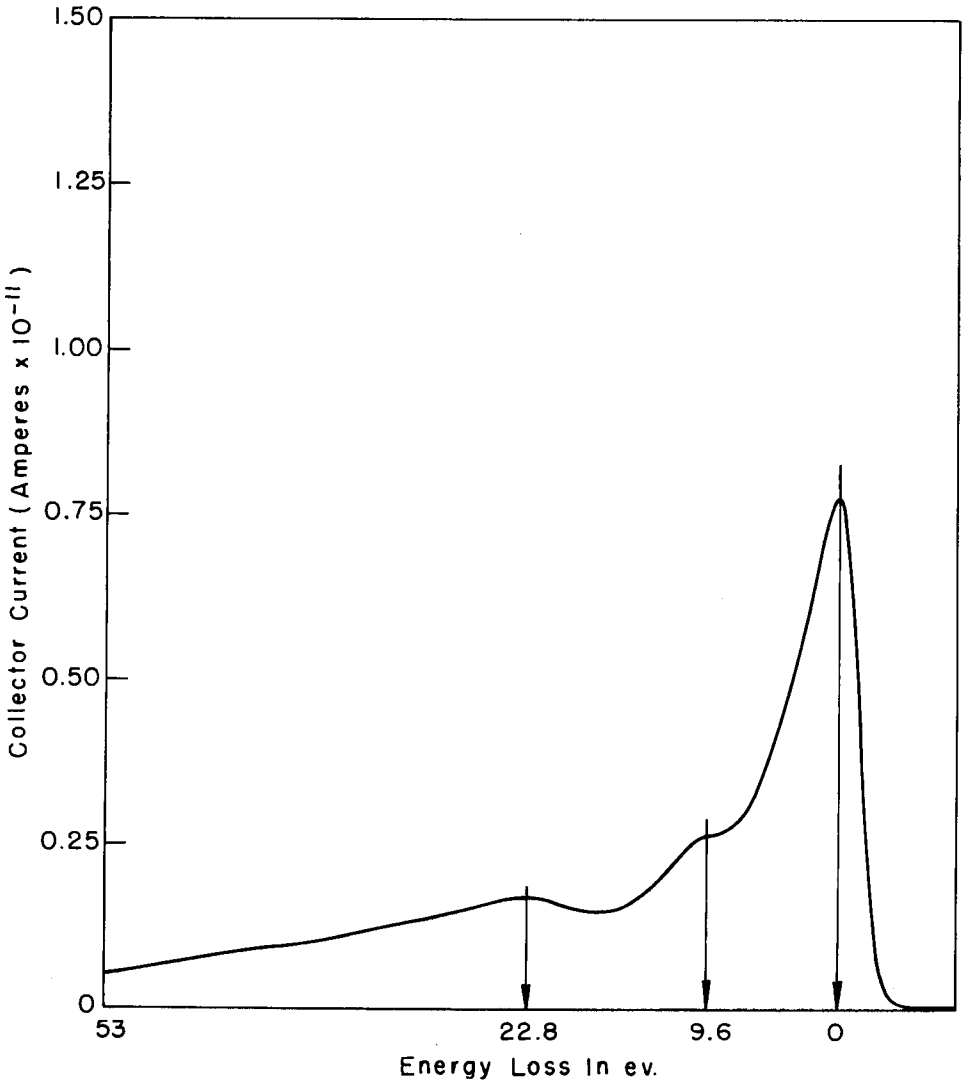

FIG. 12-ENERGY DISTRIBUTION FROM
72 $\mu g/cm^2$ MAGNESIUM FOIL
INCIDENT ELECTRON ENERGY 30 Kev.

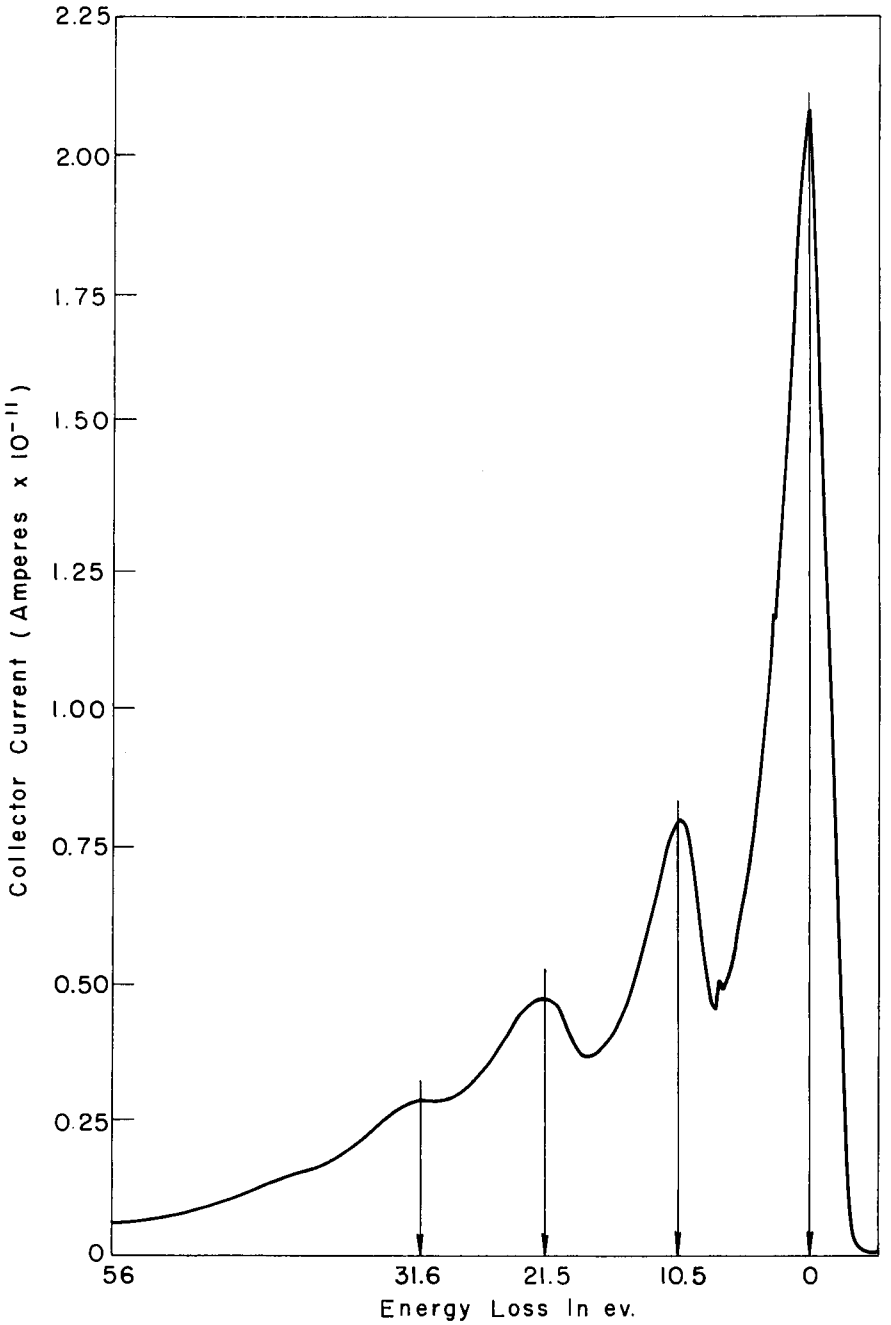

FIG.13-ENERGY DISTRIBUTION FROM
72 $\mu g/cm^2$ MAGNESIUM FOIL
INCIDENT ELECTRON ENERGY 115 Kev.

The energy distribution resulting when 45 kev electrons pass through a 66 $\mu g/cm^2$ copper foil is shown in Fig. 14. Figure 15 shows the energy distribution from the same foil resulting from electrons incident with 115 kev energy. In copper only one loss is observed.

Figure 16 shows the energy distribution from 45 kev electrons passing through a silver foil. Only one loss is observed in silver. The thickness of this foil is not accurately known but from a determination of its weight and from the inverse square law, it is thought to be between 10 and 20 $\mu g/cm^2$.

Discrete Energy Losses

The discrete energy losses found in the four metals are listed in Table 1. The mean values of the difference between successive losses in Al and Mg and the mean values of the single losses in Cu and Ag are listed in the column headed "Quantum Loss." The number in parentheses after each energy loss is the number of measurements of that loss.

Table 1
DISCRETE ENERGY LOSSES

Metal	Energy Losses (ev)				Quantum Loss (ev)
Al	14.8 (74)	30.0 (59)	44.2 (31)	59.8 (10)	14.87 ± 0.04 (174)
Mg	10.5 (44)	21.5 (44)	31.6 (9)		10.60 ± 0.03 (97)
Cu		22.6 (93)			22.6 ± 0.1 (93)
Ag		23.8 (8)			23.8 ± 0.2 (8)

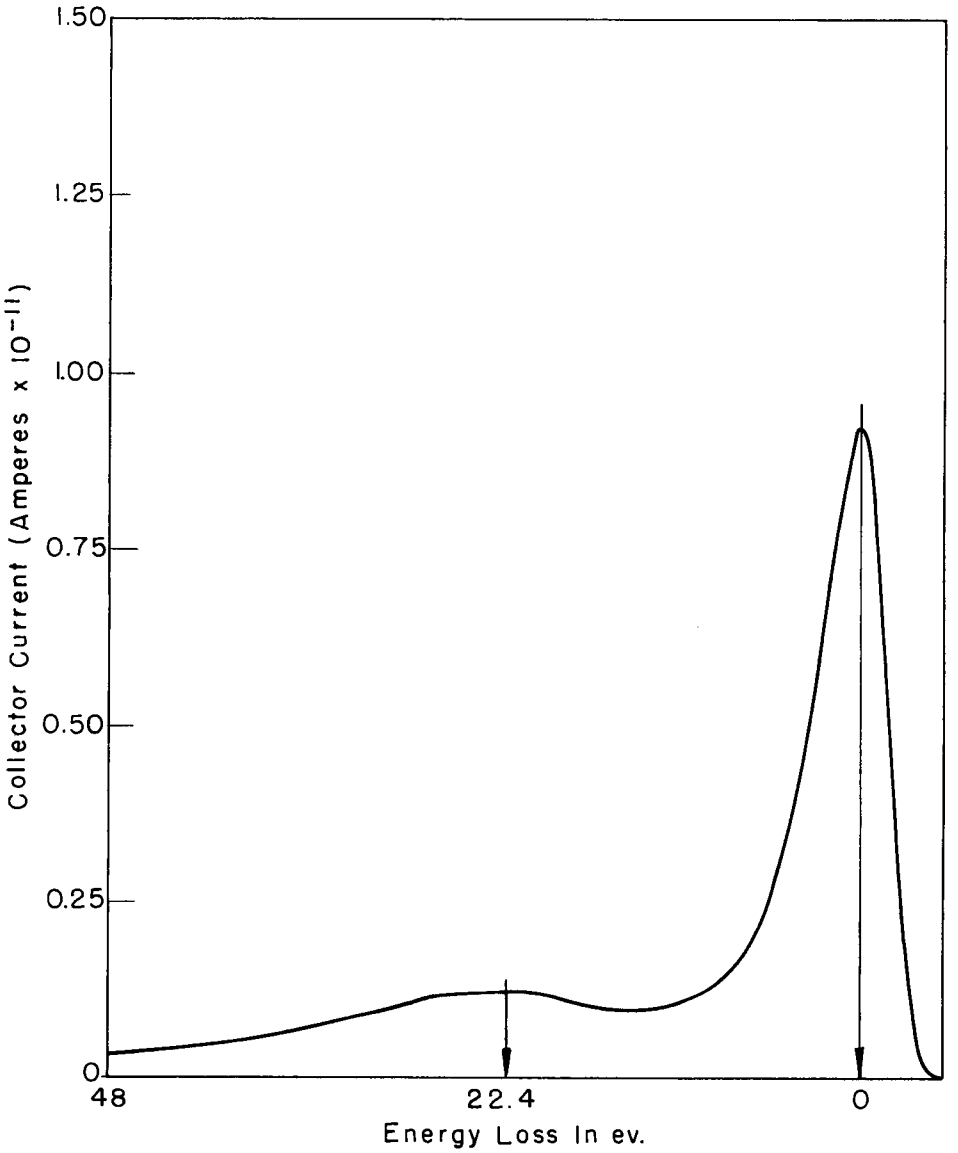

FIG. 14-ENERGY DISTRIBUTION FROM
66 $\mu g/cm^2$ COPPER FOIL
INCIDENT ELECTRON ENERGY 45 Kev.

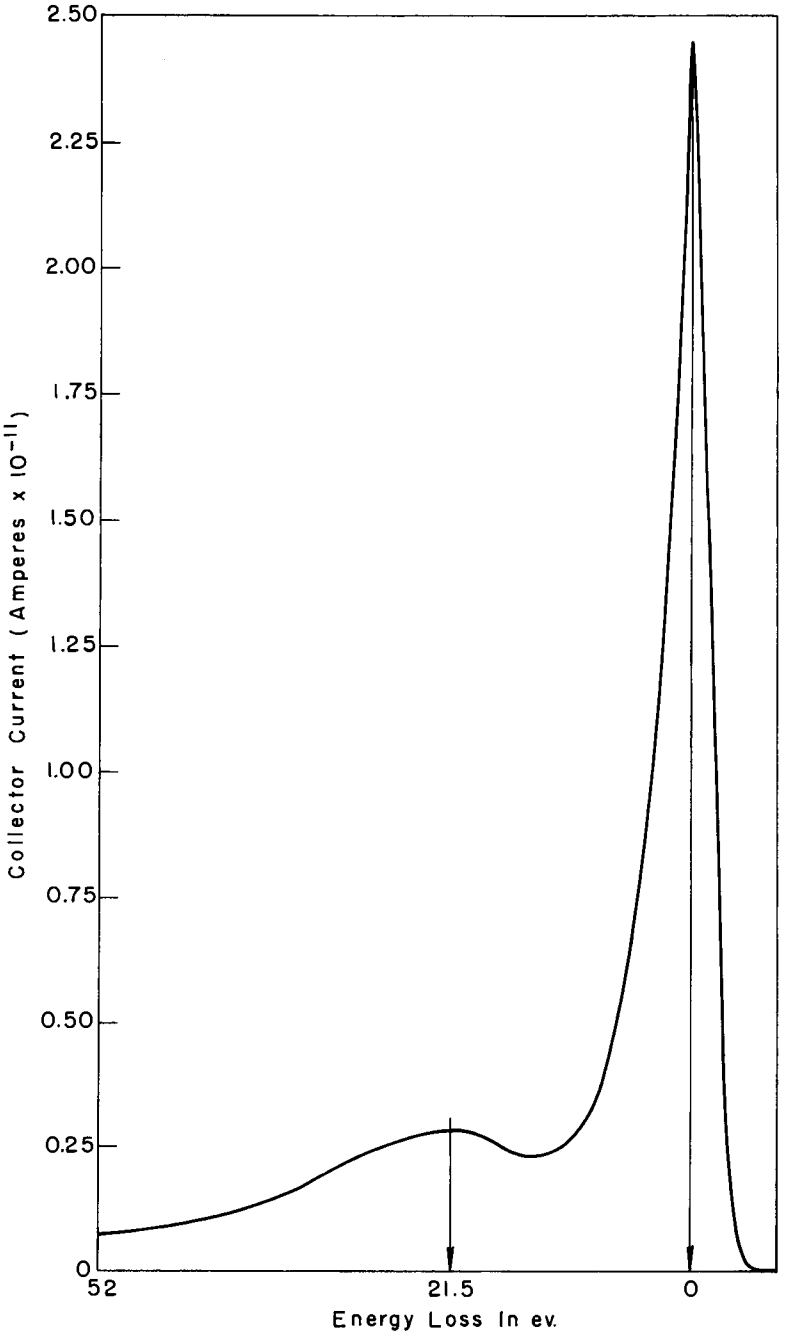

FIG. 15-ENERGY DISTRIBUTION FROM
66 $\mu g/cm^2$ COPPER FOIL
INCIDENT ELECTRON ENERGY 115 Kev.

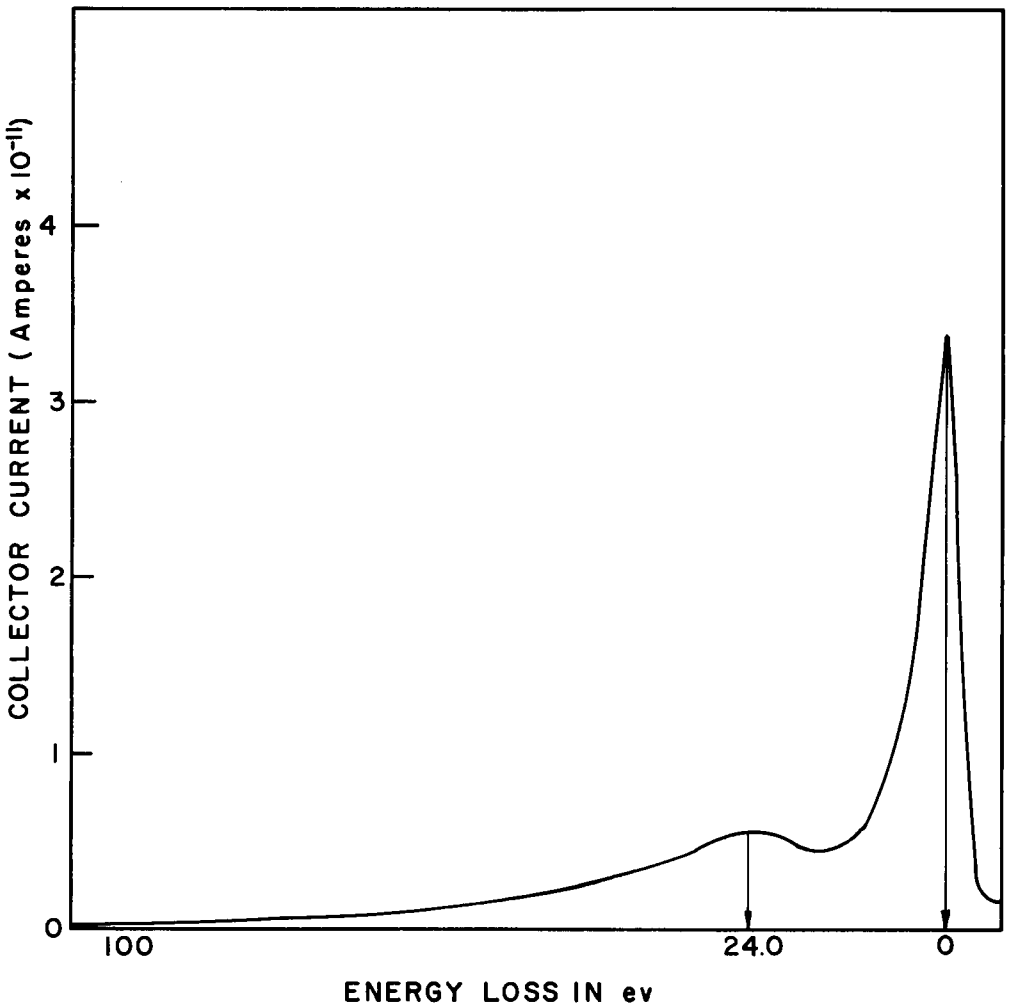

FIG.16-ELECTRON ENERGY DISTRIBUTION FROM A SILVER FOIL. INCIDENT ELECTRON ENERGY 45 KEV

The quantum loss for Al, 14.87 ev, was obtained by adding the quantities 14.8, 30.0, 44.2 and 59.8 ev, identifying the first quantity with one fundamental loss, the second with two, the third with three and the fourth with four, and dividing the sum of the four numbers by 1 + 2 + 3 + 4 = 10. The quantum loss for Mg, 10.60 ev, was obtained in the same way. Had the mean value of all differences between successive losses been taken, many of the quantities would have cancelled, eliminating many of the measurements.

The magnitudes of these losses were found to be independent of primary energy and foil thickness. The number of losses observed in Al increased with increasing foil thickness.

No energy losses were observed in gold, tin and indium. An energy loss of about 520 ev, which can be identified with the K excitation energy of oxygen, 526 ev, was indicated in Zapon films. No losses were observed in Formvar films. The δ' voltage was scanned to measure energy losses up to 600 ev in all the foils mentioned.

Comparison with Other Experiments

In Table 2 comparison is made of the measurements of the discrete losses in aluminum, copper, silver and magnesium with other measurements of such losses. The values obtained here for aluminum agree quite well with those of Ruthemann (1948) and Lang (1948) except that Ruthemann observed one, and Lang two, additional losses. Two of the present losses agree fairly well with two observed by Marton and

Table 2

ENERGY LOSSES (ev) IN ALUMINUM

Ruthemann (1948)	Lang (1948)	Möllenstedt (1949)		Marton and Leder (1954)	Watanabe (1954)	This Research
		7	9	6.2	6.5	
14.72	14.5	15		13.9	14.8	14.8
		22	18	19.2	23	
29.59	29.4			27.8	29.5	30.0
			36	35.0		
44.34	44.2					44.2
59.34	58.6		54			59.8
73.84	75.2					
	90.4					

ENERGY LOSSES (ev) IN COPPER

Rudberg (1930)	Rudberg (1936)	Lang (1948)	Möllenstedt (1949)	Reichertz-Farnsworth (1949)	Marton and Leder (1954)	Watanabe (1954)	This Research
3.4	4.2			3.0			
6.9	7.2			6.0	6.9	7	
12.3				12.3	11.3		
		19.1	20.4	20.0	19.6	19.5	
		22.9*					22.6**
25.5							
34.5							

* Cu on collodion

** Cu on zapon

Table 2 (Continued)

ENERGY LOSSES (ev) IN SILVER

Rudberg (1930)	Rudberg (1936)	Turnbull-Farnsworth (1938)	Ruthemann (1948)	Marton-Leder (1954)	Watanabe (1954)	This Research
4.6	3.9	3.9				
7.4	7.8	7.3				
				16.0		
24.8	23		22.57		22	23.8
			45.31			

ENERGY LOSSES (ev) IN MAGNESIUM

Marton-Leder (1954)	Watanabe (1954)	This Research
9.7	10.3	10.5
20.3	20.7	21.5
	31.2	31.6
	41.5	

Leder (1954) and Watanabe (1954), but they obtained additional losses in between the values obtained here. One measurement obtained here agrees fairly well with one obtained by Möllenstedt (1949), but he also obtained values in between the present ones, some of which agree with those of Marton and Leder and Watanabe. Ruthemann obtained 14.72 ev and Lang 14.8 ev for the fundamental loss, compared with 14.87 ev obtained here. The interval between the measurements of Marton and Leder does not seem to be the same in each case. However, the mean value of this interval is 6.8 ev. The interval between losses of the first set of Möllenstedt's data is 7.3 ev; there does not seem to be a constant interval between the values in the other set. The interval between losses is 7.4 ev for Watanabe's data.

The measurement of 22.6 ev for the single loss obtained here in copper agrees quite well with the value 22.9 ev observed in copper on collodion by Lang (1948). The copper foils used in the present experiment were on Zapon backings, as were the aluminum foils. Although Lang observed a difference in the energy loss in backed and unbacked copper foils, he did not report any such difference for aluminum and nickel, on which he also made measurements. The quantity 22.6 ev obtained here also agrees fairly well with the values near 20.0 ev obtained by Möllenstedt (1949), Reichertz and Farnsworth (1949), Marton and Leder (1954), and Watanabe (1954). However, Reichertz and Farnsworth, Marton and Leder, Watanabe, and Rudberg (1936) observed losses less than 20 ev and Rudberg (1930) observed greater ones as well.

Good agreement is found between the value 23.8 ev observed here for the single loss in silver and one measurement each of Rudberg (1930), Rudberg (1936), Ruthemann (1948) and Watanabe (1954). However, Rudberg, Turnbull and Farnsworth (1938) and Marton and Leder (1954) all observed losses less than this value. Ruthemann observed a loss very nearly twice as great.

The discrete losses observed in magnesium agree very well with those observed by Marton and Leder (1954) and Watanabe (1954). However, one additional loss was observed by Watanabe. The mean value of the interval between successive losses obtained here is 10.6 ev compared with 10.0 ev for Marton and Leder and 10.4 for Watanabe.

Mean Free Path

As has been shown, discrete energy losses have been observed in the metal foils. It is of interest to determine the mean free path λ for the loss of a quantum of energy $\hbar\omega_p$ in a foil. ω_p is the plasma frequency which will be discussed later. This mean free path can be obtained from the measurements taken here by application of an analysis due to Mr. R. H. Ritchie (1955).

If it is assumed that energy losses occur only in single quantum units of $\hbar\omega_p$ and that single losses involving multiples of this unit are not possible, the probability that an impinging electron will lose energy $\hbar\omega_p$ in traversing a thickness dx of the foil is given by $\frac{dx}{\lambda}$. The probability $p_o(t)$ that the electron suffers no

losses in a foil of thickness t is

$$p_o(t) = e^{-t/\lambda}$$

The probability that only one loss occurs in thickness dx at x as the electron passes through the foil is

$$p_o(x) \frac{dx}{\lambda} p_o(t - x) = e^{-x/\lambda} \frac{dx}{\lambda} e^{-(t - x)/\lambda} = e^{-t/\lambda} \frac{dx}{\lambda}$$

The probability $p_1(t)$ that only one loss occurs in the whole foil is the integral over x of this expression or

$$p_1(t) = \frac{t}{\lambda} e^{-t/\lambda}$$

The probability that one loss occurs in dx at x and another in dy at y is

$$p_o(x) \frac{dx}{\lambda} p_o(y - x) \frac{dy}{\lambda} p_o(t - y) = e^{-x/\lambda} \frac{dx}{\lambda} e^{-(y - x)/\lambda} \frac{dy}{\lambda} e^{-(t - y)/\lambda}$$

$$= e^{-t/\lambda} \frac{1}{\lambda^2} \, dx \, dy$$

If this expression is integrated first over x and then over y there results the probability for two losses in the foil

$$p_2(t) = \frac{t^2}{2\lambda^2} e^{-t/\lambda}$$

The probability that one loss occurs in dx at x, that a second occurs

in dy at y and that a third occurs in dz at z is

$$p_o(x) \frac{dx}{\lambda} p_o(y - x) \frac{dy}{\lambda} p_o(z - y) \frac{dz}{\lambda} p_o(t - z)$$

$$= e^{-x/\lambda} \frac{dx}{\lambda} e^{-(y - x)/\lambda} \frac{dy}{\lambda} e^{-(z - y)/\lambda} \frac{dz}{\lambda} e^{-(t - z)/\lambda}$$

$$= e^{-t/\lambda} \frac{1}{\lambda^3} dx\, dy\, dz$$

If this expression is integrated over dx, then dy, then dz, there results the probability of three losses in the foil

$$p_3(t) = \frac{1}{3!} \left(\frac{t}{\lambda}\right)^3 e^{-t/\lambda}$$

The probability of n losses in a foil of thickness t is then

$$p_n(t) = \frac{1}{n!} \left(\frac{t}{\lambda}\right)^n e^{-t/\lambda} ,$$

the Poisson distribution law.

Now it is assumed that the area A_o under the no loss peak is a measure of the probability that an electron will suffer no losses in passing through a foil, that the area A_1 under the first loss peak is a measure of the probability of one loss in the foil, etc. By taking ratios of the areas under the different peaks, values of the ratio t/λ can be obtained. Thus

$$\frac{A_1}{A_o} = \frac{p_1(t)}{p_o(t)} = \frac{t}{\lambda}$$

$$\frac{A_2}{A_o} = \frac{p_2(t)}{p_o(t)} = \frac{1}{2}\left(\frac{t}{\lambda}\right)^2$$

$$\frac{A_2}{A_1} = \frac{p_2(t)}{p_1(t)} = \frac{t}{2\lambda}$$

$$\frac{A_3}{A_o} = \frac{1}{6}\left(\frac{t}{\lambda}\right)^3$$

$$\frac{A_3}{A_1} = \frac{1}{6}\left(\frac{t}{\lambda}\right)^2$$

$$\frac{A_3}{A_2} = \frac{1}{3}\,\frac{t}{\lambda} \qquad \text{etc.}$$

Hence six values of t/λ can be obtained from the areas under the no loss peak and three loss peaks.

An experimental check was made to see if the data fit this analysis. The six ratios of the areas under the no loss and three loss peaks were taken for two different curves. From these ratios six values of t/λ were obtained for each curve. The mean deviation

of the values of $\frac{t}{\lambda}$ from the mean value was 7% in one case and 10% in the other. It is thought that this verifies the applicability of the analysis to the data obtained here within the limits of accuracy of the data.

As a further check a value of t/λ was determined in another way from a curve for aluminum from which t/λ had been determined by taking the ratios of the areas under the peaks. The mean free path λ is given by

$$\lambda = \frac{\Delta E}{dE/dx} = \frac{\Delta E}{\overline{\Delta E}/t}$$

where ΔE is the value of the quantum energy loss, dE/dx is the stopping power and $\overline{\Delta E}$ is the average energy loss in the foil of thickness t. The average energy loss $\overline{\Delta E}$ is given by

$$\overline{\Delta E} = \frac{\int E\ N(E)\ dE}{\int N(E)\ dE}$$

where N(E) is the energy distribution function and E is the energy loss. In order to determine $\overline{\Delta E}$, an energy distribution curve was chosen in which the trailing edge reached zero before the end of the scanning cycle. The ordinates of a number of points on the curve were multiplied by the corresponding energy losses, i.e., the energy intervals from the center of the no loss peak to the points. A second curve was plotted using the products of the original ordinates and their corresponding energy losses as ordinates. The area under

this curve as well as that under the original curve was measured with a planimeter. $\overline{\Delta E}$ is given by the ratio of the area of the second curve to the area of the original curve. t/λ is then given by

$$\frac{t}{\lambda} = \frac{\overline{\Delta E}}{\Delta E}$$

where ΔE is the value of the fundamental discrete loss, 14.9 ev for aluminum. The value of t/λ obtained in this way was 0.933 compared with 0.943 obtained from ratios of areas under the peaks. The per cent difference between the two values is 1.1%.

If the intensities of the losses, or areas under the peaks, do obey the Poisson distribution, then the ratios of the areas under the larger loss peaks to those under the smaller loss peaks should increase as the foil thickness increases. That this is the case can be seen by comparing Fig. 11 with Fig. 9, the energy distribution in a thicker Al foil at the same incident electron energy.

Figure 17 illustrates how the boundaries of the no loss and first loss peaks were extrapolated to the base line in a typical case. The leading edge of the first loss peak was extended to the base line in a manner such that when it was subtracted from the original curve there was no hump in the resulting trailing edge of the no loss peak. The trailing edge of the first loss peak was likewise obtained by subtracting the extended leading edge of the second loss peak from the original curve. It is admitted that the drawing of the extended parts of the edges of the peaks is somewhat arbitrary. However, two

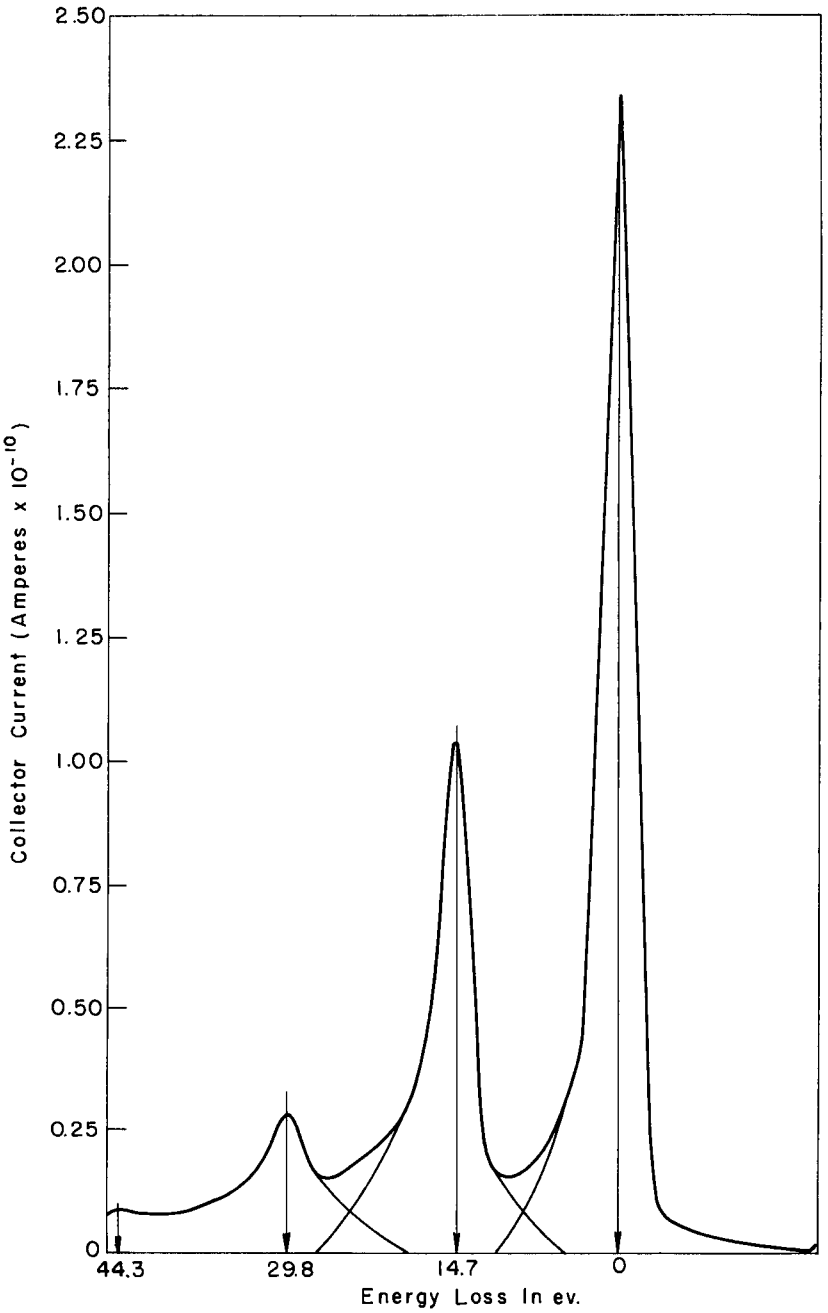

FIG. 17-ENERGY DISTRIBUTION FROM
15 $\mu g/cm^2$ ALUMINUM FOIL
INCIDENT ELECTRON ENERGY 75 Kev.

observers drew the extrapolations independently for several curves and the measured values of the areas under the peaks agreed within 10% in every case. The areas were measured with a Keuffel and Esser No. 4236 planimeter or a Dietzgen OTT Type 30/38 planimeter. The area of each curve was measured at least three times and the average of the values taken. The last peak in a curve was not used since it was difficult to draw its trailing edge and since its area was much smaller than those of the other peaks. However, in many cases four loss peaks were obtained in aluminum and the use of the first three loss peaks and the no loss peak yields six values of t/λ. If only three loss peaks were obtained, and only the first two used, three values of t/λ can be obtained. At least three, usually more, energy distribution curves were taken at each value of the bombarding electron energy for each foil. The mean value of all the values of t/λ at each incident electron energy was taken and the thickness t of the foil was determined by weighing a known area of the foil. There result values of λ as a function of incident electron energy.

Values of the mean free path in aluminum at different primary energies are listed in Table 3. The values obtained from two different experimental runs made on successive days on foil No. 1, thickness 14.3 $\mu g/cm^2$, and another run on foil No. 2, thickness 15.3 $\mu g/cm^2$, are tabulated separately. The value of the foil thickness in Angstroms is obtained assuming the density of the foil is the same as that of bulk aluminum. The probable error is given

Table 3

MEAN FREE PATH IN ALUMINUM AS A FUNCTION OF INCIDENT ELECTRON ENERGY

Incident Energy	Mean Free Path		Probable Error
kev	$\mu g/cm^2$	Angstroms	%
Foil No. 1 14.3 $\mu g/cm^2$ or 530 A ± 3.6% Run 1			
30	17 ± 1	630 ± 40	6.2
45	19 ± 1	690 ± 40	5.3
60	19.3 ± 0.8	710 ± 30	4.1
75	27 ± 1	990 ± 50	5.5
85	35 ± 1	1290 ± 50	3.8
100	33 ± 1	1230 ± 50	4.3
Foil No. 1 Run 2			
30	15 ± 1	540 ± 40	8.0
45	16.8 ± 0.7	620 ± 30	4.2
60	18.8 ± 0.7	700 ± 30	3.9
75	20.3 ± 0.8	750 ± 30	3.7
85	24.5 ± 0.9	910 ± 30	3.8
100	37 ± 2	1360 ± 70	5.2
Foil No. 2 15.3 Eg/cm^2 or 567A ± 3.0%			
25	16.9 ± 0.5	630 ± 20	3.0
45	17.2 ± 0.6	640 ± 20	3.4
60	19.0 ± 0.9	700 ± 30	4.6
75	25.7 ± 0.8	950 ± 30	3.1
100	31 ± 1	1160 ± 50	4.1

in magnitude and as a per cent of the value of λ . These data are plotted in Fig. 18. The thicknesses of these foils, determined by weighing a known area, were also estimated on the basis of the inverse square law assuming isotropic distribution in evaporation. The value obtained for foil No. 1 was 12.2 $\mu g/cm^2$ which differs from the value 14.3 $\mu g/cm^2$ obtained by weighing by 16%. The value obtained for foil No. 2 was 15.9 $\mu g/cm^2$ compared with 15.3 $\mu g/cm^2$ by weighing, a difference of 3.8%. It is believed that these differences are due to anistropy in evaporation. According to Bond (1954) actual film thicknesses may range from one-half to twice the value calculated assuming isotropic evaporation. Chase and Cox (1940) obtained a value for the thickness of an aluminum foil assuming isotropic evaporation which was 19% higher than that determined by a colorimetric microchemical method. Bayard and Yntema (1955) obtained a value for the thickness of a gold foil assuming isotropic evaporation which was 25% higher than that obtained from absolute scattering of electrons in the foil.

As can be seen from Fig. 18 the mean free path increases with increasing primary energy. This can be seen qualitatively by comparing Fig. 9, the energy distribution in an aluminum foil at 45 kev primary energy, with Fig. 10, the energy distribution in the same foil at 100 kev incident energy. A value of the mean free path λ is given by

$$\lambda = \frac{A_o}{A_1} t$$

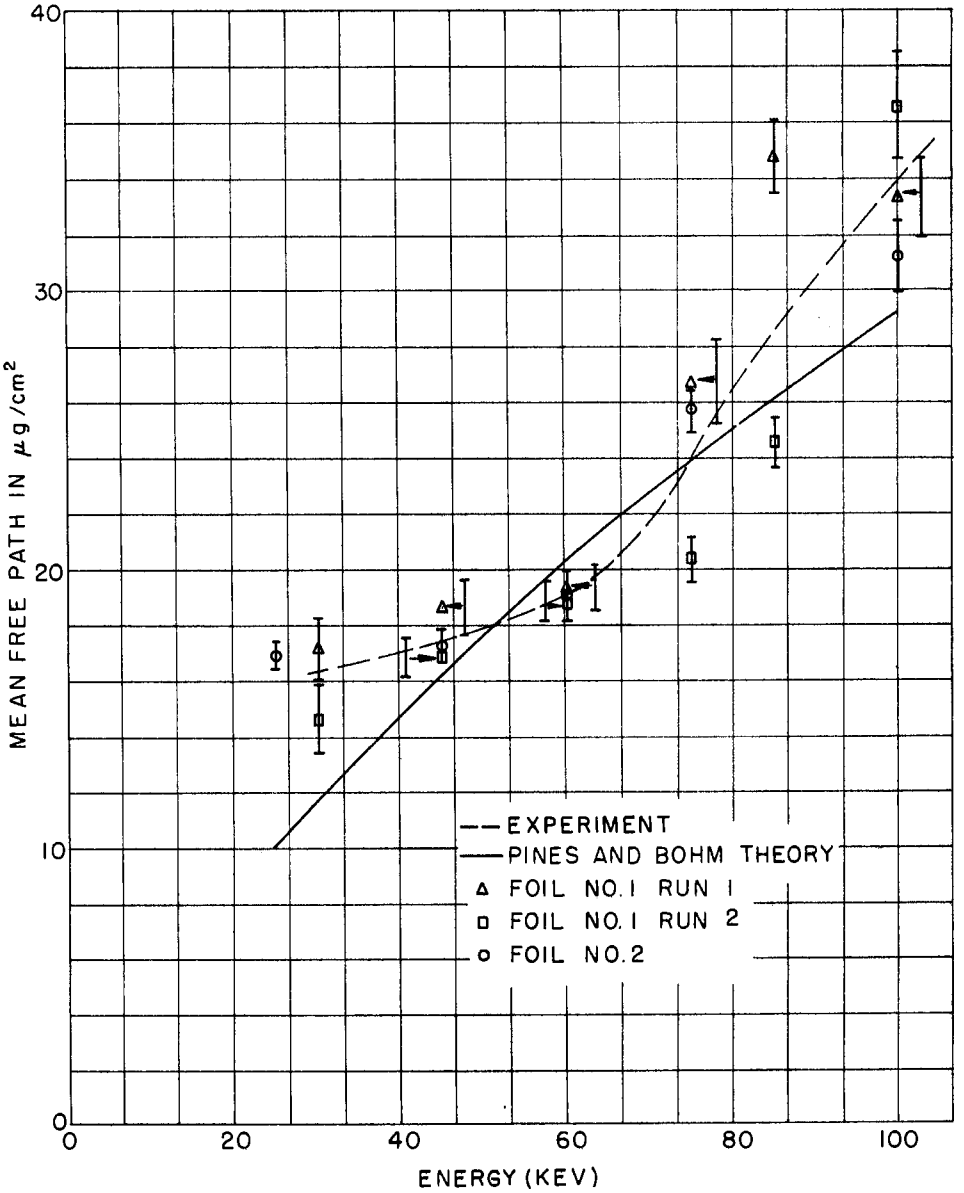

FIG.18-MEAN FREE PATH IN ALUMINUM
AS A FUNCTION OF INCIDENT ELECTRON ENERGY

where $\frac{A_o}{A_1}$ is the ratio of the area under the no loss peak to that under the first loss peak and t is the foil thickness. It can be seen that the area A_o is larger compared with the area A_1 in Fig. 10 (100 kev) than in Fig. 9 (45 kev). Hence λ is larger at 100 kev than at 45 kev. Comparison between the experimental points and the theoretical curve plotted in Fig. 18 will be discussed later.

In Table 4 are listed values of the mean free path in magnesium at different incident electron energies. The values obtained from three different foils, of thicknesses 85, 72, and 51 $\mu g/cm^2$ as determined by weighing a known area of the foils, are listed separately. For magnesium there was a wide discrepancy between the thickness values obtained by weighing the foils and those obtained from the inverse square law assuming isotropic distribution. The thicknesses obtained by the latter method for these three foils are 8.1, 10.1 and 9.4 $\mu g/cm^2$, respectively. The former values are factors of 10.5, 7.1 and 5.4, respectively, greater than the latter. In an attempt to determine which values were correct, fifteen magnesium foils were evaporated. Several of them were weighed and the others were analyzed for total magnesium content by colorimetric analysis using the titan yellow method by the Analytical Chemistry Division of ORNL. The accuracy of this method was stated to be $\pm$ 3% by the supervisor of the laboratory which made the analysis. The quantities of magnesium in the foils obtained by this analysis agreed within 30% with the values obtained by

Table 4

MEAN FREE PATH IN MAGNESIUM AT DIFFERENT INCIDENT ELECTRON ENERGIES

A. Foil Thickness Determined by Weighing

Incident Energy	Mean Free Path		Probable Error
kev	$\mu g/cm^2$	Angstroms x 10^3	%
Foil No. 1 85 $\mu g/cm^2$ = 4880A			
40	169 ± 6	9.7 ± 0.3	3.6
50	185 ± 5	10.6 ± 0.3	2.9
60	191 ± 6	11.0 ± 0.3	3.0
75	180 ± 5	10.3 ± 0.3	2.8
85	207 ± 6	11.9 ± 0.4	3.1
100	202 ± 5	11.6 ± 0.3	2.7
115	220 ± 10	12.9 ± 0.6	4.3
Foil No. 2 72 $\mu g/cm^2$ = 4140A			
45	157 ± 6	9.0 ± 0.4	4.0
60	109 ± 3	6.3 ± 0.2	2.7
75	127 ± 4	7.3 ± 0.2	3.0
85	133 ± 4	7.6 ± 0.2	3.0
100	132 ± 6	7.6 ± 0.4	4.7
115	133 ± 4	7.6 ± 0.2	2.9
Foil No. 3 51 $\mu g/cm^2$ = 2930A			
60	69 ± 3	4.0 ± 0.2	4.6
100	160 ± 10	9.0 ± 0.7	7.4

Table 4 (continued)

MEAN FREE PATH IN MAGNESIUM AT DIFFERENT INCIDENT ELECTRON ENERGIES

B. Foil Thickness Determined by Inverse Square Law

Incident Energy	Mean Free Path		Probable Error
kev	$\mu g/cm^2$	Angstroms	%
Foil No. 1 8.1 $\mu g/cm^2$ = 465A			
40	16.0 ± 0.4	920 ± 20	2.6
50	17.6 ± 0.3	1010 ± 20	1.5
60	18.2 ± 0.3	1050 ± 20	1.6
75	17.2 ± 0.2	990 ± 10	1.2
85	19.7 ± 0.4	1130 ± 20	1.8
100	19.2 ± 0.2	1100 ± 10	1.0
115	21.3 ± 0.7	1220 ± 40	3.5
Foil No. 2 10.1 $\mu g/cm^2$ = 580A			
45	22.1 ± 0.7	1270 ± 40	3.3
60	15.4 ± 0.2	890 ± 10	1.3
75	17.9 ± 0.3	1030 ± 20	1.7
85	18.7 ± 0.3	1080 ± 20	1.8
100	18.6 ± 0.7	1070 ± 40	4.0
115	18.7 ± 0.3	1080 ± 20	1.6
Foil No. 3 9.4 $\mu g/cm^2$ = 540A			
60	12.9 ± 0.5	740 ± 30	3.7
100	29 ± 2	1700 ± 100	6.9

weighing foils with the same geometry in evaporation as those analyzed, whereas they were several times as great as those obtained from the inverse square law assuming isotropic distribution. The large discrepancies between the amounts of magnesium in the foils determined both by weighing and by chemical analysis and those determined by the inverse square law are thought to be due to anisotropy in evaporation. Magnesium sublimes and does not melt before evaporating. It is thought that this might cause a greater anisotropy in the evaporation of magnesium than in the evaporation of some metal which melts, such as aluminum. The 30% difference between the quantities of magnesium determined by chemical analysis and those determined by weighing can also be accounted for by anisotropy of evaporation. Since magnesium is rather active chemically some corrosion of the foils undoubtedly occurs. Although the foils were kept in an evacuated desiccator containing a desiccant as much as possible, they were exposed to air when removed from the evaporator, when introduced into and removed from the accelerator, and when weighed. They were also exposed to the residual gases in the evaporator during and after evaporation and to residual gases in the desiccator. According to Beck (1943), Pannel (1948), the American Magnesium Corporation (1923), and Whitby (1933), the principal constituents of the corrosion of magnesium exposed to an indoor atmosphere are water and the oxide, carbonate, sulphate and hydroxide of magnesium, with the carbonate predominating. Watanabe (1954) states, "It was rather

difficult to obtain a thin Mg foil by reason of the rapid oxidation of this metal foil."

The data in Table 4 are plotted in Fig. 19. Both the mean free path determined from the foil thicknesses calculated by the inverse square law and that obtained from foil weight are plotted. It is interesting to note that the former values for the three foils agree much better with each other and with the theoretical curve than do the latter. For this reason the former determinations are included. Comparison between theory and experiment will be discussed later. Where the probable error is not shown for a point, it is smaller than the symbol indicating the point.

Table 5 lists values of the mean free path in copper at different primary energies. The values obtained from two foils, of thicknesses 66 and 81 $\mu g/cm^2$ as determined by weighing the foils, are listed separately. Values of the thickness of these foils obtained from the inverse square law assuming isotropic distribution in evaporation agreed with these values within 20%. This difference can be accounted for by anisotropy in evaporation. Some oxidation probably occurred also. Parratt (1954) states that a 2000A copper film may oxidize completely to a depth of 150A. Comparable, or even greater, oxidation may take place in the case of magnesium. The data in Table 5 are plotted in Fig. 20. Comparison with theory will be discussed later.

Since the thickness of the silver foil was not known the mean free path in silver could not be calculated. Measurements on silver

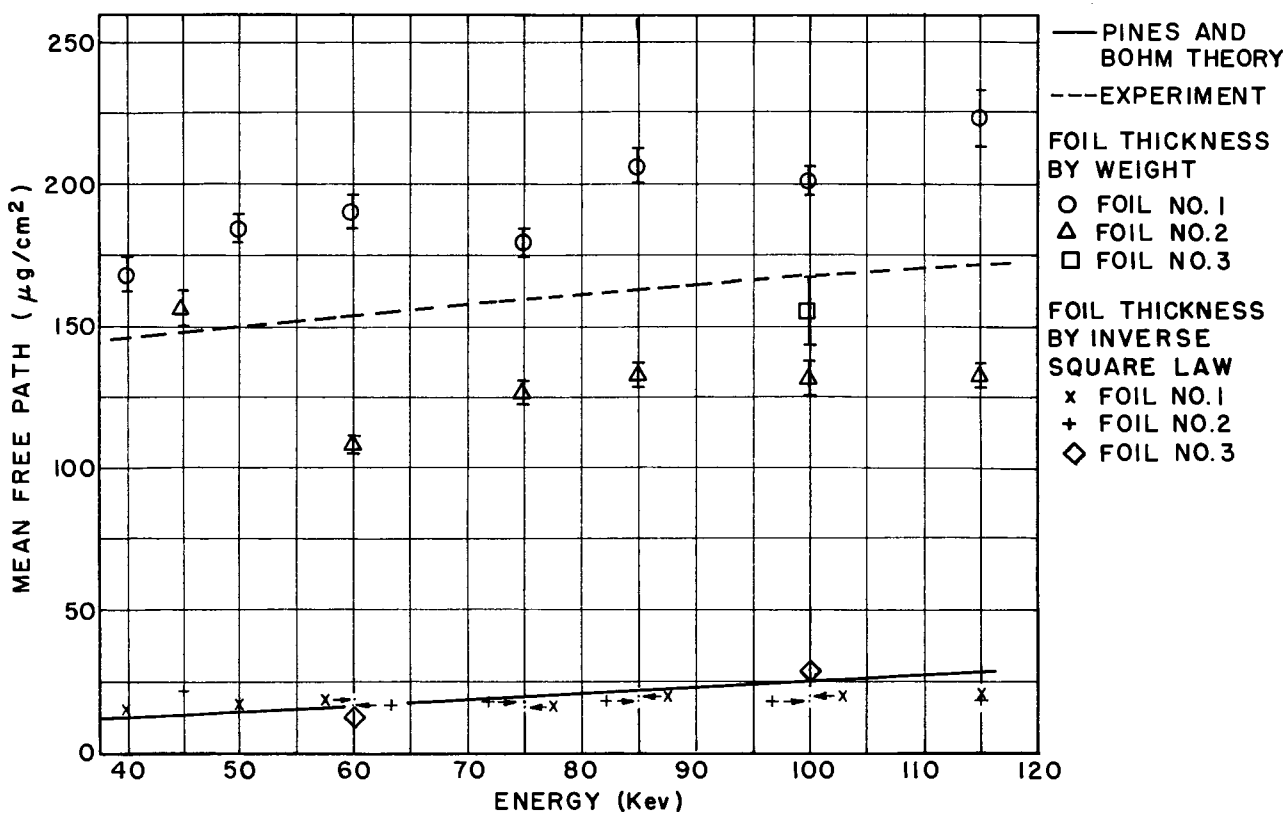

FIG. 19-MEAN FREE PATH IN MAGNESIUM AS A FUNCTION OF INCIDENT ELECTRON ENERGY

Table 5

MEAN FREE PATH IN COPPER AT DIFFERENT PRIMARY ENERGIES

Primary Energy	Mean Free Path		Probable Error
kev	$\mu g/cm^2$	Angstroms	%
Foil No. 1 66 $\mu g/cm^2$ = 742A			
45	96 ± 8	1080 ± 90	7.9
60	84 ± 4	950 ± 40	4.7
75	97 ± 4	1090 ± 40	4.0
85	120 ± 4	1350 ± 40	3.1
100	96 ± 3	1080 ± 30	3.2
115	119 ± 3	1340 ± 40	2.9
Foil No. 2 81 $\mu g/cm^2$ = 910A			
60	62 ± 3	690 ± 40	5.1
80	71 ± 4	800 ± 50	5.8
100	72 ± 2	800 ± 20	2.8

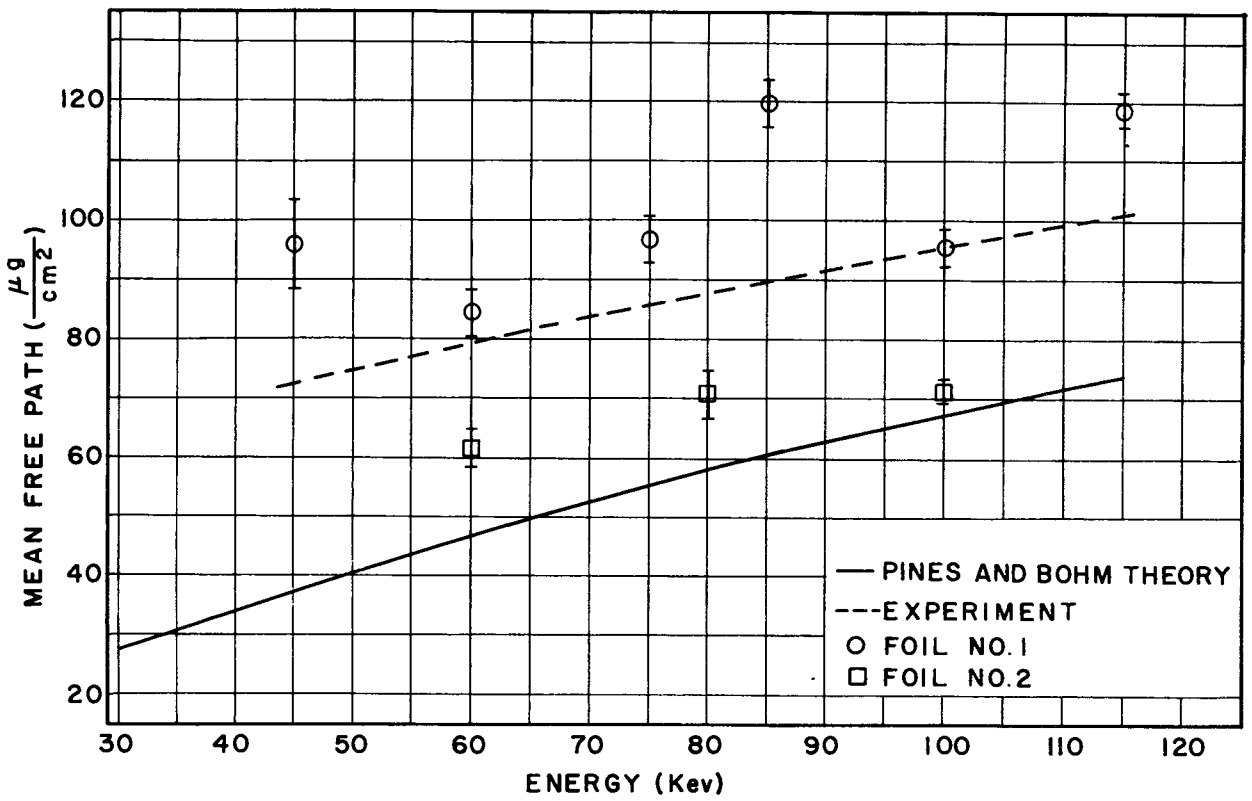

FIG.20-MEAN FREE PATH IN COPPER AS A FUNCTION OF INCIDENT ELECTRON ENERGY

were obtained only at 45 kev primary energy. Further attempts were made to get more data on silver, but no energy losses were observed.

Stopping Power

The stopping power $\frac{dE}{dx}$ is given by

$$\frac{dE}{dx} = \frac{\Delta E}{\lambda}$$

where ΔE is the quantum energy loss and λ is the mean free path for the loss of a quantum of energy.

Values of the stopping power in aluminum at different incident electron energies are listed in Table 6. As in the case of the mean free path, the values obtained from two different runs on foil No. 1, 14.3 $\mu g/cm^2$, and another run on foil No. 2, 15.3 $\mu g/cm^2$, are tabulated separately. The values are plotted in Fig. 21. It will be noted that the stopping power decreases as the incident energy increases.

In Table 7 are found values of the stopping power in magnesium as a function of primary electron energy. The values obtained for two different foils, using the values of λ obtained from the foil thicknesses determined by weighing the foils are listed separately. Values of the stopping power determined from values of λ obtained from the foil thicknesses determined by the inverse square law are also listed for each foil. The values are plotted in the graph of Fig. 22.

Table 6

STOPPING POWER IN ALUMINUM AT DIFFERENT INCIDENT ELECTRON ENERGIES

Incident Energy kev	Stopping Power $\frac{ev}{\mu g/cm^2}$	Probable Error %
Foil No. 1 14.3 $\mu g/cm^2$ = 530A ± 3.6% Run 1		
30	0.87 ± 0.05	6.3
45	0.80 ± 0.04	5.3
60	0.77 ± 0.03	4.1
75	0.56 ± 0.03	5.5
85	0.43 ± 0.02	3.8
100	0.45 ± 0.02	4.3
Foil No. 1 Run 2		
30	1.02 ± 0.08	8.0
45	0.89 ± 0.04	4.2
60	0.79 ± 0.03	3.9
75	0.73 ± 0.03	3.7
85	0.61 ± 0.02	3.8
100	0.41 ± 0.02	5.2
Foil No. 2 15.3 $\mu g/cm^2$ = 567A ± 3.0%		
25	0.88 ± 0.03	3.0
45	0.86 ± 0.03	3.4
60	0.78 ± 0.04	4.6
75	0.58 ± 0.02	3.1
100	0.48 ± 0.02	4.1

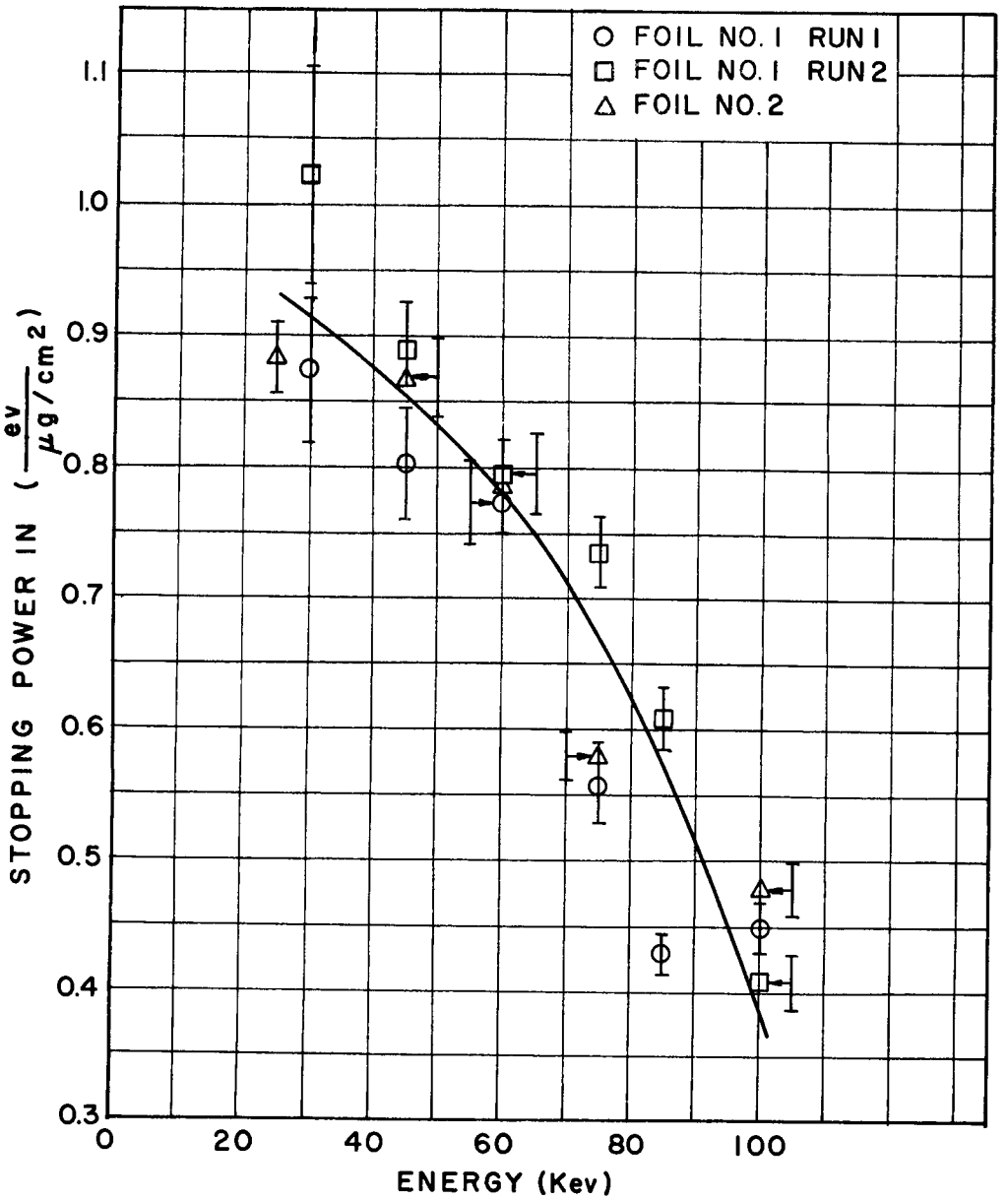

FIG. 21-STOPPING POWER IN ALUMINUM AS A FUNCTION OF INCIDENT ELECTRON ENERGY

Table 7

STOPPING POWER IN MAGNESIUM AS A FUNCTION OF PRIMARY ELECTRON ENERGY

A. Foil Thickness Determined by Weighing

Primary Energy kev	Stopping Power $\frac{ev}{\mu g/cm^2}$	Probable Error %
Foil No. 1 85 $\mu g/cm^2$ = 4880A		
40	0.063 ± 0.002	3.6
50	0.057 ± 0.002	2.9
60	0.056 ± 0.002	3.0
75	0.059 ± 0.002	2.8
85	0.051 ± 0.002	3.1
100	0.052 ± 0.001	2.7
115	0.047 ± 0.002	4.4
Foil No. 2 72 $\mu g/cm^2$ = 4140A		
45	0.068 ± 0.003	4.0
60	0.097 ± 0.003	2.7
75	0.083 ± 0.002	3.0
85	0.080 ± 0.002	3.0
100	0.080 ± 0.004	4.7
115	0.080 ± 0.002	2.9

Table 7 (continued)

STOPPING POWER IN MAGNESIUM AS A FUNCTION OF PRIMARY ELECTRON ENERGY

B. Foil Thickness Determined by Inverse Square Law

Primary Energy kev	Stopping Power $\frac{ev}{\mu g/cm^2}$	Probable Error %
Foil No. 1 8.1 $\mu g/cm^2$ = 465A		
40	0.66 ± 0.02	2.6
50	0.602 ± 0.009	1.5
60	0.582 ± 0.009	1.6
75	0.616 ± 0.007	1.2
85	0.54 ± 0.01	1.8
100	0.552 ± 0.006	1.0
115	0.50 ± 0.02	3.5
Foil No. 2 10.1 $\mu g/cm^2$ = 580A		
45	0.48 ± 0.02	3.3
60	0.688 ± 0.009	1.3
75	0.59 ± 0.01	1.7
85	0.57 ± 0.01	1.8
100	0.57 ± 0.02	4.0
115	0.567 ± 0.009	1.6

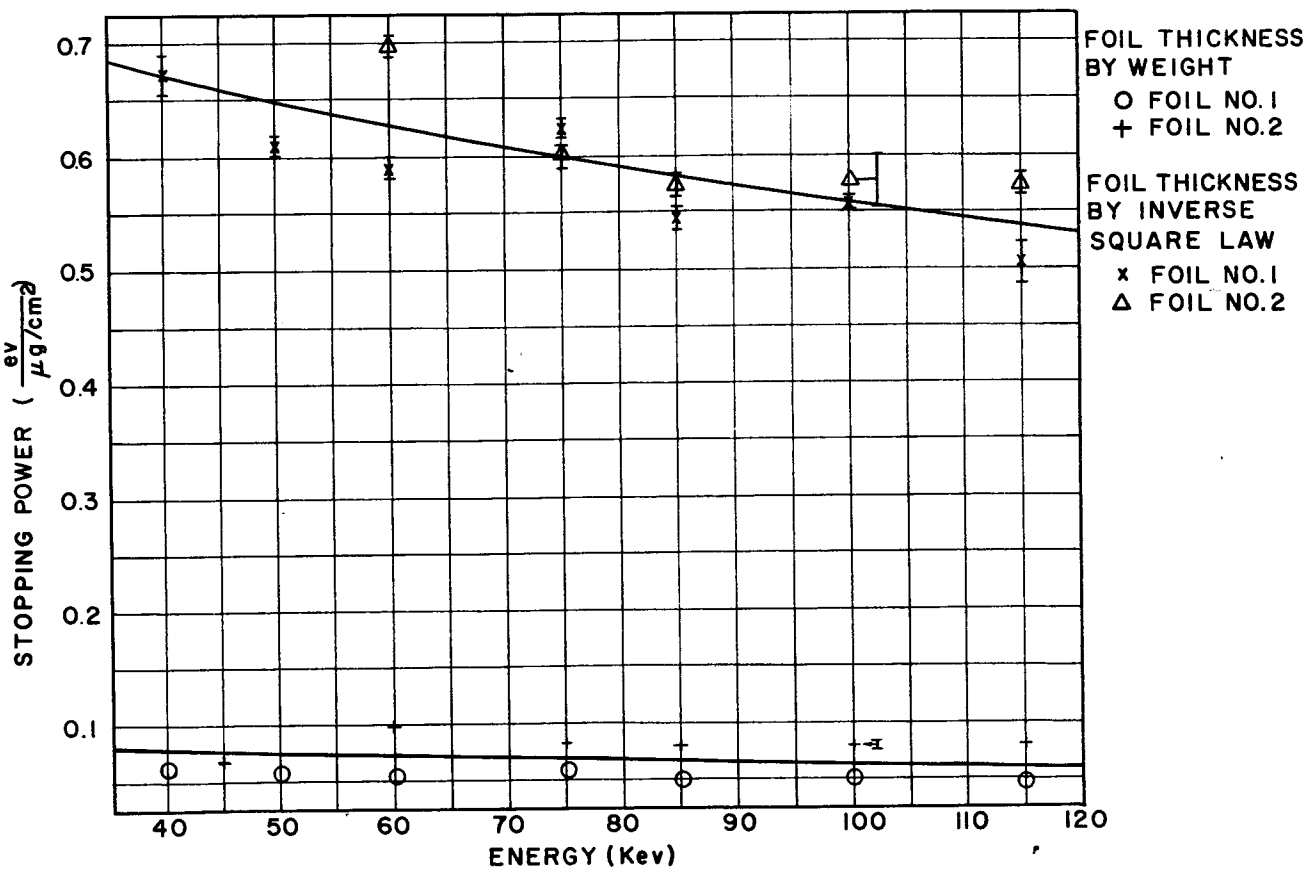

FIG.22-STOPPING POWER IN MAGNESIUM AS A FUNCTION OF INCIDENT ELECTRON ENERGY

Table 8 lists values of the stopping power in copper at different primary electron energies. The values obtained for the two copper foils are tabulated separately and the data are plotted in Fig. 23.

Since the thickness of the silver foil was not known the stopping power in silver could not be calculated.

Cross Sections

The cross section per free electron σ is related to the mean free path λ for the loss of a quantum of energy ΔE by

$$\sigma = \frac{1}{n\lambda} \frac{\text{cm}^2}{\text{free electron}} \tag{1}$$

where n is the number of free electrons per cm^3. n is given by

$$n = \frac{m\,\omega_p^{\,2}}{4\pi e^2} \tag{2}$$

where ω_p is the plasma oscillation frequency and m and e are the mass and charge of the electron. This equation will be discussed in the section on theory. ω_p is related to ΔE, the quantum energy loss, by

$$\omega_p = \frac{\Delta E}{\hbar} \tag{3}$$

Table 8

STOPPING POWER IN COPPER AT DIFFERENT PRIMARY ELECTRON ENERGIES

Primary Energy kev	Stopping Power $\frac{ev}{\mu g/cm^2}$	Probable Error %
Foil No. 1 66 $\mu g/cm^2$ = 742A		
45	0.24 ± 0.02	8.0
60	0.27 ± 0.01	4.7
75	0.233 ± 0.009	4.0
85	0.188 ± 0.006	3.1
100	0.236 ± 0.008	3.3
115	0.190 ± 0.006	2.9
Foil No. 2 81 $\mu g/cm^2$ = 910A		
60	0.37 ± 0.02	5.1
80	0.32 ± 0.02	5.8
100	0.316 ± 0.009	2.8

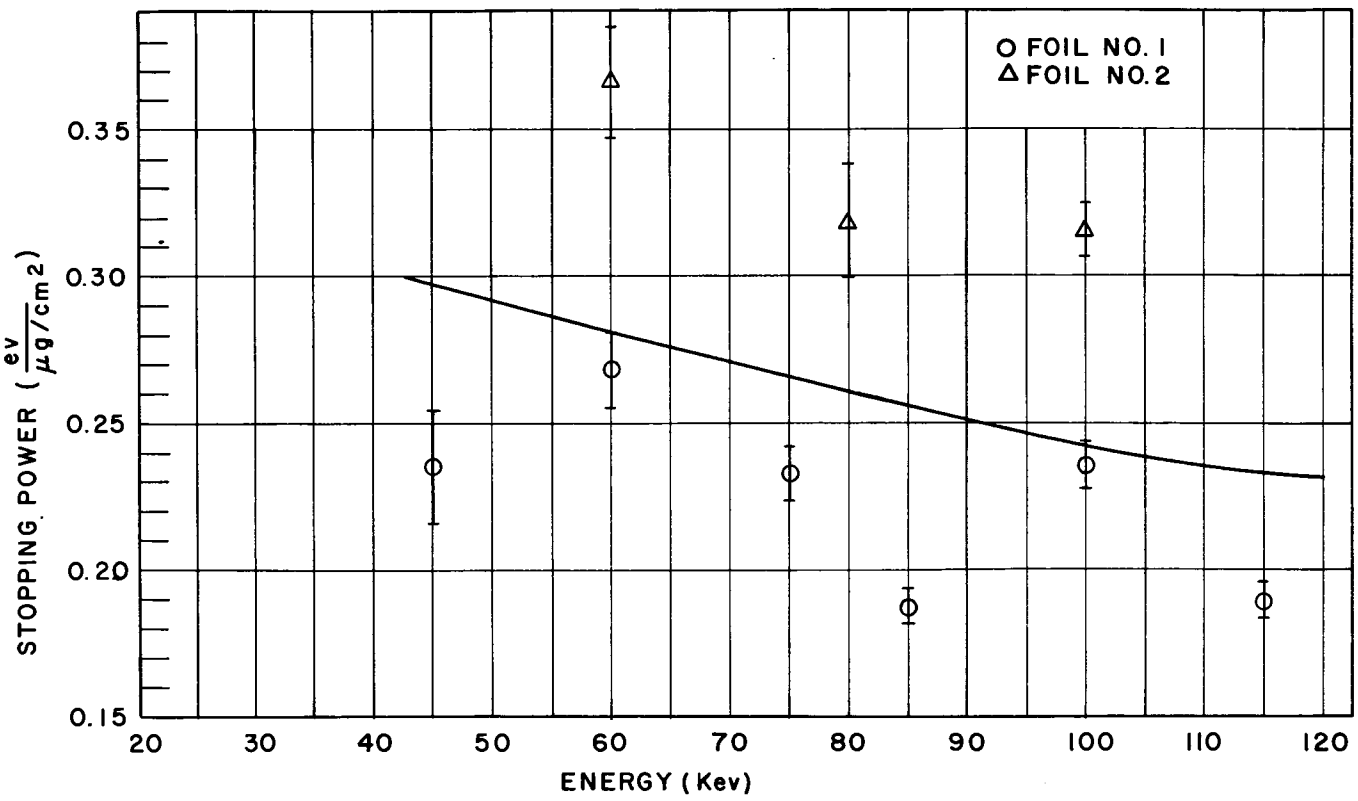

FIG. 23-STOPPING POWER IN COPPER AS A FUNCTION OF INCIDENT ELECTRON ENERGY

Substitution of relation (3) into (2) and then (2) into (1) results in

$$\sigma = \frac{1}{\pi m \lambda}\left(\frac{eh}{\Delta E}\right)^2 \qquad (4)$$

Values of the cross section per free electron in aluminum as a function of incident electron energy are given in Table 9. Again the values obtained from two different runs on foil No. 1 and another run on foil No. 2 are listed separately. The values are plotted in Fig. 24. As can be seen the cross section decreases with increasing incident energy.

In Table 10 are found values of the cross section per free electron in magnesium as a function of electron primary energy. The values obtained for two different foils are listed separately. Values obtained using the foil thickness determined by weighing the foils are tabulated separately for each foil from those obtained using the foil thickness determined by assuming isotropic evaporation. The data are plotted in Fig. 25.

Table 11 lists values of the cross section per free electron in copper at various electron incident energies. Values obtained from two copper foils are given separately. The data appear in the graph of Fig. 26.

Table 9

CROSS SECTION PER FREE ELECTRON IN ALUMINUM AS A FUNCTION OF INCIDENT ELECTRON ENERGY

Incident Energy kev	Cross Section barns x 10^5	Probable Error %
Foil No. 1 14.3 $\mu g/cm^2$ = 530A ± 3.6% Run 1		
30	9.8 ± 0.6	6.3
45	9.0 ± 0.5	5.3
60	8.7 ± 0.4	4.1
75	6.3 ± 0.3	5.5
85	4.8 ± 0.2	3.8
100	5.0 ± 0.2	4.3
Foil No. 1 Run 2		
30	11.5 ± 0.9	8.1
45	10.0 ± 0.4	4.2
60	8.9 ± 0.4	4.0
75	8.3 ± 0.3	3.8
85	6.8 ± 0.3	3.8
100	4.6 ± 0.2	5.2
Foil No. 2 15.3 $\mu g/cm^2$ = 567A ± 3.0%		
25	9.9 ± 0.3	3.1
45	9.7 ± 0.3	3.4
60	8.8 ± 0.4	4.6
75	6.5 ± 0.2	3.1
100	5.4 ± 0.2	4.1

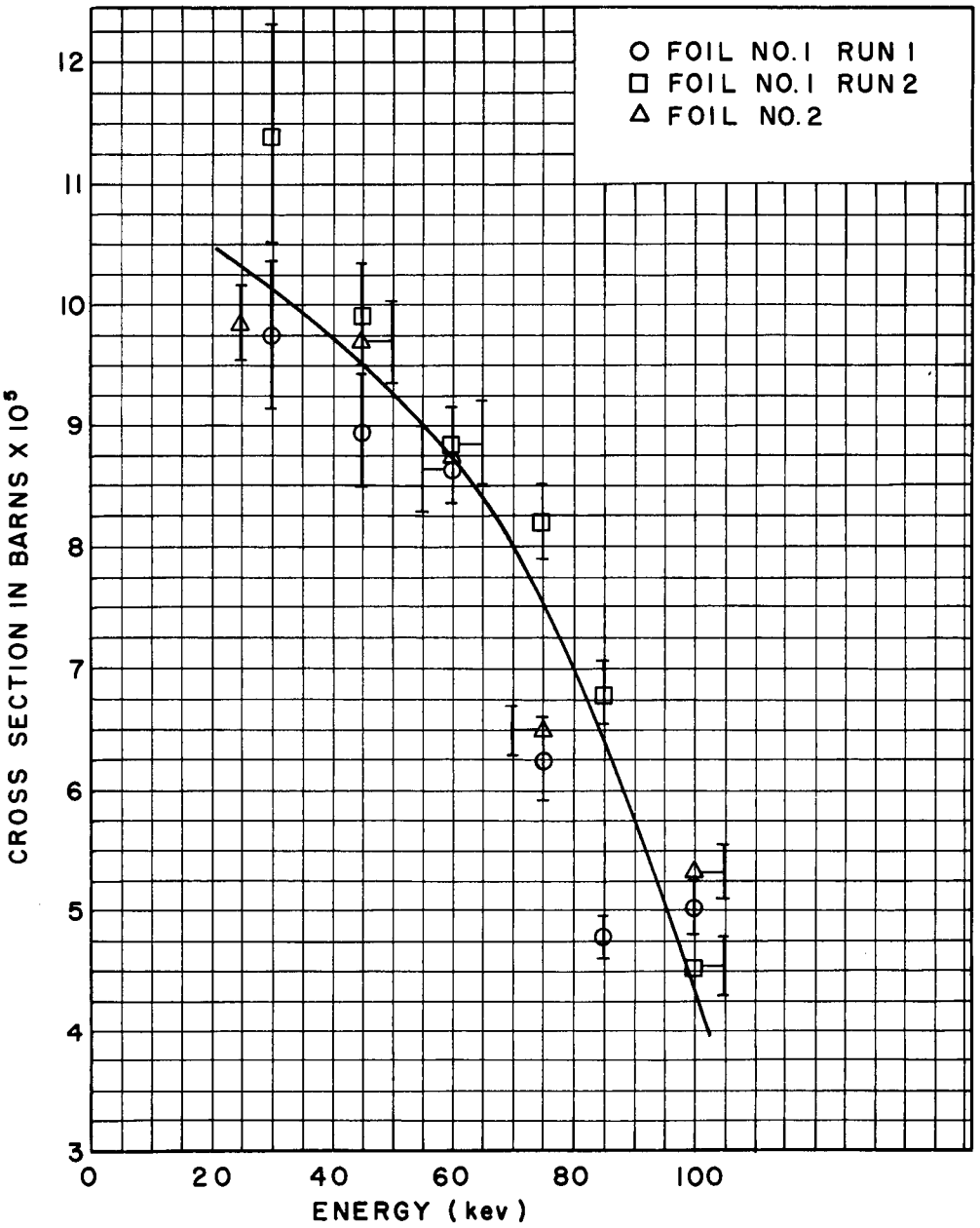

FIG.24-CROSS SECTION PER FREE ELECTRON IN ALUMINUM AS A FUNCTION OF INCIDENT ELECTRON ENERGY

Table 10

CROSS SECTION PER FREE ELECTRON IN MAGNESIUM AS A FUNCTION OF ELECTRON PRIMARY ENERGY

A. Foil Thickness Determined by Weighing

Primary Energy kev	Cross Section barns x 10^5	Probable Error %
Foil No. 1 85 $\mu g/cm^2$ = 4880A		
40	1.26 ± 0.05	3.6
50	1.15 ± 0.03	2.9
60	1.11 ± 0.03	3.0
75	1.18 ± 0.03	2.8
85	1.03 ± 0.03	3.1
100	1.05 ± 0.03	2.7
115	0.95 ± 0.04	4.4
Foil No. 2 72 $\mu g/cm^2$ = 4140A		
45	1.35 ± 0.06	4.1
60	1.95 ± 0.05	2.7
75	1.67 ± 0.05	3.0
85	1.60 ± 0.05	3.0
100	1.61 ± 0.08	4.7
115	1.60 ± 0.05	2.9

Table 10 (continued)

CROSS SECTION PER FREE ELECTRON IN MAGNESIUM AS A FUNCTION OF ELECTRON PRIMARY ENERGY

B. Foil Thickness Determined by Inverse Square Law

Primary Energy kev	Cross Section barns x 10^5	Probable Error %
Foil No. 1 8.1 $\mu g/cm^2$ = 465A		
40	13.3 ± 0.3	2.6
50	12.1 ± 0.2	1.6
60	11.6 ± 0.2	1.7
75	12.3 ± 0.2	1.3
85	10.8 ± 0.2	1.8
100	11.1 ± 0.1	1.1
115	10.0 ± 0.3	3.5
Foil No. 2 10.1 $\mu g/cm^2$ = 580A		
45	9.6 ± 0.3	3.3
60	13.8 ± 0.2	1.4
75	11.8 ± 0.2	1.7
85	11.3 ± 0.2	1.8
100	11.4 ± 0.5	4.0
115	11.3 ± 0.2	1.7

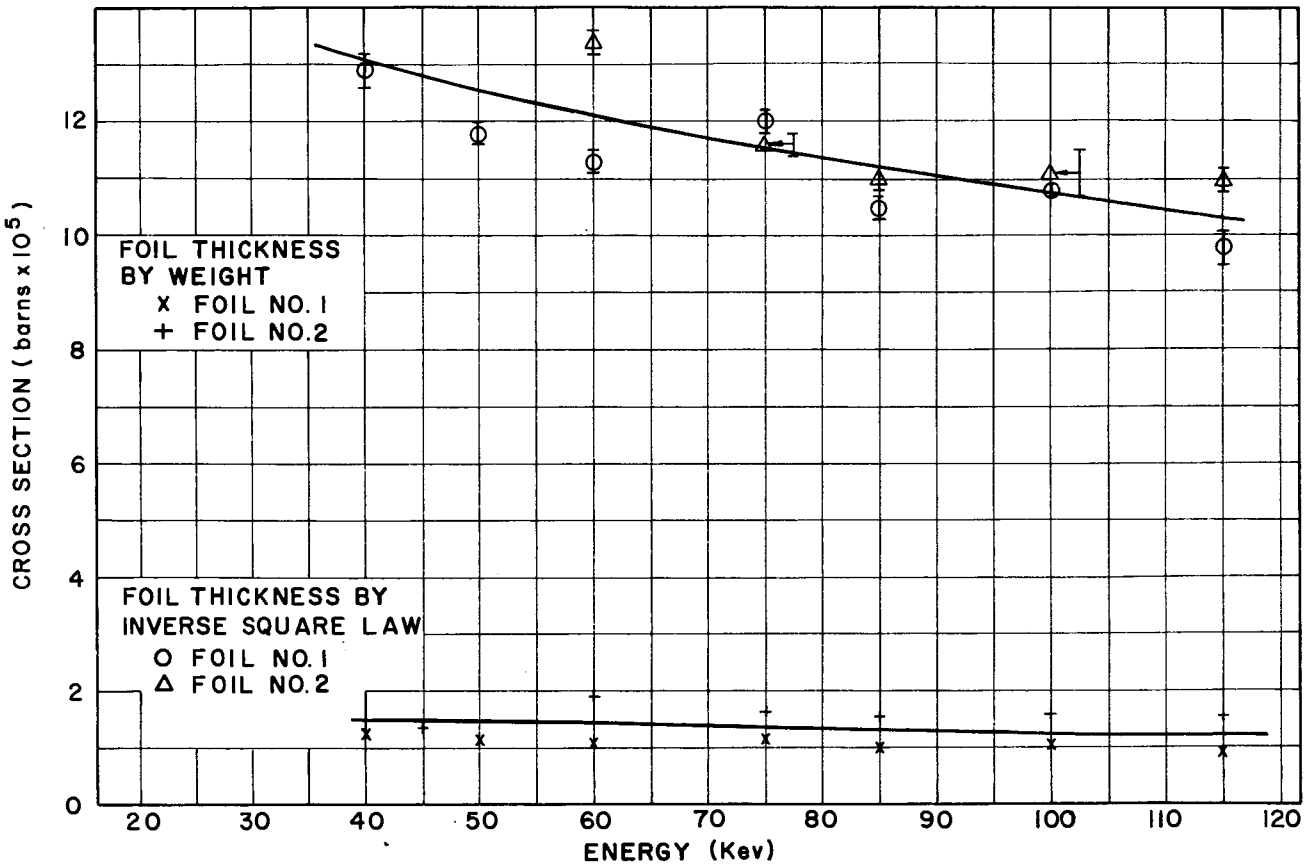

FIG. 25-CROSS SECTION PER FREE ELECTRON IN MAGNESIUM AS A FUNCTION OF INCIDENT ELECTRON ENERGY

Table 11

CROSS SECTION PER FREE ELECTRON IN COPPER AT VARIOUS ELECTRON INCIDENT ENERGIES

Incident Energy kev	Cross Section barns x 10^5	Probable Error %
Foil No. 1 66 $\mu g/cm^2$ = 742A		
45	2.5 ± 0.2	8.0
60	2.8 ± 0.1	4.7
75	2.5 ± 0.1	4.0
85	1.99 ± 0.06	3.2
100	2.49 ± 0.08	3.3
115	2.01 ± 0.06	3.0
Foil No. 2 81 $\mu g/cm^2$ = 910A		
60	3.9 ± 0.2	5.1
80	3.4 ± 0.2	5.8
100	3.3 ± 0.1	2.9

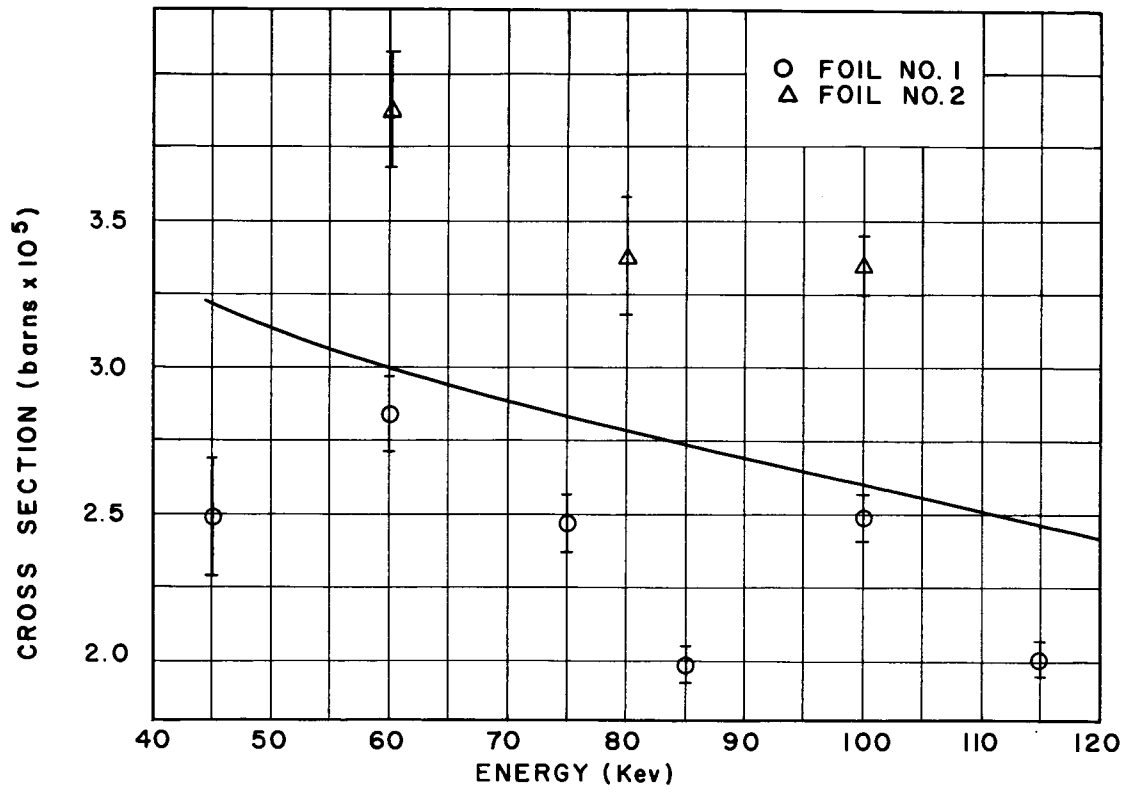

FIG. 26-CROSS SECTION PER FREE ELECTRON IN COPPER AS A FUNCTION OF INCIDENT ELECTRON ENERGY

Theory

Plasma oscillations were discussed as early as 1906 by Rayleigh in connection with the constitution of the atom. Plasma in its normal equilibrium state is characterized by a substantially equal density distribution of positive and negative charge so that the volume distribution of charge is practically zero. The positive charges are heavy and their motion can be neglected. Any disturbance in the plasma will primarily disturb the distribution of electrons and produce polarization in the medium. Tonks and Langmuir (1929) first derived the expression for the frequency of the electron plasma oscillations. However, a later derivation will be given here. Tonks and Langmuir (1929), Merrill and Webb (1939), Looney and Brown (1954), and others have observed such oscillations experimentally.

Weizsäcker (1933) attempted to determine the effect of the conduction electrons in a metal on the stopping process. He considered the electronic motion caused by the passage of the incident particle to be damped by a force proportional to the velocity of the electrons. The proportionality factor ω_σ is inversely proportional to the electrical conductivity σ of the medium and is given by

$$\omega_\sigma = \frac{ne^2}{m\sigma}$$

where n is the number of conduction electrons per unit volume and

m and e are the mass and charge of the electron. The stopping power for electrons obtained in this manner due to conduction electrons only is

$$\frac{dE}{dx} = \frac{4\pi ne^4}{mv^2} \ln \frac{2mv^2}{\hbar \omega_\sigma} \tag{5}$$

where v is the velocity of the incident electron. Thus $\frac{dE}{dx}$ depends on the factor ω_σ which in turn depends on the conductivity of the medium. Since the conductivity is a function of temperature, the stopping power should also change with the temperature of the bombarded medium.

Kronig and Korringa (1943) treated the problem by means of a classical hydrodynamical model of an electron gas. The conduction electrons were considered to constitute a negatively charged fluid flowing with respect to the fixed metallic ions which in turn exerted a frictional force on the fluid. An additional frictional force within the fluid was also assumed. The principal contribution of this treatment seems to have been the casting of doubt on the temperature dependent stopping power formula by Weizsäcker, for this treatment predicted no such dependence. Gerritsen (1946) measured the stopping power of aluminum and tin for alpha particles from room temperature down to liquid helium temperatures. No change in the range of the alpha particles with temperature was found within an experimental accuracy of 0.5%.

In the U.S.S.R. in 1945 Vlasov gave a discussion of the

kinetic theory of an assembly of particles with collective interaction and Landau (1946) gave a further discussion of vibrations of the electronic plasma.

In a later treatment of the problem Kramers (1947) used a macroscopic description in which the electrons were treated as a continuum characterized by an effective dielectric constant. He used the conventional form of the dielectric constant of an assembly of free stationary electrons and calculated the stopping power by means of classical electrodynamics. Both the polarizability of the medium and the damping effect of the collisions of the conduction electrons were considered. Using the quantum mechanical limit for the minimum impact parameter as did Weizsäcker, Kramer's expression for the stopping power for electrons is

$$\frac{dE}{dx} = \frac{4\pi ne^4}{mv^2} \ln \frac{2mv^2}{\hbar(\omega_p + \frac{\pi}{4}\omega_\sigma)} \tag{6}$$

where

$$\omega_p = \left(\frac{4\pi ne^2}{m}\right)^{1/2}$$

is the frequency of the electron plasma oscillations and all the other symbols have the same meaning as previously. The relative sizes of $\hbar\omega_p$ and $\hbar\omega_\sigma$ can be obtained for a representative metal such as aluminum. If three conduction electrons per atom are

assumed in aluminum, then

$$\hbar\omega_p = 15.8 \text{ ev}$$

$$\hbar\omega_\sigma = 0.088 \text{ ev}$$

and the term in ω_σ may be neglected. This affords an explanation of the fact that no temperature dependence of the stopping power was observed experimentally.

A. Bohr (1948) has given a microscopic description of the collisions between a charged particle and the individual electrons, both free and bound, in which the influence of the electron-electron interactions is taken into account explicitly. He obtained an expression for the characteristic frequency associated with the excitation of the conduction electron plasma. The electric field of the incident electron is given by

$$\underline{E} = \underline{D} - 4\pi\underline{P}$$

where $\underline{D}$ is the displacement and $\underline{P}$ is the polarization. The force experienced by a conduction electron is $\underline{E}e$ and may be considered to arise from the term $\underline{D}e$ which would exist in the absence of any polarization effects in the medium diminished by a term $4\pi e\underline{P}$ which represents the force on the electron due to the polarization produced by the incident particle. In effect the electric field is screened by the setting up of a dipole moment per unit volume $\underline{P}$. If there are n electrons per unit volume and each experiences a

displacement $\underline{X}$ due to the polarization force, then $\underline{P} = -ne\underline{X}$, and the force on the electron may be equated to $m\ddot{\underline{X}}$. Thus

$$m\ddot{\underline{X}} = 4\pi e\underline{P}$$

$$m\ddot{\underline{X}} = -4\pi ne^2\underline{X}$$

The square of the frequency of oscillation of the electron plasma is then given by

$$\omega_p^{\ 2} = \frac{4\pi ne^2}{m} \tag{7}$$

Kronig (1949) compared the results of Kronig and Korringa (1943) and Kramers (1947). He showed that for a suitable choice of the coefficient of viscosity in the stopping power formula of Kronig and Korringa agreement could be obtained with the Kramers expression if the quantum mechanical minimum impact parameter is used in the latter.

Bohm and Gross (1949) gave further discussions on the theory of plasma oscillations. An extensive treatment of collective interactions of electrons has been given in a series of four papers, Bohm and Pines (1951), Pines and Bohm (1952), Bohm and Pines (1953), and Pines (1953). The effect of the velocity of the conduction electrons on the stopping power has been included in this treatment. For $v^2 >> \overline{v_i^{\ 2}}$, where v is the velocity of the incident particle and $\overline{v_i^{\ 2}}$ is the mean square velocity of the electrons in the plasma,

Pines (1953) found for the stopping power due to conduction electrons in which only the plasma oscillations are excited

$$\frac{dE}{dx} = \frac{4\pi n Z^2 e^4}{mv^2} \ln \frac{\beta k_o v}{\omega_p} \tag{8}$$

where Ze is the charge of the incident particle. The quantity βk_o is equal to $\frac{1}{b}$, where b is the minimum impact parameter for collective interactions or plasma oscillations. According to Pines and Bohm, collisions with impact parameters greater than b can be best treated in terms of interactions between the incident particle and the collection of electrons constituting the plasma; collisions with impact parameters less than b can be better described in terms of individual particle interactions. For the minimum impact parameter Pines and Bohm use $b = \lambda_D$, the Debye length in the plasma.

The Debye length was originally introduced by Debye and Hückel (1923) as a screening distance in ionized electrolytes. A similar screening distance holds for an electron plasma if the positive charges in the medium are assumed to be at rest and spread out to a uniform density. An amount of work $-e\phi$ is required to move an electron into the medium to a point where the electrostatic potential is ϕ. Considering a volume element dv and a Maxwell-Boltzman distribution of electron energies, the number of electrons in dv is

$$n \epsilon^{e\phi / kT} dv$$

and the number of positive ions in dv is ndv. The charge density is then

$$\rho = ne(1 - \epsilon^{e\phi / kT})$$

which for $e\phi$ small compared with kT, the thermal energy of the electrons, becomes

$$\rho = -\frac{ne^2}{kT}\phi$$

Poisson's equation for the medium may be written

$$\Delta\phi = -4\pi\rho$$

which upon substituting for ρ becomes

$$\Delta\phi = \frac{4\pi ne^2}{kT}\phi$$

In polar coordinates the equation is

$$\frac{1}{r^2}\frac{d}{dr}\left(r^2\frac{d\phi}{dr}\right) = \frac{4\pi ne^2}{kT}\phi$$

which has a solution of the form

$$\phi = \frac{A\,\epsilon^{-r/\lambda_D}}{r}$$

where

$$\lambda_D^{\,2} = \frac{kT}{4\pi ne^2}$$

For a Maxwell-Boltzmann distribution this may be written

$$\lambda_D^2 = \frac{1}{3} \frac{\overline{v_i^2}}{\omega_p^2}$$

where $\overline{v_i^2}$ is the mean square velocity of the electrons in the medium. However, the conduction electrons constituting the plasma in a metal have a Fermi-Dirac distribution of energies. For this case Neufeld and Ritchie (1955) have shown that λ_D is given by

$$\lambda_D^2 = \frac{1}{3} \frac{v_F^2}{\omega_p^2} \tag{9}$$

where v_F is the electron velocity at the maximum Fermi energy at a temperature T = 0.

Thus

$$\beta k_o = \frac{1}{b} = \frac{1}{\lambda_D} = \sqrt{3} \frac{\omega_p}{v_F}$$

Substituting this expression for βk_o and setting Z = 1 for electrons as incident particles, equation (8) becomes

$$\frac{dE}{dx} = \frac{4\pi ne^4}{mv^2} \ln\left(\sqrt{3} \frac{v}{v_F}\right) \tag{10}$$

The maximum Fermi energy at T = 0 is given by, for instance, Slater (1939) p. 476, as

$$E_F = \frac{mv_F^2}{2} = \frac{h^2}{2m}\left(\frac{3n}{8\pi}\right)^{2/3}$$

whence

$$v_F = \frac{h}{2m}\left(\frac{3n}{\pi}\right)^{1/3} \tag{11}$$

The mean free path for the loss of a quantum of energy $\hbar\omega_p$ to the plasma is, using equation (10),

$$\lambda = \frac{\hbar\omega_p}{dE/dx} = \frac{\hbar\omega_p\, mv^2}{4\pi ne^4 \ln\left(\sqrt{3}\,\frac{v}{v_F}\right)} \tag{12}$$

The stopping power formula of Kramers, equation (6) includes not only collisions in which plasma oscillations are excited but also much closer collisions involving large transfers of energy. Since only small energy losses were observed in this experiment, comparison will be made with the Pines and Bohm theory.

Comparison of Experiment with Theory

The number of free electrons per cubic centimeter n is given by

$$n = \frac{N\rho f}{A} \tag{13}$$

where N is Avogadro's number, ρ is the density and A the atomic weight of the material and f is the number of free electrons per atom. If this expression for n is substituted in equation (7), the resultant expression for the energy loss quantum $\hbar\omega_p$ is

$$\hbar\omega_p = he\left(\frac{N\rho f}{\pi mA}\right)^{1/2} \text{ ergs} \tag{14}$$

Inserting the values of the constants in equation (14) and converting to ev there results

$$\hbar\omega_p = 28.8\left(\frac{\rho f}{A}\right)^{1/2} \text{ ev} \tag{15}$$

Pines and Bohm use the number of valence electrons for f in their calculations. The values of $\hbar\omega_p$ calculated for aluminum, magnesium, copper, and silver from equation (15) using the valence for f in each case are compared with the experimental energy losses ΔE in the following table:

Table 12

Metal	Valence	$\hbar\omega_p$ (ev) Calculated	ΔE (ev) Experimental
Al	3	15.8	14.9
Mg	2	10.9	10.6
Cu	1,2	10.8,15.3	22.6
Ag	1	9.0	23.8

Pines and Bohm calculated values of $\hbar\omega_p$ of 15.9 ev for aluminum and 10.8 ev for magnesium. The values in Table 12 agree rather well for Al and Mg, but not for Cu and Ag.

An alternative method of comparison is to calculate the number of free electrons per atom f from the observed energy loss and compare this value with the valence of the element. If equation (15) is solved for f and ΔE is substituted for $\hbar\omega_p$, there results

$$f = 1.21 \times 10^{-3} \frac{A}{\rho} (\Delta E)^2 \qquad (16)$$

where ΔE is in ev. This is a more sensitive check than comparing the values of the energy loss, since f depends on the square of ΔE. Thus any experimental error in the value of ΔE will be magnified in the value of f. The values of f for the four metals obtained from equation (16) are compared with the respective valences in Table 13.

Table 13

Metal	ΔE (ev) Observed	No. Free Electrons per Atom f	Valence
Al	14.9	2.69	3
Mg	10.6	1.90	2
Cu	22.6	4.39	1,2
Ag	23.8	7.05	1

Just as in Table 12, there is rather good agreement for Al and Mg, but not for Cu and Ag.

The experimentally determined values of the mean free path λ for the loss of a quantum of energy ΔE are compared with those given by the Pines and Bohm relation, equation (12). In order to facilitate the calculation of values of λ by means of equation (12), this equation will be modified somewhat. Using equation (7), replacing $\hbar\,\omega_p$ by ΔE and introducing the factor for converting ΔE from ev to ergs, there results

$$\lambda = \frac{6.25 \times 10^{11}}{\Delta E \ln\left(\sqrt{3}\,\frac{v}{v_F}\right)}\left(\frac{\hbar v}{e}\right)^2 \quad \text{cm} \tag{17}$$

Inserting the values of h and e and introducing the density ρ of the material and the factor to convert λ from g/cm^2 to μg/cm^2, equation (17) becomes

$$\lambda = \frac{3.02 \times 10^{-18}\,\rho\, v^2}{\Delta E \ln\left(\sqrt{3}\,\frac{v}{v_F}\right)} \quad \mu\text{g/cm}^2 \tag{18}$$

The density of the foil is assumed to be the same as that of the bulk metal. If equation (7) is solved for n and ΔE is substituted for $\hbar\,\omega_p$, the resultant expression is

$$n = \pi m\left(\frac{\Delta E}{he}\right)^2$$

If this expression for n is substituted in equation (11) that equation becomes

$$v_F = \frac{(3h)}{2}^{1/3} \left(\frac{\Delta E}{me}\right)^{2/3}$$

which, upon inserting the constants and introducing the conversion factor so that ΔE in ev can be inserted directly, becomes

$$v_F = 3.22 \times 10^7 \, (\Delta E)^{2/3} \text{ cm/sec} \tag{19}$$

The logarithmic term in equation (18) then becomes

$$\ln \left(\sqrt{3} \frac{v}{v_F}\right) = \ln \left[5.38 \times 10^{-8} v \, (\Delta E)^{-2/3}\right] \tag{20}$$

or alternatively

$$\ln \left(\sqrt{3} \frac{v}{v_F}\right) = \ln v - 16.74 - \frac{2}{3} \ln \Delta E \, . \tag{21}$$

The velocity of the incident electrons, v, is obtained from the relativistic equation

$$v = \beta c = \left[1 - \left(\frac{mc^2}{E + mc^2}\right)^2\right]^{1/2} c$$

Inserting the constants and the conversion factor so that E, the energy of the incident electron, can be introduced directly in kev

there results

$$v = 3.00 \times 10^{10} \left[1 - \left(\frac{8.20 \times 10^{-7}}{1.60 \times 10^{-9}\, E + 8.20 \times 10^{-7}} \right)^2 \right]^{1/2} \frac{\text{cm}}{\text{sec}} \qquad (22)$$

The value of v obtained from equation (22) is used with the observed value of ΔE in equation (20) or (21) to obtain the value of the logarithmic term. This in turn is used with ΔE, v and the density ρ of the material in equation (18) to determine the value of λ.

Values of λ for Al, Mg and Cu obtained from equation (18) for incident energies covering the range of experimental measurements are plotted in Figures 18, 19 and 20, respectively, with the experimental values of λ. The curves resulting from the points obtained from equation (18) are labeled "Pines and Bohm Theory."

Rather good agreement between the experimental values and those obtained from equation (18) is found in Fig. 18 for Al. However, the curve through the experimental points has a different slope at nearly every point from that obtained from equation (18).

If equation (18) is solved for v^2/λ, the result is

$$\frac{v^2}{\lambda} = \frac{3.31 \times 10^{17}\, \Delta E}{\rho} \ln\left(\frac{\sqrt{3}}{v_F}\, v \right)$$

This equation can be put in the form

$$\frac{v^2}{\lambda} = \frac{3.31 \times 10^{17}\, \Delta E}{\rho} \ln \frac{\sqrt{3}}{v_F} + \frac{3.31 \times 10^{17}\, \Delta E}{\rho} \ln v \qquad (23)$$

Since ρ, ΔE and, therefore, v_F are all constants for a particular element, equation (23) is of the form

$$\frac{v^2}{\lambda} = c \ln v + K$$

Therefore, if $\frac{v^2}{\lambda}$ is plotted versus ln v, the resulting graph should be a straight line. Values of $\frac{v^2}{\lambda}$ for Al resulting from equation (23), along with the experimental values, are plotted as a function of ln v in Fig. 27. The v_o of Fig. 27 is the same as v, the incident velocity of the electrons. The departure of the experimental points from a straight line is immediately evident.

Very poor agreement is found in Fig. 19 between the values of λ for Mg obtained from equation (18) and the experimental values obtained using the foil thickness determined by weighing the foils. Much better agreement exists between the theoretical values and the experimental values obtained using the foil thickness determined from the mass of metal evaporated assuming isotropic distribution. However, as has been stated before, the amount of magnesium in the foils determined independently by colorimetric analysis agreed within 30% with the amount obtained by weighing whereas it was several times that obtained assuming isotropic evaporation. Therefore the value of foil thickness obtained from foil weight is thought to be the more correct value. It may be recalled that the Formvar backings for the foils were placed on a rectangular piece, about 1-3/8" x 7/8", of thin stainless steel or aluminum sheet with a 5/8" circular hole in it. The metal was evaporated onto the backings and the electron beam

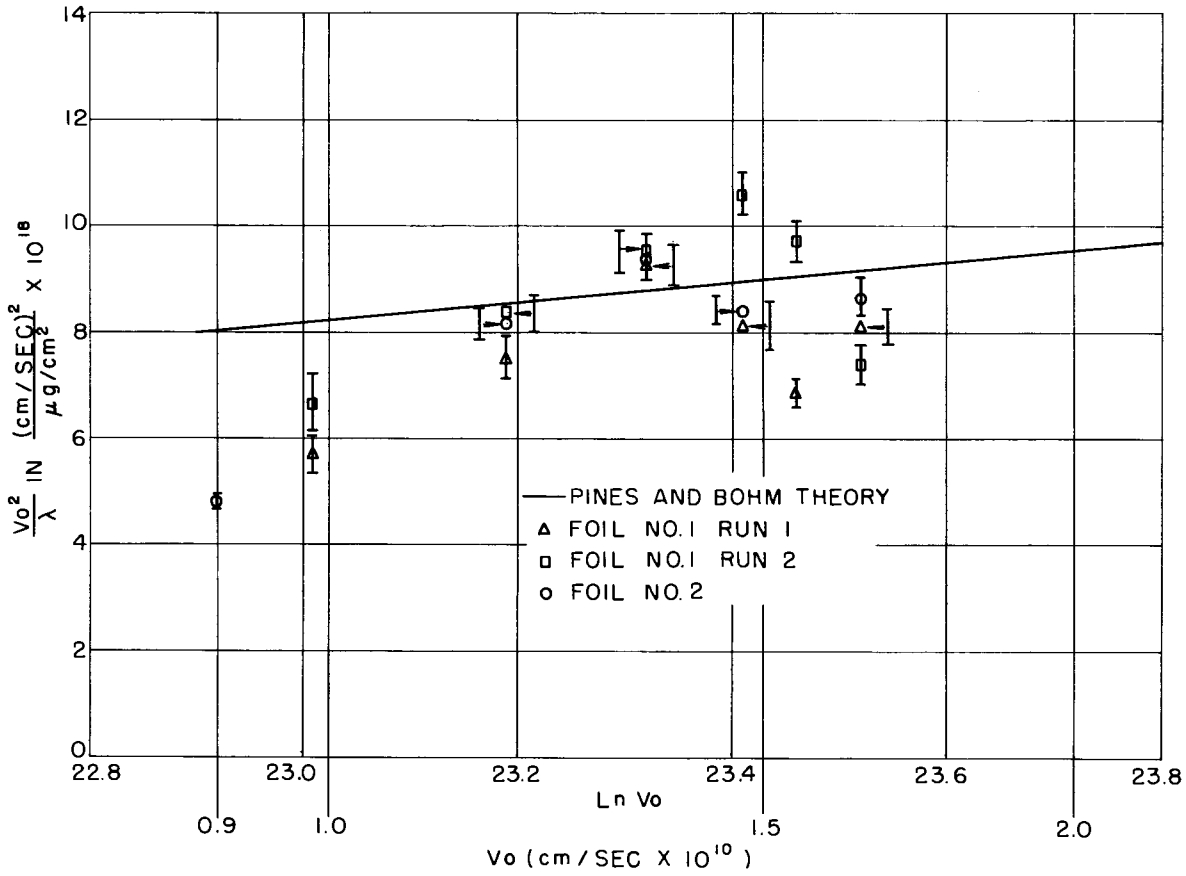

FIG.27-$\frac{Vo^2}{\lambda}$ AS A FUNCTION OF LnVo IN ALUMINUM

traversed that part of the foil within the 5/8" circle. It was noticed that, in the case of magnesium, there was always a ring of Formvar at the outer edge of the 5/8" circle adjacent to the stainless steel or aluminum frame on which there was no magnesium. The effect of this ring is to increase the number of electrons which pass through the foil with no energy loss, that is to increase the area under the no loss peak, A_o. Thus, since $\lambda/t = A_o/A_1$, the experimental value of λ is too large. This effect is a possible explanation for part of the difference between the experimental values of λ determined from foil weight and the theoretical values. However, it does not seem that this effect could account for the total difference since the area of the ring is much smaller than the area of the foil covered by Mg and, hence, the current through the former area should be much less than that through the latter.

Rather poor agreement is also found in Fig. 20 between the experimental values of λ for copper and those obtained from equation (18).

Other Considerations

It is of interest to see what magnitude of energy loss might be expected from elastic collisions between the incident electrons and the atoms or free electrons in the target. Suppose that an incident electron of mass m and initial velocity u collides elastically with a target particle of mass M initially at rest. The incident electron is scattered with a velocity v at an angle θ with the

initial direction of motion. The target particle recoils with a velocity V at an angle ϕ with the direction of motion of the incident electron. Using non-relativistic relations and applying the principles of conservation of momentum and kinetic energy the following equations relating the energy loss ΔE to the incident energy E are obtained:

$$\Delta E = \frac{4\ M\ m \cos^2 \phi}{(m + M)^2}\ E \tag{24}$$

$$\Delta E = \frac{2m}{(M + m)^2} \left[M + m \sin^2 \theta - \cos \theta \left(M^2 - m^2 \sin^2 \theta\right)^{1/2} \right] E \tag{25}$$

Consider first a collision between the incident electron and the target atom as a whole. For $M >> m$, equation (24) reduces to

$$\Delta E = \frac{4m}{M}\ E \cos^2 \phi \tag{26}$$

and equation (25) to

$$\Delta E = \frac{2m}{M} (1 - \cos \theta)\ E \tag{27}$$

It can be seen from equation (27) that ΔE increases with increasing E and θ, the scattering angle of the incident electron. If θ is taken to be 1.2°, the angle subtended at the foil by the largest

dimension of the entrance slit to the current collector, the energy lost by an electron with 115 kev initial energy, the largest incident energy used in the experiment, in an elastic collision with a magnesium atom is 0.0011 ev. This loss is, of course, far too small to be detected with the instrument used in this experiment. The energy losses will be even smaller in collisions with aluminum, copper and silver atoms since M is larger for each of these than for magnesium.

For a head-on collision $\phi = 0$ and $\theta = 180^{\circ}$; in this case both equations (24) and (25) reduce to the well known equation

$$\Delta E = \frac{4\ Mm}{(M + m)^2}\ E \tag{28}$$

which is the maximum energy loss the electron can experience in an elastic collision. For $M >> m$ the maximum energy loss from either equation (26), (27) or (28) is given by the equally well known relation

$$\Delta E = \frac{4m}{M}\ E \tag{29}$$

The maximum energy that an electron with 115 kev incident energy can lose in an elastic collision with a magnesium atom is 10.3 ev; with an aluminum atom, 9.3 ev; with a copper atom, 3.9 ev; and with a silver atom, 2.3 ev. However, in this case the incident electron will, of course, recoil in a direction opposite to that of its

original motion and will not enter the collector unless scattered again in the original direction.

In the case of a collision between the incident electron and a free electron, M = m and equations (24) and (25) become, respectively

$$\Delta E = E \cos^2 \phi \tag{30}$$

and

$$\Delta E = E \sin^2 \theta \tag{31}$$

As can be seen by comparing equations (30) and (31), the angle between the directions of motion of the two electrons after the collision is $\theta + \phi = 90^\circ$. Using E = 115 kev and $\theta = 1.2^\circ$, equation (31) gives 50.2 ev for the energy lost in a collision with a free electron. For a head-on collision with a free electron, both equations (28) and (30) with $\phi = 0$ yield, as is well known, $\Delta E = E$, a complete transfer of energy. In this case, since the incident electron comes to rest, there is no scattering angle θ.

From this non-relativistic treatment, it appears that there should be a continuous distribution of energy losses due to elastic collisions with free electrons in the target in the energy range in which the discrete losses were observed. As can be seen in Figs. 9 through 17, the discrete loss peaks are superimposed on a continuous distribution.

Inelastic collisions should also be considered. Inelastic collisions with target atoms will result in ionization or

excitation of the atoms. According to Ferrell (1955), electrons which suffer plasma losses are scattered through smaller angles than those which suffer equal losses in causing atomic excitations.

In order to determine whether or not the losses observed here correspond to transitions between atomic energy levels, a survey was made of the optical and X-ray levels in the four metals investigated. These data were taken from Fine and Hendee (1955), Hill, Church and Mihelich (1952), Moore (1949, 1952) Eucken (1950), Compton and Allison (1935), Bacher and Goudsmit (1932), and Washburn (1929). Pertinent data found are listed together with the observed energy losses in Table 14. Since the probability of an atom's being ionized to a degree higher than two by the bombarding electrons is relatively small and since the excitation energies will in general be larger for the higher ions, ions of degree greater than two were not considered. In the column headed "Excitation Energies", the lowest and highest excitation energies found for each ion are listed together with the intermediate values nearest the observed energy losses. Likewise only those absorption edges and lines with energies nearest the observed losses are listed for each series.

Of the energy levels found for Mg, the value closest to the value of the first discrete loss in Mg, 10.5 ev, is 10.35 ev, an excitation level for the neutral atom. The value 22.58 ev, the second ionization potential of the neutral atom, is the closest value found to the second discrete loss in Mg, 21.5 ev. None of the values found are very close to the third loss, 31.6 ev.

Table 14

Comparison of Transitions between Atomic Energy Levels

with the Observed Energy Losses

Ion	Excitation Energy	Ionization Energy	Lowest Energy Lines		Absorption Edges						Observed Energy Losses
			K	L	K	L_{III}	M_I	M_{II}	M_{III}	M_{IV}	
	ev	ev	kev	ev	kev	ev	ev	ev	ev	ev	ev
Mg	2.71 10.35	7.64 22.58	1.25	39.1	1.30	49.5	7.65	6.80			10.5 21.5 31.6
Mg^+	4.42 10.00 11.51 14.65	15.03									
Mg^{++}	52.8 78.2	80.12									
Al	3.14 9.94	5.98	1.49	42.8	1.56	72.7		5.44			14.8 30.0 44.2 59.8
Al^+	4.64 14.89 18.7	18.82									
Al^{++}	6.66 14.39 15.56 26.9	28.44									
Cu	1.39 10.1	7.72	8.03	810.	8.98	933			74.7	3.81	22.6

Table 14 (continued)

Comparison of Transitions between Atomic Energy Levels

with the Observed Energy Losses

Ion	Excitation Energy	Ionization Energy	Lowest Energy Lines			Absorption Edges						Observed Energy Losses
			K	L	M	K	L_{III}	M_V	N_{II} N_{IV} N_V (1)	III (2)	Y_I Y_{II}	
	ev	ev	kev	kev	ev	kev	kev	ev	ev	ev	ev	ev
Cu^+	2.72 19.02	20.29										22.6
Cu^{++}	7.54 19.1 24.0 24.6	36.8										
Ag	3.68 11.2	7.58	22.0	2.64	73.8	25.5	3.36	369	58.2 6.1 4.9	80 29 26	31.5 2.18	23.8
Ag^+	4.86 19.8	21.38										
Ag^{++}	7.83 17.8	35.9										

(1) Eucken (1950)

(2) Hill, Church and Mihelich (1952)

For aluminum, the value found closest to the quantum energy loss, 14.87 ev, is 14.89 ev, an excitation level in the singly ionized atom. The value closest to the second discrete loss, 30.0 ev, is 28.44 ev, the ionization energy of the doubly ionized atom. The value 42.75 ev for the $L_I - L_{II\ III}$ transition is the one found nearest the third loss, 44.2 ev. This amount of energy could not be absorbed, however, unless there were a vacancy in the L_{II} or L_{III} shell. None of the energies found are very near the fourth discrete loss, 59.8 ev.

The value 24.0 ev, an excitation level in the doubly ionized copper atom, is the value found nearest to the discrete loss in copper, 22.6 ev.

The value found nearest the discrete loss in silver, 23.8 ev, is 26 ev, the value given for the N_V absorption edge by Hill, Church and Mihelich (1952); however, Eucken (1950) gives 4.9 ev for this edge.

It must be remembered, however, that the optical spectra were measured with the metals in the gaseous state, in which state the atoms are essentially free. As is well known, when atoms are combined in a metal, the outer energy levels containing the valence electrons broaden to form the conduction bands which contain many levels. It is therefore difficult to correlate energy transitions involving the outer levels in a free atom with those in an atom bound in a lattice. With two exceptions all the energy values which were near the discrete loss values were taken from optical data and

are transitions involving the outer levels. The two exceptions are the value 42.75 ev for the L_I - $L_{II\ III}$ transition in Al, which is near the third discrete loss in Al, 44.2 ev, and the value 26 ev for the N_V absorption edge in Ag, which is near the single loss in Ag, 23.8 ev. Therefore, with these two possible exceptions, none of the discrete losses observed can be definitely identified with transitions between the atomic energy levels. Moreover, as has been stated previously, there is disagreement on the value of the N_V absorption edge in Ag; Hill, Church and Mihelich (1952) give the value 26 ev whereas Eucken (1950) gives 4.9 ev.

Diffraction effects should also be considered. The de Broglie wave length of the incident electrons is given by

$$\lambda = \frac{h}{p}$$

where the momentum p is given by the relativistic relation

$$p = \frac{1}{c}\left[E\ (E + 2mc^2)\right]^{1/2}$$

where E is the incident energy and m the rest mass of the electron. For E = 25 kev, the lowest incident energy used, $\lambda = 7.70 \times 10^{-2}$ A and for E = 115 kev, the highest primary energy used, $\lambda = 3.43 \times 10^{-2}$ A. In order for Bragg reflection to occur from the crystal planes, λ must satisfy the relation

$$n\ \lambda = 2d \sin \theta \qquad (32)$$

If the beam is parallel to the axis of the accelerator upon striking the foil, the maximum angle θ at which electrons can be reflected and still be accepted by the collector is $\theta = \frac{\phi}{2} = 0.3^{\circ}$, where ϕ is half the angle subtended at the foil by the largest dimension of the entrance slit to the collector, the whole angle being 1.2°. According to Wyckoff (1951) the lattice spacings of Mg are 3.20 and 5.20 A and of Ag, Al and Cu are 4.08, 4.04 and 3.61 A, respectively. The minimum atomic separations are 3.20, 2.88, 2.86 and 2.55 A, respectively. Ag, Al and Cu have face centered cubic structures and Mg has a hexagonal close packed structure. Bragg reflection can occur from planes with spacings smaller than the minimum atomic separation, but the intensity of the reflected beam decreases as the plane spacing decreases, since the planes with smaller spacings contain fewer atoms. From equation (32), θ decreases as λ decreases and as d increases. Taking n = 1 for the first order, $\lambda = 3.43 \times 10^{-2}$ A, the smallest value of λ in the primary energy range 25 to 115 kev, and d = 4A, the value of θ obtained from equation (32) is 0.246°. Hence, for these conditions, a part of the maximum nearest the central maximum will enter the collector, since the collector will accept electrons reflected at angles θ up to 0.3°. If electrons in the beam make an angle as great as $3\phi = 1.8^{\circ}$ with the axis of the accelerator when striking the foil, those suffering Bragg reflections at angles as great as $\theta = 2\phi = 1.2^{\circ}$ can enter the collector. This analysis indicates that maxima other than the central maximum can enter the collector. The problem is complicated by the fact that the focussing properties

of the decelerator are not accurately known. If the observed energy losses were due to diffraction effects, it would seem that the separation of the loss peaks would vary with incident electron energy. However, the separation of the peaks was found to remain constant over the range of bombarding energies used, 25 to 115 kev.

In this connection, attempts were made to see whether or not there is a resonance effect in which there is excitation of oscillations with the de Broglie wave length between the crystal planes. If the crystallites have a preferred orientation, this effect might be expected to result in a change in the separation of the discrete loss peaks as the foil is rotated to angles other than 90° with the incident beam. However, no change in the peak separations was observed in aluminum when the foil was rotated to positions making angles of 45° and 60° with the incident beam. The normal foil position is perpendicular to the incident beam.

Calculations

In order to show how the calculations were made, the calculation of each quantity for aluminum foil No. 2 and 100 kev incident electron energy will be shown here. The method of calculation is the same for other incident energies and for the other foils.

Three values of the weight of the Al foil plus the Zapon backing obtained from three separate weighings are 46, 48 and 47 μg. The mean value of the weight is 47.0 ± 0.3 μg. The results of three weighings of each of two Zapon films prepared at the same time and

under the same conditions as the foil backing are 16, 13 and 17 μg and 19, 17 and 19 μg. The mean of these values is 16.8 ± 0.5 μg. The difference between the weight of the aluminum plus the Zapon and the weight of the Zapon is 30.2 ± 0.6 μg. The area of the foil is the area within a 5/8 inch circle, which is 1.98 cm^2. The foil thickness in $\mu g/cm^2$ is then

$$t = \frac{30.2\ \mu g}{1.98\ cm^2} = 15.3 \pm 0.5\ \mu g/cm^2$$

The foil thickness was also calculated from the mass of metal evaporated assuming isotropic distribution from the relation

$$t = \frac{mh}{4\pi r^3}$$

where m is the mass of metal evaporated, h is the perpendicular distance between the source of evaporation and the plane of the foil and r is the distance from the source to the foil. Aluminum foil No. 2 was vertically above the source so that h = r and the relation becomes

$$t = \frac{m}{4\pi h^2}$$

The mass of metal evaporated was 58.4 mg and h = 17.1 cm so that

$$t = \frac{5.84 \times 10^4\ \mu g}{4\pi(17.1\ cm)^2} = 15.9\ \mu g/cm^2$$

There is a difference of 3.8% between the two values.

Three values of the area A_o under the no loss peak from three different measurements with a planimeter are 1.46, 1.49 and 1.47 sq. in., the mean value of which is 1.47 sq. in. Three measurements of the area A_1 under the first loss peak are 0.67, 0.65 and 0.66 sq. in., the mean value of which is 0.66 sq. in. A value of t/λ is given by

$$\frac{t}{\lambda} = \frac{A_1}{A_o} = \frac{0.66}{1.47} = 0.449$$

Since three loss peaks were observed at 100 kev in Al foil No. 2, two other values of t/λ can be obtained from the ratios $\frac{A_2}{A_o}$ and $\frac{A_2}{A_1}$, where A_2 is the area under the second loss peak. The last (third) loss peak is not used since its area is too small and it is difficult to extrapolate its trailing edge properly. Two other distribution curves were used, each yielding three more values of t/λ, making a total of nine values. The mean of all values of t/λ is 0.491 ± 0.014.

The mean free path λ in $\mu g/cm^2$ is given by

$$\lambda = \frac{t}{t/\lambda} = \frac{15.3\ \mu g/cm^2}{0.491} = 31.2 \pm 1.3\ \mu g/cm^2$$

Assuming the foil density ρ is the same as that of bulk aluminum, 2.70 g/cm^3, the value of λ in Angstroms is

$$\lambda = \frac{31.2 \times 10^{-6}\ g/cm^2}{\rho} = \frac{31.2 \times 10^{-6}\ g/cm^2}{2.70\ g/cm^3} = 1160 \pm 50\ A$$

The stopping power $\frac{dE}{dx}$ is given by

$$\frac{dE}{dx} = \frac{\Delta E}{\lambda} = \frac{14.9\ ev}{31.2\ \mu g/cm^2} = 0.48 \pm 0.02\ \frac{ev}{\mu g/cm^2}$$

The cross section per free electron is given by equation (4) as

$$\sigma = \frac{1}{\pi m \lambda} \left(\frac{eh}{\Delta E}\right)^2$$

Inserting the values of the constants, the conversion factor so that ΔE can be introduced in ev, and converting to barns, there results

$$\sigma = \frac{1.38 \times 10^3}{\lambda\ (\Delta E)^2}\ \text{barns}$$

Inserting the values of ΔE and λ for Al and 100 kev incident energy,

$$\sigma = \frac{1.38 \times 10^3}{11.6 \times 10^{-6}\ (14.9)^2} = (5.4 \pm 0.2) \times 10^5\ \text{barns}$$

The theoretical value of λ is obtained from equation (18). But the value of the incident electron velocity must be calculated first. From equation (22) for E = 100 kev

$$v = 3.00 \times 10^{10} \left[1 - \left(\frac{8.20 \times 10^{-7}}{1.60 \times 10^{-9} \times 100 + 8.20 \times 10^{-7}} \right)^2 \right]^{1/2}$$

$$v = 1.64 \times 10^{10} \text{ cm/sec}$$

The logarithmic term in equation (18) is given by either equation (20) or (21). Choosing equation (20),

$$\ln \left(\sqrt{3} \frac{v}{v_F} \right) = \ln \left[5.38 \times 10^{-8} \times 1.64 \times 10^{10} \, (14.9)^{-2/3} \right]$$

$$\ln \left(\sqrt{3} \frac{v}{v_F} \right) = 4.98$$

Substituting these values together with the value of the density ρ in equation (18) there results

$$\lambda = \frac{3.02 \times 10^{-18} \times 2.70 \times (1.64 \times 10^{10})^2}{14.9 \times 4.98}$$

$$\lambda = 29.7 \ \mu g/cm^2$$

The values of v^2/λ for Fig. 27 were obtained simply by dividing the values v^2 by the values of λ. The experimental value at 100 kev is

$$\frac{v^2}{\lambda} = \frac{(1.64 \times 10^{10})^2}{31.2} = (8.6 \pm 0.4) \times 10^{18} \frac{(\text{cm/sec})^2}{\mu\text{g/cm}^2}$$

The theoretical value is

$$\frac{v^2}{\lambda} = \frac{(1.64 \times 10^{10})^2}{29.7} = 9.06 \times 10^{18} \frac{(\text{cm/sec})^2}{\mu\text{g/cm}^2}$$

V. SUMMARY OF FINDINGS AND CONCLUSIONS

Summary of Findings

The discrete energy losses found in the four metals are listed in the following table. The magnitude of these losses was found to be independent of primary energy and foil thickness. The number of losses observed in Al increased with increasing foil thickness. The mean values of the difference between successive losses in Al and Mg and the mean values of the single losses in Cu and Ag are listed in the column headed "Quantum Losses".

Table 15

Metal	Energy Losses (ev)				Quantum Losses (ev)
Al	14.8	30.0	44.2	59.8	14.87 ± 0.04
Mg	10.5	21.5	31.6		10.60 ± 0.03
Cu		22.6			22.6 ± 0.1
Ag		23.8			23.8 ± 0.2

The values of the mean free path for the loss of a quantum of energy at the lowest and highest incident electron energies used are listed in Table 16. The mean free path increases with increasing primary energy. Mg(a) designates the values for Mg obtained from the foil thickness determined from foil weight. Mg(b) refers to the values for Mg determined from the foil thickness calculated assuming isotropic evaporation.

Table 16

Metal	Incident Energy kev	Mean Free Path $\mu g/cm^2$	A
Al	25	16	590
	100	34	1250
Mg (a)	40	150	8600
	115	180	10300
Mg (b)	40	12	690
	115	20	1150
Cu	45	70	790
	115	100	1120

In Table 17 are listed the extreme values of the stopping power. Mg(a) and Mg(b) have the same meaning as in Table 16. The stopping power decreases with increasing primary energy.

Table 17

Metal	Primary Energy (kev)	Stopping Power $\left(\frac{ev}{\mu g/cm^2}\right)$
Al	25	0.93
	100	0.45
Mg (a)	40	0.08
	115	0.06
Mg (b)	40	0.66
	115	0.54
Cu	45	0.30
	115	0.23

Table 18 lists the extreme values of the cross section per free electron. Mg(a) and Mg(b) have the same meaning as in Table 16. The cross section also decreases with increasing primary energy.

Table 18

Metal	Incident Energy (kev)	Cross Section (barns x 10^5)
Al	25	10.3
	100	5.0
Mg (a)	40	1.5
	115	1.2
Mg (b)	40	13
	115	10
Cu	45	3.2
	115	2.5

Conclusions

The observed discrete energy losses suffered by electrons traversing thin foils cannot be identified with transitions between the atomic energy levels of the element. The quantum energy losses and the number of free electrons per atom in magnesium and aluminum agree well with those predicted by the plasma oscillation theory. Both the single discrete loss and the number of free electrons per atom in copper and silver disagree with the plasma oscillation theory. Pines (1953) states that the valence electrons in Cu and Ag are probably not sufficiently free to take part in undamped collective

motion. The broad single peaks observed in Cu and Ag are in contrast to the sharp peaks found in Mg and Al. Wolff (1953) has suggested that this broadening may be due to strong coupling between electrons in overlapping s and d conduction bands which makes possible a rapid transfer of energy from a plasma oscillation in the s band to a single d electron, thus leading to a short life and large energy width for the oscillations in accordance with the uncertainty principle. Based on this interpretation he predicts that the widths of the absorption peaks should increase in Sc through Ni as the 3d shell is filled. However, the band widths estimated in Ti, Cr, Mn, Fe, Co and Ni by Marton and Leder (1954) "indicate that this may not be the case." According to Wolff, a shift in the plasma energy of the order of 10 ev toward higher energy due to interaction with the 3d electrons is also to be anticipated in Cu and Ag. If 10 ev is subtracted from the magnitudes of the discrete energy losses in Cu and Ag, 22.6 and 23.8 ev, respectively, the resulting values agree better with the plasma energies calculated assuming the number of free electrons per atom equals the number of valence electrons. The quantity for Cu to be compared with 10.8 and 15.3 ev, for valence 1 and 2, respectively, is then 12.6 ev; for Ag, the loss 13.8 ev is then to be compared with 9.0 ev for valence 1.

The mean free path for loss of a quantum of energy in aluminum agrees within experimental error with that predicted by the plasma oscillation theory. The mean free path in magnesium determined from the foil thickness obtained from foil weight is in wide

disagreement with the plasma oscillation theory. Rather large disagreement is found between the mean free path in copper and that predicted by the plasma oscillation theory.

The agreement of the discrete energy losses in Mg and Al and the mean free path in Al with the plasma oscillation theory does not constitute a unique proof of this theory. Evidently there are aspects of the phenomenon which are not covered by this theory.

BIBLIOGRAPHY

American Magnesium Corporation. 1923. Magnesium - a handbook. American Magnesium Corporation, Niagara Falls.

Allison, S. K., Frankel, S. P., Hall, T. A., Montague, J. H., Morrish, A. H., and Warshaw, S. D. 1949. Construction and calibration of a cylindrical electrostatic analyzer. Rev. Sci. Instr. 20: 735-44.

Allison, S. K., Skaggs, L. S., and Smith, N. M. 1938. A precise measurement of the energy change in the transmutation of beryllium into lithium by proton bombardment. Phys. Rev. 54: 171-75.

Bacher, R. F., and Goudsmit, S. 1932. Atomic energy states. McGraw-Hill Book Company, Inc., New York.

Backus, J. 1945. The beta-ray spectra of Cu^{64} at low energies. Phys. Rev. 68: 59-63.

Bainbridge, K. T., and Jordan, E. B. 1936. Mass spectrum analysis. Phys. Rev. 50: 282-96.

Bayard, R. T., and Yntema, J. L. 1955. Scattering of 0.6-, 1.0-, and 1.7- Mev electrons from aluminum and gold. Phys. Rev. 97: 372-79.

Beck, A. 1943. The technology of magnesium and its alloys. F. A. Hughes and Company Limited, London.

Bergstein, J., and Birkhoff, R. D. 1953. Performance of a 125- kev accelerator and spectrometer. Phys. Rev. 91: 223.

Blackstock, A. W., Birkhoff, R. D., and Slater, M. 1954. Discrete electron energy losses in thin foils. Phys. rev. 95: 303.

_____. 1955. Electron accelerator and high resolution analyzer. Rev. Sci. Instr. 26: 274-75.

Bohm, D., and Gross, E. P. 1949. Theory of plasma oscillations. A. Origin of medium-like behavior. Phys. Rev. 75: 1851-64.

_____. 1949. Theory of plasma oscillations. B. Excitation and damping of oscillations. ibid. pp. 1864-76.

Bohm, D., and Pines, D. 1951. A collective description of electron interactions. I. Magnetic interactions. Phys. Rev. 82: 625-34.

_____. 1953. A collective description of electron interactions. III. Coulomb interactions in a degenerate electron gas. ibid. 92: 609-25.

Bohr, A. 1948. Atomic interaction in penetration phenomena. Kgl. Danske Videnskab. Selskab, Mat.-fys. Medd. 24: No. 19: 1-52.

Bond, W. L. 1954. Notes on solution of problems in odd job vapor coating. J. Opt. Soc. Amer. 44: 429-38.

Cauchois, Y. 1952. Etude comparée du spectre K d'absorption de l'aluminum métallique. Acta Cryst. 5: 351-56.

Chase, C. T., and Cox, R. T. 1940. The scattering of 50-kilovolt electrons by aluminum. Phys. Rev. 58: 243-51.

Chen, J. J. L. 1950. Test of rupture strength of thin plastic films. Rev. Sci. Instr. 21: 491-92.

Compton, A. H., and Allison, S. K. 1935. X-rays in theory and experiment. D. Van Nostrand Company, Inc., New York.

Debye, P., and Hückel, E. 1923. Zur theorie der elektrolyte. Physik. Z. 24: 185-206.

Dempster, A. J. 1937. Electric and magnetic focusing in mass spectroscopy. Phys. Rev. 51: 67-69.

Eucken, A. 1950. Landolt-Börnstein; zahlenwerte und functionen. I. band 1. teil. Springer-Verlag, Berlin.

Ferrell, R. A. 1955. Angular dependence of the characteristic energy loss of electrons passing through metal foils. Bull. Am. Phys. Soc. 30, No. 3: 47.

Fine, S., and Hendee, C. F. 1955. X-ray critical-absorption and emission energies in kev. Nucleonics 13, No. 3: 36-37.

Fowler, W. A., Lauritsen, C. C., and Lauritsen, T. 1947. Electrostatic analyzer for 1.5 Mev protons. Rev. Sci. Instr. 18: 818-20.

Franck, J., and Hertz, G. 1914. Über zusammenstösse zwischen elektronen und den molekülen des quecksilberdampfes und die ionisierungsspannung desselben. Verh. Deut. Phys. Ges. 16: 457-67.

Gerritsen, A. N. 1946. An attempt to measure the influence of the temperature on the stopping power of a metal for polonium α-particles. Physica 12: 311-20.

Glass, F. M. 1952. A simple low-drift electrometer. Nucleonics 10, No. 2: 36-39.

Hamilton, D. R., and Gross, L. 1950. An electrostatic beta spectrograph. Rev. Sci. Instr. 21: 912-17.

Hanson, A. O. 1944. Voltage-measuring and control equipment for electrostatic generators. Rev. Sci. Instr. 15: 57-63.

Haworth, L. J. 1935. The energy distribution of secondary electrons from molybdenum. Phys. Rev. 48: 88-95.

Herzog, R. 1934. Ionen- und elektronenoptische zylinderlinsen und prismen. I. Z. Physik 89: 447-73.

Hill, R. D., Church, E. L., and Mihelich, J. W. 1952. The determination of gamma-ray energies from beta-ray spectroscopy and a table of critical X-ray absorption energies. Rev. Sci. Instr. 23: 523-28.

Hillier, J., and Baker, R. F. 1944. Microanalysis by means of electrons. J. Appl. Phys. 15: 663-75.

Hughes, A. L., and McMillen, J. H. 1929. Re-focussing of electron paths in a radial electrostatic field. Phys. Rev. 34: 291-95.

Hughes, A. L., and Rojansky, V. 1929. On the analysis of electronic velocities by electrostatic means. Phys. Rev. 34: 284-90.

Hunt, S. E. 1952. Some absolute determinations of proton-gamma resonances in the energy range below 500 kev. Proc. Phys. Soc. (London) 65: 982-92.

Kramers, H. A. 1947. The stopping power of a metal for alpha particles. Physica 13: 401-12.

Kronig, R. 1949. A note on the stopping of fast charged particles in metallic conductors. Physica 15: 667-70.

Kronig, R., and Korringa, J. 1943. Zur theorie der bremsung schneller geladener teilchen in metallischen leitern. Physica 10: 406-18.

Landau, L. 1946. On the vibrations of the electronic plasma. J. Phys. U.S.S.R. 10: 25-34.

Lander, J. J. 1953. Auger peaks in the energy spectra of secondary electrons from various materials. Phys. Rev. 91: 1382-87.

Lang, W. 1948. Geschwindigkeitsverluste mittelschneller elektronen beim durchgang durch dünne metallfolien. Optik 3: 233-46.

Leder, L. B., and Marton, L. 1954. Effect of chemical combination on the characteristic energy loss of electrons. Phys. Rev. 95: 1345-46.

Looney, D. H., and Brown, S. C. 1954. The excitation of plasma oscillations. Phys. Rev. 93: 965-69.

Marton, L., and Leder, L. B. 1954. Energy loss of electrons in passage through thin films. Phys. Rev. 94: 203-204.

Mattauch, J., and Herzog, R. 1934. Über einen neuen massenspektrographen. Z. Physik 89: 786-95.

Merrill, H. J., and Webb, H. W. 1939. Electron scattering and plasma oscillations. Phys. Rev. 55: 1191-98.

Möllenstedt, G. 1949. Die elektrostatische linse als hochauflösender geschwindigkeitsanalysator. Optik 5: 499-517.

_____. 1952. Diskrete energieverluste von 35-kev electronen bei wechselwirkung mit atomen und molekülen. Z. Naturforsch. 7a: 465-70.

Moore, C. E. 1949. Atomic energy levels. National Bureau of Standards Circular 467, Vol. I, Washington.

_____. 1952. ibid, Vol. II.

Neufeld, J., and Ritchie, R. H. 1955. Passage of charged particles through plasma. Phys. Rev. (to be published).

Pannell, E. V. 1948. Magnesium; its production and use. Sir Isaac Pitman and Sons, Ltd., London.

Parratt, L. G. 1954. Surface studies of solids by total reflection of X-rays. Phys. Rev. 95: 359-69.

Phillips, J. A. 1953. The energy loss of low energy protons in some gases. Phys. Rev. 90: 532-37.

Pines, D. 1953. A collective description of electron interactions: IV. Electron interaction in metals. Phys. Rev. 92: 626-36.

Pines, D., and Bohm, D. 1952. A collective description of electron interactions: II. Collective vs individual particle aspects of the interactions. Phys. Rev. 85: 338-53.

Rayleigh, Lord. 1906. On electrical vibrations and the constitution of the atom. Phil. Mag. 11: 117-23.

Reichertz, P. P., and Farnsworth, H. E. 1949. Inelastic scattering of low speed electrons from a copper single crystal. Phys. Rev. 75: 1902-08.

Ritchie, R. H. 1955. Private communication.

Rogers, M. M., McReynolds, A. W., and Rogers, F. T. 1940. A determination of the masses and velocities of three radium B beta-particles. Phys. Rev. 57: 379-83.

Rudberg, E. 1930. Characteristic energy losses of electrons scattered from incandescent solids. Proc. Roy. Soc. (London) A127: 111-40.

_____. 1936. Inelastic scattering of electrons from solids. Phys. Rev. 50: 138-50.

Ruthemann, G. 1941. Diskrete energieverluste schneller elektronen in festkörpern. Naturwiss. 29: 648.

_____. 1942. Elektronenbremsung an röntgenniveaus. ibid. 30: 145.

_____. 1948. Diskrete energieverluste mittelschneller elektronen beim durchgang durch dünne folien. Ann. Physik 2: 113-34.

_____. 1948. Elektronenbremsung an röntgenniveaus. ibid. pp. 135-46.

Slater, J. C. 1939. Introduction to chemical physics. McGraw-Hill Book Company, Inc., New York.

Tonks, L., and Langmuir, I. 1929. Oscillations in ionized gases. Phys. Rev. 33: 195-210.

Turnbull, J. C., and Farnsworth, H. E. 1938. The inelastic scattering of slow electrons from a silver single crystal. Phys. Rev. 54: 509-14.

Vlasov, A. 1945. On the kinetic theory of an assembly of particles with collective interaction. J. Phys. U.S.S.R. 9: 25-40.

Warren, R. E., Powell, J. L., and Herb, R. G. 1947. Electrostatic analyzer for selection of homogeneous ion beam. Rev. Sci. Instr. 18: 559-63.

Washburn, E. W. 1929. International critical tables. Vol's. V and VI. McGraw-Hill Book Company, Inc., New York.

Watanabe, H. 1954. Energy losses of electrons passing through an MgO foil. Phys. Rev. 95: 1684-86.

_____. 1954. On the velocity analysis of electrons scattered by thin foils. J. Phys. Soc. Japan. 9: 920-28.

_____. 1954. Multiple lines in the energy spectrum of electrons passing through an Mg foil. ibid. pp. 1035-36.

Weizsäcker, C. F. v. 1933. Durchgang schneller korpuskularstrahlen durch ein ferromagnetikum. Ann. Physik 17: 869-96.

Whitby, L. 1933. The atmospheric corrosion of magnesium. Trans. Faraday Soc. 29: 844-53.

Wolff, P. A. 1953. Theory of plasma waves in metals. Phys. Rev. 92: 18-23.

Wyckoff, R. W. G. 1951. Crystal structures, Vol. I. Interscience Publishers, Inc., New York.